Optimizing the configuration of tidal turbines in storm surge barriers

Verbeek, Merel C.

DOI
10.4233/uuid:a370be10-b49d-4f4d-a074-39f464c3d8f9

Publication date
2023

Document Version
Final published version

Citation (APA)
Verbeek, M. C. (2023). *Optimizing the configuration of tidal turbines in storm surge barriers*. [Dissertation (TU Delft), Delft University of Technology]. https://doi.org/10.4233/uuid:a370be10-b49d-4f4d-a074-39f464c3d8f9

OPTIMIZING THE CONFIGURATION OF TIDAL TURBINES IN STORM SURGE BARRIERS

OPTIMIZING THE CONFIGURATION OF TIDAL TURBINES IN STORM SURGE BARRIERS

Proefschrift

for the purpose of obtaining the degree of doctor
at Delft University of Technology
by the authority of the Rector Magnificus prof. dr. ir. T.H.J.J. Van der Hagen,
chair of the Board for Doctorates
to be defended publicly on
Thursday 22^{th} of June, 2023 at 12:30 AM

by

Merel Clasien VERBEEK

Master of Science in Earth and Environment,
Wageningen University, The Netherlands,
Born in The Hague, The Netherlands.

This dissertation has been approved by:

promotor: prof. dr. ir. W.S.J. Uijttewaal
copromotor: dr. ir. R.J. Labeur

Composition of the doctoral committee:

Rector Magnificus, chair person
Prof. dr. ir. W.S.J. Uijttewaal, Delft University of Technology
Dr. ir. R.J. Labeur, Delft University of Technology

Independent members:
Ir. A.C. Bijlsma, Deltares
Prof. dr. R.H.J. Willden, Oxford University
Prof. dr. ir. A.J.F. Hoitink, Wageningen University & Research
dr. ir. H. Polinder, Delft University of Technology
Prof. dr. ir. B.J. Boersma, Delft University of Technology
Prof. dr. ir. Z.B. Wang, Delft University of Technology, reserve member

Keywords: Tidal energy, storm surge barrier, hydrodynamics, turbine performance, environmental impact

Printed by: Ridderprint

Front & back: Clarify

Graphical abstract: Clarify

Financed by: NWO, The New Delta programme (project 869.15.008)

ISBN 978-94-6483-182-5

An electronic version of this dissertation is available at
http://repository.tudelft.nl/.

CONTENTS

SUMMARY

The flow between bridge piers and through storm surge barriers and barrages is an untapped and promising source of water energy. This energy can be harvested with tidal or hydro turbines. In 2015, five turbines with a total capacity of 1.2 MW were retrofit in a flow opening of the Eastern Scheldt storm surge barrier (the Netherlands). These turbines form world's first commercial-scale tidal fence. However, there is still a major challenge to optimize the configuration of these turbines based on their energy yield and their possible environmental effects to the hinter-lying estuary.

This thesis presents a model tool to optimize the energy yield and impact on the environment of installing turbines in flood defences by altering the turbine placing. Mapping out the effects of turbines on the flow is the central question. To answer this question, this research consists of three parts: (1) measuring the field situation, (2) testing a turbine in the laboratory and (3) setting up an analytical model that is coupled to a regional flow model.

In the first part of this study (1), unique, high-resolution data of the flow through the Eastern Scheldt storm surge barrier and around the turbines were investigated. In particular, for the first time in the literature, commercial-scale turbines are used to determine the effect of tidal turbines on the water flow. The power output of the turbines is also quantified. The data is used to derive an analytical model of the flow around a turbine in a barrier. This model can calculate the power of tidal turbines and the resistance of the barrier and turbine for different forms of the installation and variable strength of the external flow.

In the second part of this study (2), these insights were refined in laboratory tests, in which the configuration of the turbine and barrier was varied. This method is more representative of real turbines because it has a larger scale factor (1:9) than is usual in the literature. The tests show that the generated power strongly depends on the position of the turbine relative to the barrier. The data also show that the combined resistance of a barrier and turbine is lower than the sum of the individual resistances. These outcomes are used to successfully validate the previously developed analytical model.

In the last part of this study (3), the developed analytical model was implemented in a larger-scale numerical flow model. In this larger-scale model, the small-scale flow around a barrier with turbines is linked in an efficient way to the large-scale water movement in a tidal basin. This makes it possible to optimize existing or new tidal power stations, both at the level of the entire barrier and at that of a single flow opening. The impact on the environment can therefore be determined with the model, even more accurately than was previously possible.

The research in this thesis shows that the effect of the turbines on the flow at a larger distance is smaller than previously thought. This offers the possibility, for example, to install more turbines and harvest more energy without exceeding the acceptable environmental impact (e.g. ecological effects). This study has contributed to confidence in the technical and economic feasibility of turbine installations that can be built in hydraulic engineering works in the Dutch Delta. The developed calculation tool is freely available to investigate energy yield and environmental effects of tidal energy projects worldwide.

SAMENVATTING

De stroming tussen brugpijlers en door stormvloedkeringen is een nog niet benutte en veelbelovende bron van waterenergie. Deze energie kan worden gewonnen met getij- of waterturbines. In een doorstroomopening van de Oosterscheldekering (Nederland) zijn in 2015 vijf turbines met een totaal vermogen van 1,2 MW gebouwd. Dit zijn de eerste in een rij geplaatste op ware grootte gebouwde getijturbines ter wereld. Er ligt echter nog een grote uitdaging om de plaatsing van dit soort turbines te optimaliseren gebaseerd op een maximale energieopbrengst en minimale effecten op de omgeving.

Dit proefschrift presenteert een tool om bij de plaatsing van turbines in keringen te optimaliseren gebaseerd op de energieopbrengst en de impact op de omgeving. Het in beeld brengen van de effecten van turbines op de stroming is daarbij de centrale vraag. Om hierop antwoord te geven bestaat dit onderzoek uit drie delen: (1) het doen van metingen van de veldsituatie, (2) het testen van een turbine in het laboratorium en (3) het opstellen van een analytisch model dat met een regionaal stromingsmodel is gekoppeld.

In het eerste deel van dit onderzoek (1) zijn unieke, hoge resolutie data van de stroming door de Oosterscheldekering en rondom de turbines onderzocht. Hiermee kan, voor het eerst in de literatuur, met prototype-schaal turbines het effect van getijturbines op de waterstroming bepaald worden. Met de set aan gegevens kan ook het geleverde vermogen van de turbines worden bepaald. En op basis van deze gegevens kan een analytisch model worden afgeleid van stroming rond een turbine. Dit model is zo ontwikkeld om bij verschillende vormen van de installatie en de sterkte van de externe stroming te bepalen wat het vermogen van de getijturbines en de weerstand van de kering en turbine in verschillende situaties zijn.

In het tweede deel van dit onderzoek (2) zijn deze inzichten worden aangescherpt in laboratoriumproeven, waarbij is gevarieerd met de opstelling van turbine en kering. Deze methode is representatiever voor echte turbines omdat ze een grotere schaalfactor (1:9) heeft dan gebruikelijk is in de literatuur. Uit de proeven blijkt dat het opgewekte vermogen sterk afhankelijk is van de positie van de turbine ten opzichte van de kering. Ook blijkt dat de gecombineerde weerstand van een kering plus turbine lager is dan de som van de afzonderlijke weerstanden. Met deze uitkomsten is het analytische model succesvol gevalideerd.

In het laatste deel van dit onderzoek (3) is het ontwikkelde analytische model geïmplementeerd als onderdeel van een grootschaliger numeriek stromingsmodel. In dit grootschaliger model wordt de kleinschalige stroming rondom een kering met turbines op een slimme en efficiënte manier gekoppeld met de grootschalige waterbeweging in een getijbekken. Dit maakt het mogelijk om bestaande of nieuw te bouwen getijcentrales te optimaliseren, zowel op het niveau van de gehele kering als op dat van een enkele doorstroomopening. De impact op de omgeving kan dan ook met het model worden vastgesteld, zelfs nauwkeuriger

dan voorheen mogelijk was.

Met het onderzoek in dit proefschrift wordt aangetoond dat het effect van de turbines op de stroming op grotere afstand kleiner is dan eerder gedacht. Dit biedt de mogelijkheid om bijvoorbeeld meer turbines te plaatsen zonder de acceptabele omgevingsimpact (ecologische effecten) te overschrijden. Deze studie heeft draagt bij aan het vertrouwen in de technische en economische haalbaarheid van turbine-installaties die gebouwd kunnen worden in waterbouwkundige werken in de Nederlandse Delta. De ontwikkelde rekentool is vrij beschikbaar om energieopbrengst en omgevingseffecten van getij-energieprojecten wereldwijd te onderzoeken.

1

INTRODUCTION

1

Challenges in low-lying deltas

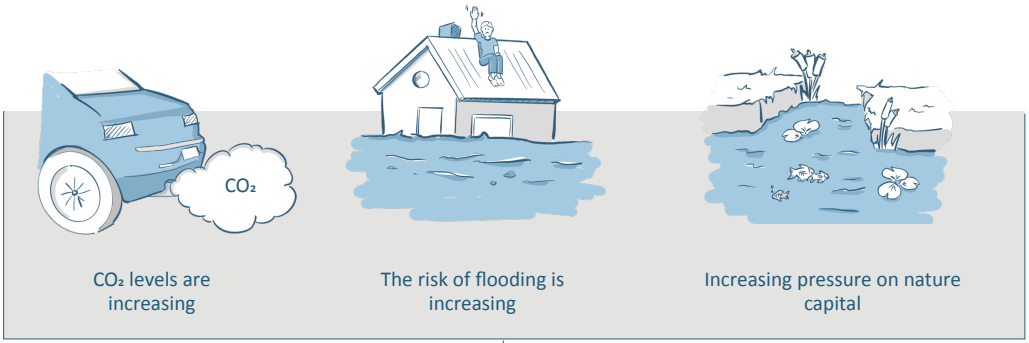

Upcoming technology: storm surge barriers with tidal turbines

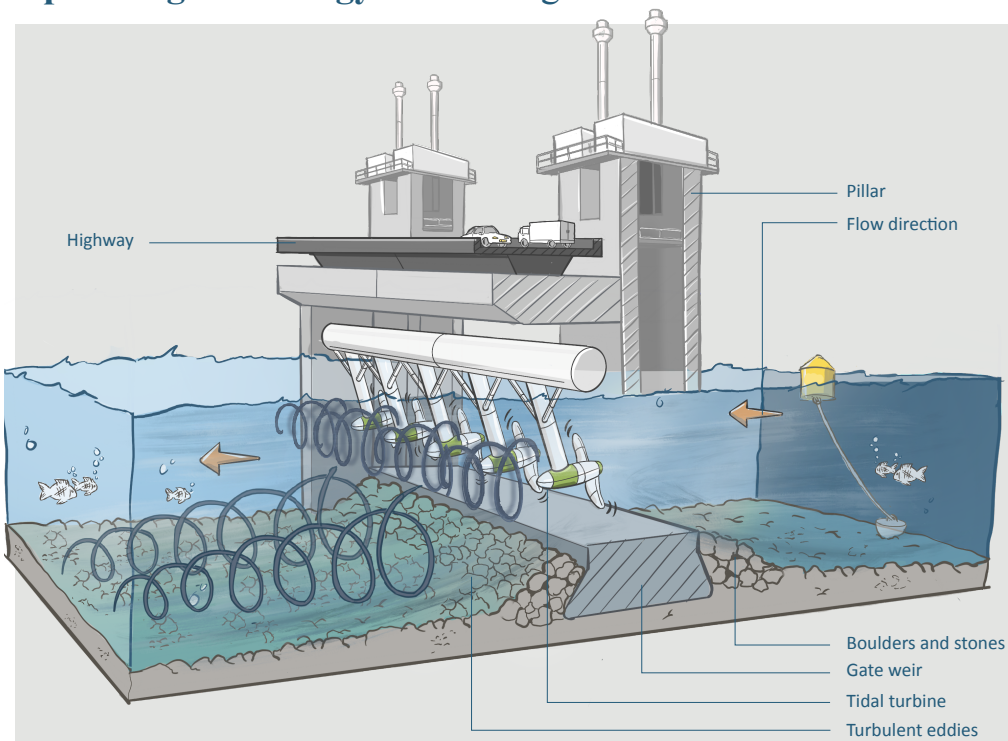

Advantages

Tidal energy generation

- Sustainable energy harvesting
- Small turbine size
- Predictable energy resource
- Little environmental impact

Protection against flooding

- Storm surge barrier protects hinter-lying delta against flooding

Sustaining nature capital

- Flexible discharge capacity is an asset to ecology
- Tidal currens transport nutrients, sealife and sediments

1.1. PROBLEM DESCRIPTION: CHALLENGES IN DELTAS

A changing climate and an increasing number of citizens will bring major challenges to low-lying deltas around the world in the coming decades. A river delta is often a densely populated and bio-diverse landform where the river enters the sea or a tidal basin. The New Delta call financing this project (*NWO*, 2016) formulates three challenges in deltas that are leading.

Firstly, the increasing energy demand needs to be furnished in a sustainable way, as both fossil fuels are depleting and CO_2 levels are increasing worldwide. Secondly, the sea level is rising and weather events are getting more extreme, leading to higher flood risk. This is a problem to low-lying deltas in particular, as some deltas are sinking as a result of the extraction of water from the subsurface. And thirdly, nature capital can compete for space with other societal needs, such as housing, as human activity in delta regions intensifies and available space is limited (*Hoitink et al.*, 2017). The European Green Deal (*EU*, 2019) and the Netherlands Organisation for scientific research (*NWO*, 2016) prescribe the need to act upon these three challenges jointly.

GENERATING RENEWABLE ENERGY WITH TIDAL TURBINES

Firstly, to meet the challenge of generating renewable energy, several technical solutions have been proposed in recent years. The European Offshore Energy Strategy aims to generate up to 40 GW in 2050 using wind, solar, and marine energies. Parts of this strategy involve tidal energy (and wave) turbines envisaged for an installed power of 100 MW in 2025 and 1 GW in 2050. The predictable character of the tide makes tidal energy an attractive addition to other, more stochastic, renewables such as wind (see Fig. 1.1). There are various forms of tidal energy converters, including oscillating, cross flow and axial flow systems, but the most mature technology is the horizontal axis, or tidal stream, turbine (Technology Readiness Level of 7-9, *Neill et al.* (2012)).

The tidal stream sector is currently in the pre-commercial fase, as first tidal stream farms are being installed worldwide. In 2016, four bottom-fixed turbines (1.5 MW each) are installed in the Meygen project, six floating turbines (600 MW in total) are installed in the Shetland Tidal array and the five barrage-mounted turbines (1.5 MW in total) are installed in Tocardo's tidal fence. In 2018, the floating Orbital SRS2000 tidal turbine (2 MW) became operational and later also the 02 turbine (2 MW). In 2020, the tidal stream power sector in Europe produced 60 GWh of power cumulatively (*Europe*, 2023).

PROTECTING AGAINST FLOODING WITH TIDAL BARRAGES

Secondly, there are a few infrastructural solutions that combine coastal protection with tidal energy generation. An example is a, more established, hydropower dam, such as the planned barrage in Severn (UK), that extracts energy from the tidal head difference. Another, interesting and upcoming solution is an open barrage (or storm surge barrier) with tidal stream turbines in its parallel gates, that uses the tidal current to extract energy. An example is the Brouwersdam barrier which is planned in the Grevelingen Lake (the Netherlands). This barrage consists of parallel gates, small channels consisting of side pillars and a bed beam, that can be closed during storm surges to protect the hinterland

1

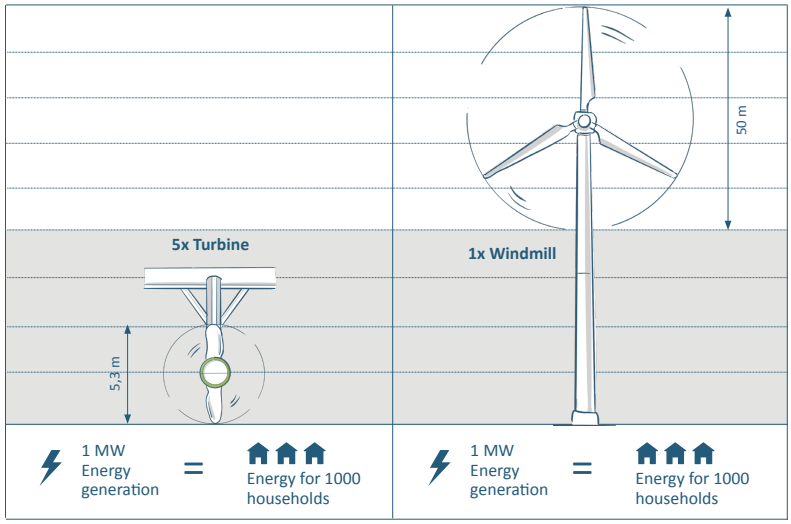

Figure 1.1: Schematic drawing of the comparison of a tidal turbine to a small windmill.

against flooding. Turbines inside these gates can be used to harvest energy from the tidal currents and to control the discharge in normal conditions. However, hydropower dams have typically large impact to their surroundings (e.g. *Xia et al.*, 2010), while it is desirable that impact to nature capital is minimized.

WITHIN ENVIRONMENTAL CONSTRAINTS WITH OPEN FLOW GATES

Thirdly, a barrier consisting of parallel open gates forms an interesting alternative to closed hydropower dams, as tidal currents can pass the structure freely. These currents transport nutrients, sealife and sediments to the hinterlying habitat. Open gates of storm surge barriers can contribute to coastal ecosystem services of hinter-lying delta areas, as the discharge capacity can be tuned using turbines or because they can create locations sheltered from high flow velocities. It would be interesting to know how a high energy yield, flood protection and nature capital are sustained by this technology.

Figure 1.2: Photo of a gate of the Dutch storm surge barrier with five tidal turbines (here: the turbines are parked above the water and not in operation).

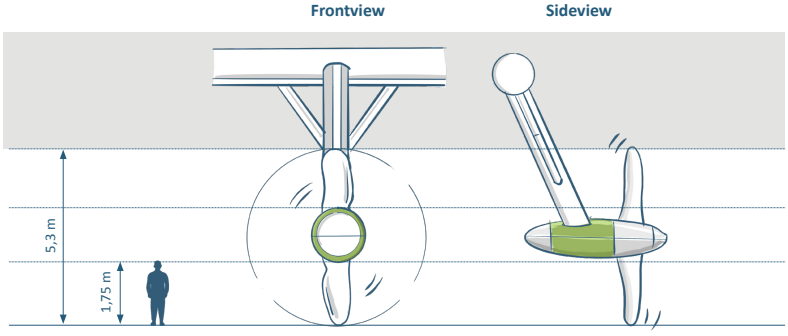

Figure 1.3: Schematic drawing of the ratio of one of the tidal turbines of the Dutch storm surge barrier to a human.

1.2. APPLICATION: A PILOT STUDY

A direct cause for this research is the initiation of a tidal energy pilot in the storm surge barrier in the Dutch delta (see Fig. 1.2 and 1.3). The project was running between the end of 2015 and 2019 and between 2021 and 2023. Five horizontal-axis tidal turbines (1.2 MW in total) were retrofitted in a single gate of the barrier. The gates of the barrier in the Eastern Scheldt are an attractive location for tidal energy harvesting as the flow velocities range up to 5 ms^{-1}. Learning from this pilot is an essential first step for applying this technology in low-lying deltas. This is particularly valuable if, in addition, it is investigated how the EU objectives are affected when more turbines are installed in a tidal energy project to harvest more energy from the flow.

For the latter, a modelling tool is needed that can predict the influence of alternative configurations of tidal turbines in a storm surge barrier on turbine power production as well as the impact of the modified barrier and on the adjacent delta. By incorporating the main

1

physical processes, such a tool should also be instrumental in applying lessons learned to other suitable tidal sites in deltas worldwide.

1.3. APPROACH: MODELLING THE SMALL AND LARGE SCALE

Specifically, the desired tool must be able to predict how small-scale flow processes associated with the turbines affect larger-scale flow processes in a delta, and vice versa. At small scales, an individual turbine device influences its neighbour turbine through bypass flow and wakes (*Nishino and Willden*, 2013; *Cooke et al.*, 2016) (see Fig. 1.4). Besides, the flow through the barrier itself also interacts with the turbine. At larger scales, the distribution and amplitude of the tidal current over the barrier is affected by the sum of these processes, and vice versa. In turn, these large-scale processes have impact on e.g. discharge distribution and sediment transport, which are important to flood- and nature protection of a delta. A major issue to this modelling tool is that little is known about these small scale processes. In particular, while the behaviour of single or arrayed turbines in a tidal flow has received a lot of attention in literature, the combination with a storm surge barrier or other hydraulic structure is completely new.

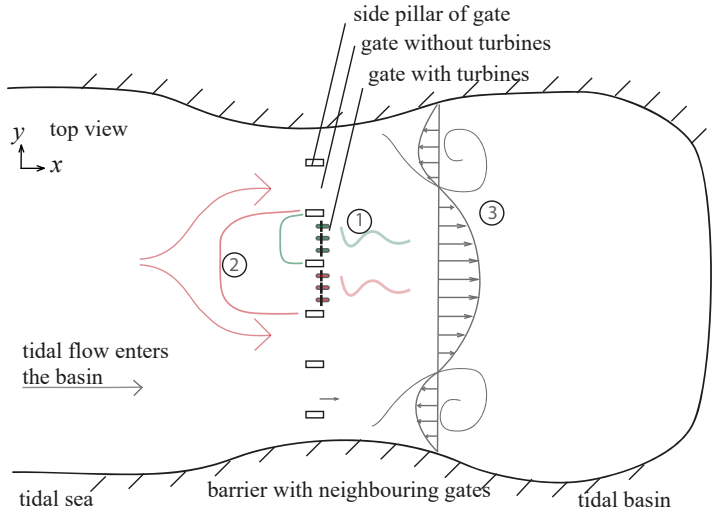

Figure 1.4: A schematic of the flow in a delta or tidal basin with a storm surge barrier in top view. The small-scale flow processes associated with turbines in barriers (e.g. blockage effects and bypassing of flow, numbers 1 and 2 respectively) affect the larger-scale flow processes in a delta (e.g. (re)distribution of the tidal current, number 3).

A good way to investigate these turbine-barrier processes for the purpose of developing a modelling tool is by combining intensive monitoring of commercial-scale turbines and physical modelling of lab scale turbines inside barriers (*Stallard et al.*, 2015; *Myers and Bahaj*, 2010). The field monitoring, on one hand, results in insights about the flow distribution through and bypassing turbines, as no scale effects are present at commercial-scale

turbines. Furthermore, detailed flow- and performance measurements of commercial-scale turbines in representative environments are rare in literature (*Jeffcoate et al.*, 2015). A physical model study, on the other hand, has the advantage that it can show whether the assumptions hold for a larger set of turbine-barrier geometries. In particular, turbine-barrier distance, water depth, and gate-bottom beam height can be varied in a laboratory setting, while these may be fixed in a field environment. In the end, information from both the field and the physical model can be used to validate a resulting modelling tool for turbines in barriers. This tool that can predict small scale processes, needs to be coupled to a larger scale model to reproduce flow effects in the adjacent tidal basin or delta.

Due to the above mentioned interaction of scales, an important requirement for the desired tool is the dynamic coupling of flow phenomena at both scale levels: from flow patterns at the scale of a single turbine device, of O(1-10) m, up to flow patterns at the scale of a barrier and the wider tidal basin, of O(1-10) km. The described coupling of scales usually comes at the cost of a prohibitively increased computational effort. Obviously, it is desirable to minimize this effort where possible. This can be achieved in two ways. Firstly, by modelling small-scale turbine processes (such as the flow through and bypassing a turbine device) in a sub-grid manner, using a parametrization which accounts for the relevant physical processes, and coupling this to a larger-scale numerical flow model. Examples of this approach are: incorporating a momentum sink at the turbine location, which is a common method to parameterize turbines (e.g. *Neill et al.* (2012); *Fallon et al.* (2014); *Kramer and Piggott* (2016); *Bray et al.* (2016)), and a head-discharge relation, which is often used to calculate flow through gates or over weirs (*Talstra et al.*, 2019). And secondly, by applying local mesh refinement in the larger scale model near the barrier and turbine devices (to accurately and efficiently resolve the coupling of scales), while using a coarser mesh resolution in the far field. Such a model is needed to help designing and optimizing the future delta with barriers combined with tidal turbines.

1.4. DISSERTATION AIM AND QUESTIONS

Based on the above considerations, the aim of this dissertation can be formulated as:

> *To develop a physics-based modelling tool to determine an optimal placing of horizontal-axis turbines mounted in a storm surge barrier, with regard to their energy yield and hydrodynamic effects.*

This aim will be achieved by answering five questions:

1. What are the main processes governing energy yield and flow effects of commercial-scale tidal stream turbines inside storm surge barriers?

2. How to predict the energy yield of turbines in barriers using an analytical flow model that can serve as a sub-grid formulation in a regional flow model?

3. How does the geometry of a gate of a storm surge barrier affect energy yield and hydrodynamics of turbines mounted inside a gate of a storm surge barrier?

4. How to develop a model for storm surge barriers with turbines, from the turbine device to the estuary scale, for the purpose of optimizing turbine configuration in barriers based on their energy yield and their hydrodynamic effects?

5. What are effects of multiple turbine configurations on energy yield, nature capital and flood protection in a tidal pilot (case study)?

The answer to question 1 reveals the physics of turbines in barriers, providing the fundamental basis to schematise the flow through and bypassing turbines in barriers in a analytical model, as an answer to question 2. The answer to question 3 is a parameter study that can be used to validate the analytical model. This model is coupled to a regional flow model, covering the turbine device scale to the barrier/estuary scale, for the simulation of flow effects and energy yield of turbines mounted in barriers as an answer to question 4. And when answering question 5, the coupled model is applied to a tidal pilot, where and alternative placings of turbines in a storm surge barrier are considered exploring an optimal configuration for turbine placement.

1.5. OUTLINE AND METHOD

Questions 1 and 2 are answered in Chapter 2, question 3 in Chapter 3 and question 4 and 5 in Chapter 4. Fig. 1.5 presents the coupling of these chapters in a schematic way by presenting the products and associated activities.

In Chapter 2, flow and performance data are measured in the world's first commercial-scale tidal stream array of turbines operating in a gate of the Dutch Eastern Scheldt basin. The data of these commercial-scale turbines are used to schematize the hydrodynamics of turbines inside barriers in a model, describing physics of the small scale, and to validate the resulting model. Also, this model will be applied to a range of barrier-gate geometries (with different weir height, water depth, turbine-weir distance) to find an optimal geometry. In the end, this chapter delivers a dataset of the hydrodynamics for full scale operating turbines and a validated analytical model, which can predict the performance of tidal stream turbines inside a gate of a storm surge barrier.

In Chapter 3, flow and performance data will be collected from a physical model of a turbine inside a storm surge barrier. In essence a parameter study is done on the performance of turbines in barriers. These data will be used to validate the model for the small scale and show its range of application for alternative turbine-weir geometries. This chapter delivers a dataset of detailed turbine wakes, bypasses and performance.

In Chapter 4, the model for the small turbine scale will be coupled to a model for the large (estuarine) scale processes. The coupled model will be validated using the datasets from Chapter 2 and 3. Lastly, the coupled model will be applied to study the placing of turbines in a storm surge barrier in a relevant case study: the Eastern Scheldt tidal estuary; the same location as the field study of Chapter 2. The model outcome for this study site will be used to discuss trade-offs and compromises of different configurations of turbines in barriers for a high energy yield and small impact to the surrounding.

In the end, the results are synthesized in Chapter 5.

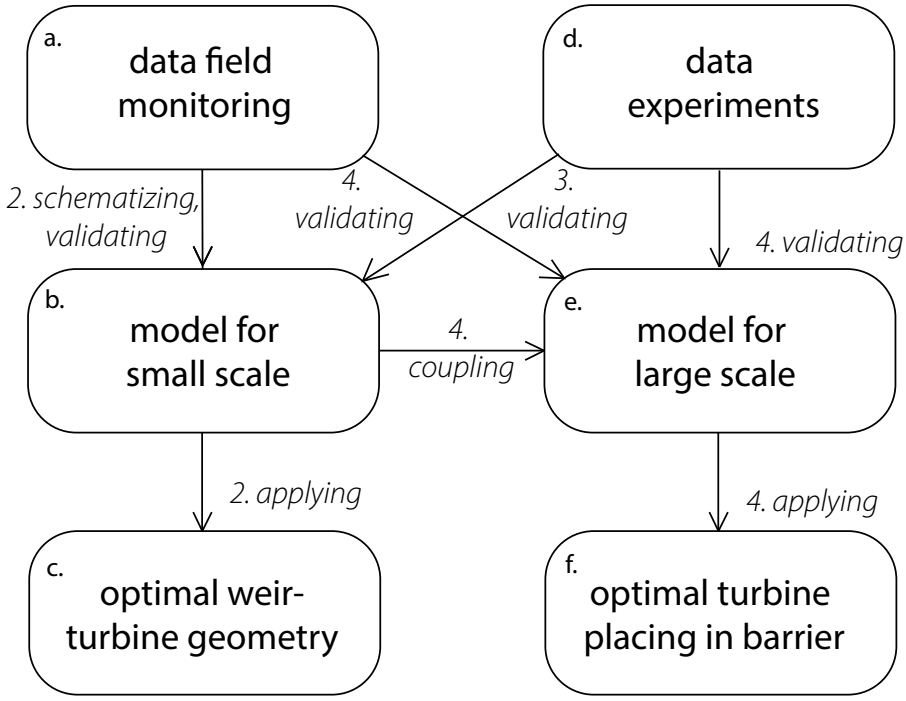

Figure 1.5: Schematic of the dissertation structure. Panels indicate products and arrows in between panels indicate activities. Numbers of the activities refer to the chapters in which they are described. In the end, a small scale model coupled to a large scale model is developed. The model is validated with data from the field and experiments and applied to study an optimal configuration of turbines in a storm surge barrier.

2

THE PERFORMANCE OF A WEIR-MOUNTED TIDAL TURBINE: FIELD OBSERVATIONS AND THEORETICAL MODELLING

This chapter has been published as M. C. Verbeek, R. J. Labeur, and W. S. J. Uijttewaal, 2020, "The performance of a weir-mounted tidal turbine: Field observations and theoretical modelling", Renewable Energy, 153, 601 – 614, https://doi.org/10.1016/j.renene.2020.02.005

2. Field observations and theoretical modelling

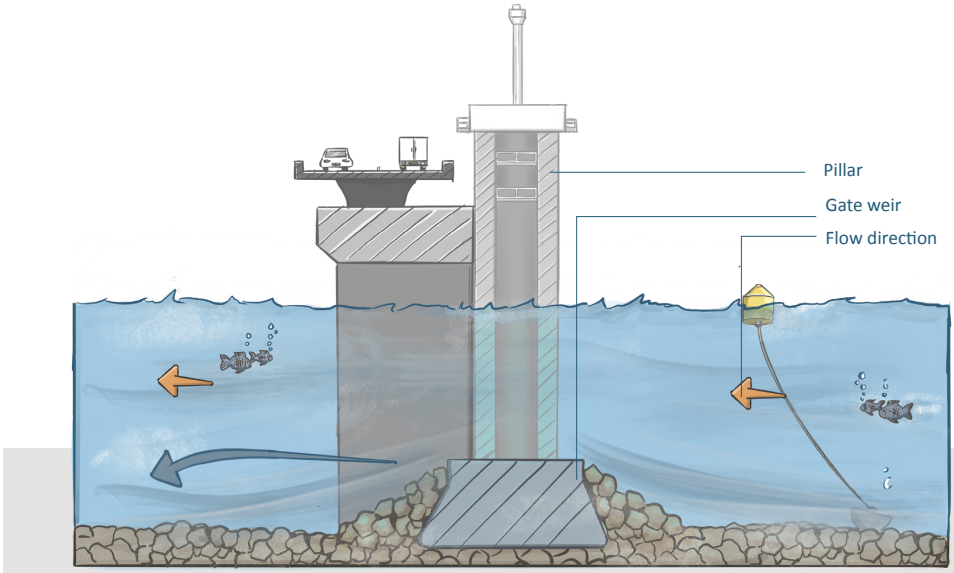

Field observation of the flow through a barrier without turbines

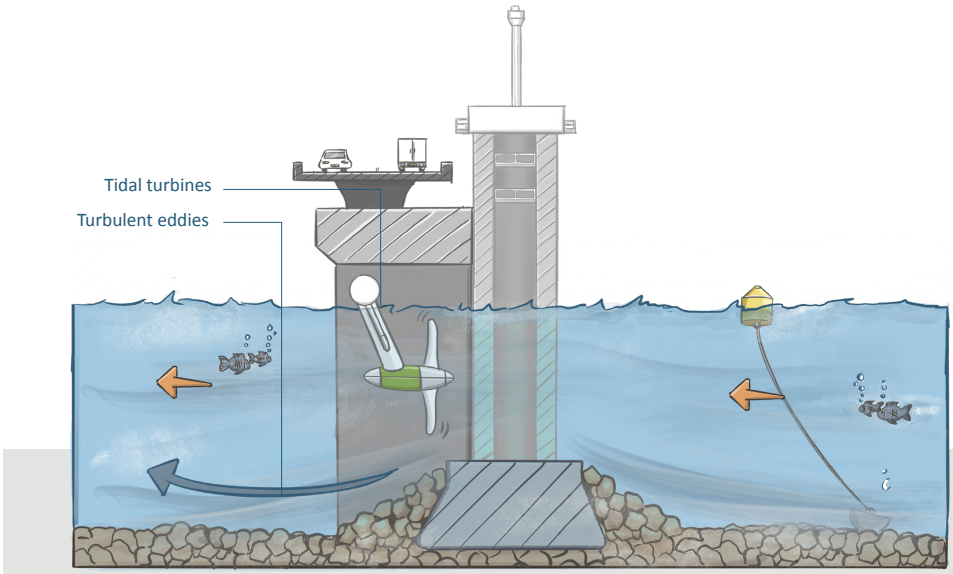

Field observation of the flow through a barrier with turbines: flow is altered by the turbines.

To reach the thesis objective described in Chapter 1, processes need to be studied that govern the energy yield and flow effects of turbines inside storm surge barriers. This will form the key ingredient to develop a physics-based model to study turbine placing inside barriers.

While numerous studies have investigated how turbines should be arranged in idealized geometries to optimize their performance, only a few have considered the influence of realistic bed features, like piers and weirs present in barriers. Besides, detailed flow- and performance measurements of full scale turbines in representative environments are absent in literature.

To fill this gap, this chapter describes the influence of a hydraulic structure on the performance of a tidal turbine, using the combination of field monitoring of prototype-scale turbines installed in a Dutch storm surge barrier - comprising a weir and pillars - and by developing a corresponding analytical model.

Section 2.3 describes detailed measurements at the tidal turbines. Both the flow field, its turbulence, the velocity magnitude in the turbine wake and bypass and turbine performance are described. Thereafter, in Section 2.4, an analytical model for turbines inside barrier geometries is presented based on these measurements.

The observed production by the turbines was large compared to situations with an unconstrained flow for two reasons. Firstly, the flow contraction caused by the weir increased the mass flux through the rotor plane. Secondly, the turbine suppressed energy losses in the recirculation zone downstream of a weir. The proposed model provides a quantitative estimate of these effects and is validated against field data. The analytical model can be used as a design tool of turbines, providing performance estimates covering a range of turbine-weir configurations, and it can be coupled to a regional flow model, providing large scale flow and performance effects of multiple turbine installations in a basin or estuary.

2.1. INTRODUCTION

Energy generation using tidal turbines is a promising new technology, which can supply a significant amount of power to countries with tidal coasts. For example the waters around UK's coast have the potential to provide half of the electricity need of the country (*Bahaj*, 2011). The Levelized Cost of Energy of tidal stream is quantified two to five times higher than exploiting other renewable energy sources such as onshore wind in the UK (*Borthwick*, 2016). A cost reduction may be realized by installing turbines in existing coastal infrastructure - such as dams, storm surge barriers or levees - provided their power output is not significantly reduced. In this light, many researchers have investigated how the performance of turbines is affected when changing their configuration in a tidal channel (e.g. *Vennell*, 2010).

Betz (1920), *Lanchester* (1915), and *Joukowsky* (1920) provided the basis for performance studies of wind - and tidal energy turbines, by describing the turbine as an inverse propeller which extracts power proportional to the rotor swept area. *Betz* (1920) derived an expression for the maximum fraction of energy that can be extracted from the flow by applying the 1D balances for mass, energy and momentum to a stream tube passing the rotor area. The theoretical maximum power extraction amounts to 16/27 of the undisturbed energy flux through the rotor plane for a turbine placed in an unconstrained flow (*Betz*, 1920). *Garrett and Cummins* (2005) demonstrated that this limit can be exceeded

if turbines are installed in a channel, as the lateral confinement of the flow by the channel boundaries enforces a larger mass flux through the rotor plane of the turbines. *Garrett and Cummins* (2005) elaborated on the formulation of *Betz* (1920) by adding an energy balance for the flow bypassing the turbines. They found that power output can be optimized by changing the *local blockage*, defined as the ratio of the total turbine area and the channel area.

Theories to assess the performance of turbines in channels generally consider a flat bed only and can therefore not be applied to situations with an abrupt step in the bathymetry, as is the case for a weir. *Smeaton et al.* (2016) discussed how turbine performance is affected by a smooth constriction in a channel, excluding the effects of flow separation and recirculation. For turbines in the wake of a weir however, these turbulence phenomena govern the volume flux of water bypassing the rotor, while also energy losses downstream of the weir may be affected by the presence of the turbines. The coupled effects of separating flow and the turbine's effect on the flow field will thus determine the turbine's performance.

Many studies have investigated the performance of tidal turbines by using theoretical or numerical modelling. Validation of such models is generally limited as data from turbines operating at full scale is relatively scarce. For this reason, verification of the underlying model assumptions has mainly relied on laboratory experiments which imposes some restrictions deriving from moderate scalability of intricate details of the flow past turbines. Validation of the calculated performance - using measurements from full-scale turbines - would on the other hand warrant the predictive capability of such models rendering them valuable tools to obtain a quick scan of the power potential of a tidal site.

This study extends the 1D model of *Garrett and Cummins* (2007) and *Houlsby et al.* (2008) to tidal channels with a locally non-flat bed in order to assess the performance of turbines mounted in a hydraulic structure or a weir. Data from a monitoring program of full scale horizontal axis turbines are used to schematize the flow and to verify various other model assumptions. The field data are obtained from turbines installed at the storm surge barrier in the Eastern Scheldt, a tidal estuary in The Netherlands. These observations demonstrate that turbine performance may exceed the theoretical limit, derived by *Betz* (1920), when the turbines are installed nearby a weir. The model can predict an optimal trade-off between energy losses at flood defences and energy harvesting by the turbines.

This chapter consists of two parts: (1) field data analyses, and (2), data interpretation through theoretical modelling. In the next section, the methods to acquire the flow - and performance data of the commercial-scale turbines are discussed and the general modelling concepts are introduced. The field data are presented in the third section for a representative situation during flood and ebb, respectively. These data provide a basis for conceptualization of the flow at a turbine near a weir, where the following two cases are discerned: (1) the turbine is situated downstream of a weir, which at the test site corresponds to flood, and (2), the turbine is situated upstream of a weir, corresponding to the observed ebb tidal stage. The model equations are presented and verified in Section 4, which are used to estimate the turbine thrust coefficient and the fraction of extracted power for different turbine-weir geometries. Conclusions are drawn in Section 5.

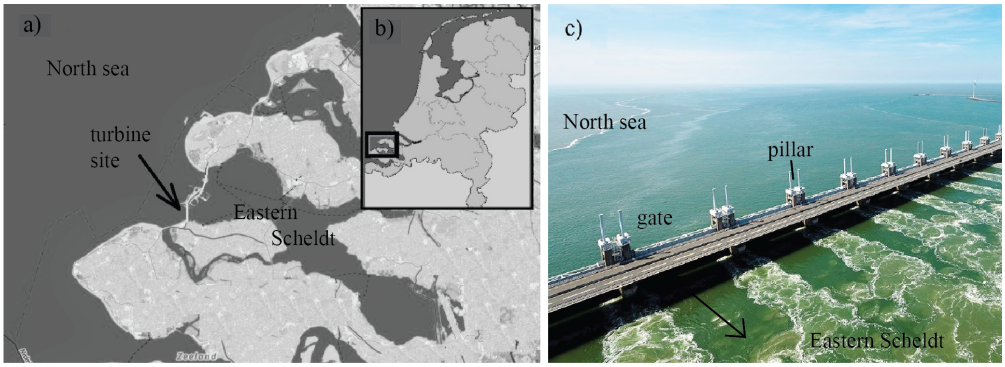

Figure 2.1: a) A map of the Eastern Scheldt basin, with the barrier with turbine site indicated with an arrow and b) its location in the Netherlands. c) An aerial photograph of the storm surge barrier and its gates. The arrow indicates the flow direction in one of the gates of the barrier during the flood phase. (source: Rijkswaterstaat)

2.2. METHODS OF MONITORING AND MODELLING

2.2.1. FIELD OBSERVATIONS

The hydrodynamics and performance of an array of full-scale turbines is studied in a monitoring programme at a semi-open storm surge barrier in the Eastern Scheldt basin, a tidal estuary in The Netherlands (Fig. 2.1). The basin is connected to the southern part of the North Sea (Fig. 2.1a, 2.1b). The barrier is a prospective location for harvesting tidal energy, as in principle all gates can be retrofitted with turbines and flow velocity is high. The flow passing the barrier is constrained by both the islands and the bathymetry in the basin mouth, and the pillars and weirs of the barrier (Fig. 2.1c, *Hartsuiker et al.* (1989). The barrier is positioned on top of a submarine sill, which is covered with asphalt mastic and boulders. The structure consists of 62 gates - with an equal amount of weirs - which can be closed during storm surges to protect the hinterland from coastal flooding (Fig. 2.1c). Since the end of 2015, five horizontal-axis turbines have been installed in the 8th gate of the southern channel.

Each turbine has two blades, a rotor diameter of 5.3 m and an installed capacity of 250 kW. The turbine axes are mounted at a height of -4.83 m NAP (national reference datum) and 6.13 m basin-ward of the gate weir (Fig. 2.2). The turbine blade tip-to-tip spacing is a quarter rotor diameter. The blade-swept area to channel area ratio amounts to 0.20, with respect to the mean local cross section, and 0.29 with respect to the mean cross-sectional area at the crest of the weir. The turbines are lifted in case the hydraulic head loss over the barrier exceeds 0.6 m during outflow from the basin, or 0.8 m during inflow towards the basin, in order to avoid potentially high structural loading on the barrier and its downstream bed protection. The gauges, which record the corresponding water levels, are located in the approach harbours up- and downstream of the barrier 1 km north of the installation site.

Tab. 2.1 summarizes the characteristics of the five sets of data that were obtained in the context of the monitoring: one before the turbines were installed, in 2011, and four after installation of the turbines (Tab. 2.1 and Fig. 2.2). Two- and three beam Teledyne Acoustic

Doppler Current Profiler (ADCP) transducers recorded the flow during a spring neap cycle in August 2011. The transducers have a three degree beam angle slanted 20 degrees with respect to the transducer centre line. The transducers were mounted at the gate pillar looking sideways and at the gate sill looking upwards (Fig. 2.2b). The second and third datasets were recorded with horizontal ADCPs (Signature 1000, *Nortek AS*) mounted in the turbine hub and strut of the outer and centre turbines (Fig. 2.2c, d, Fig. 2.3) with one 16 Hz beam along the mean flow direction. The transducers have an acoustic frequency of 1 MHz and map the flow velocity 25 m up- and downstream of the turbines in 50 bins of 0.5 m each. The fourth and fifth datasets are obtained similarly, but with three ADCP beams at 8 Hz.

The flow field at the turbines in dataset 2 to 5 is studied discerning two modes of operation: (1) idle, with the turbines operating at a constant and minimal tip speed relative to the incoming flow velocity at a distance 25 m upstream, taking out no kinetic energy, and (2), loaded, with the turbines operating at a constant and optimal tip speed ratio, extracting energy. The corresponding tip speed ratios are similar for the measured ebb and flood situation. Various variables were recorded for both modes: flow velocity [ms^{-1}] at 8 Hz and 16 Hz, turbine loads [N] at 1 MHz, including the axial thrust force, bending moments [Nm] at 1 MHz, rotational speed at 1 Hz and net production [kWh] at 1 Hz.

2.2.2. DATA PROCESSING

The data of dataset 1 (2011) were processed, giving vertical, lateral and streamwise flow velocity profiles. Hereby, isotropy of the flow between the inclined beams is assumed. The data from the turbine transducer beams (datasets 2 to 5) are not combined into a velocity vector in three directions, because the flow in the turbine wake is strongly anisotropic (*Schmitt et al.*, 2015). Here only the component along the mean flow direction is used in the analysis. This component is a consistent approximation of the mean flow velocity as long as the flow direction is not perpendicular to the transducer beam. This holds since the mean flow direction deviates only up to 10 degrees from the turbine rotation axis when the flow enters the basin during flood. The flow velocity in between the turbines is measured with the side-looking ADCP beams (Fig. 2.3), quantifying the acceleration of the flow bypassing the array and devices when the turbines are positioned close to each other *Nishino and Willden* (2012b).

The data analyses are not limited to the time-averaged flow fields since the flow over the weir is highly turbulent, which is associated with the sharp local velocity gradient. The turbulence characteristics give insight in the shear layer between the wakes and ambient

Table 2.1: Overview of the characteristics of the five sets of ADCP-data used in the analysis. The exact tip speed ratio (TSR) of the turbines cannot be disclosed. (hor. is horizontal and vert. is vertical.)

Type	Dates	Turbine Tip speed ratio	ADCP Height	ADCP Direction	ADCP Configuration	ADCP Frequency
1.	08 16 - 08 23 2011	No turbine	-9.5 m	vert.	1 device, 3 beams	2 Hz
	08 16 - 08 23 2011	No turbine	-4.8 m	hor.	1 device, 2 beams	2 Hz
2.	10 10 - 10 26 2016	Optimal TSR	-4.8 m	hor.	6 devices, 1 beam	16 Hz
3.	08 28 - 08 29 2017	Minimal TSR	-4.8 m	hor.	6 devices, 1 beam	16 Hz
4.	06 20 - 06 22 2017	Optimal TSR	-4.8 m	hor.	6 devices, 3 beams	8 Hz
5.	06 01 - 06 06 2017	Minimal TSR	-4.8 m	hor.	6 devices, 3 beams	8 Hz

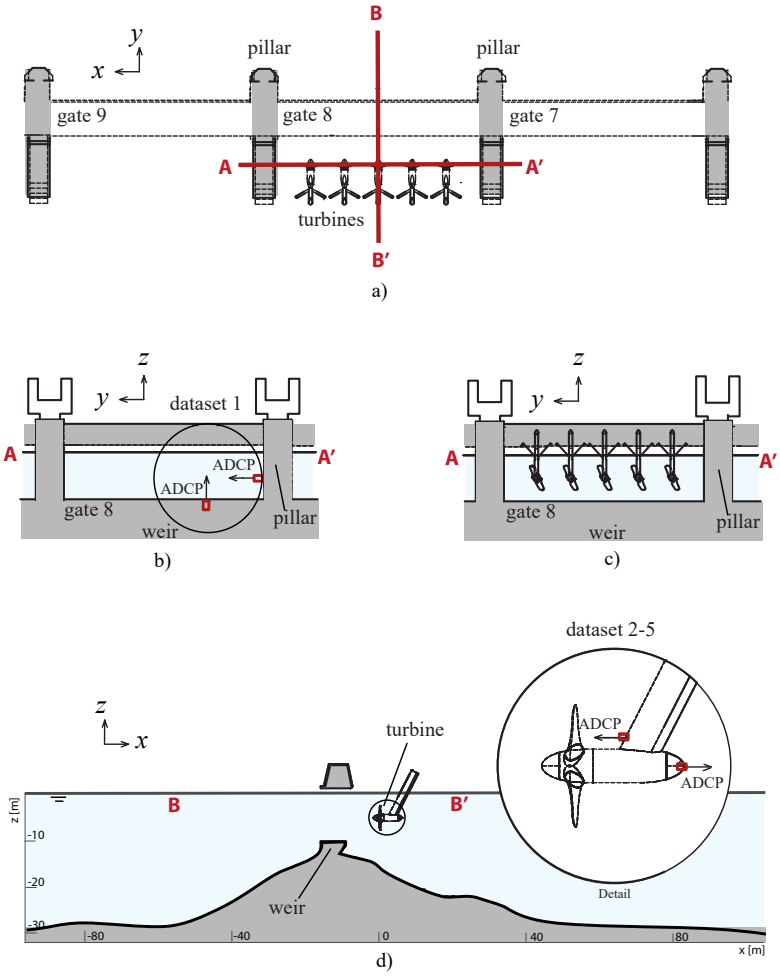

Figure 2.2: a) A schematic drawing of the gate with turbines in top-view indicating cross sections A and B (a projection of a 3D view is presented in Fig. 2.3), b) cross section A showing the gate from the side (looking to the east) with the positions of the two ADCPs mounted during the 2011 survey prior to turbine installation, c) cross section A gives a side view of the turbines to the east, d) cross section B showing the bathymetry over the gate from the side (looking north) and a detail of the turbine with ADCPs.

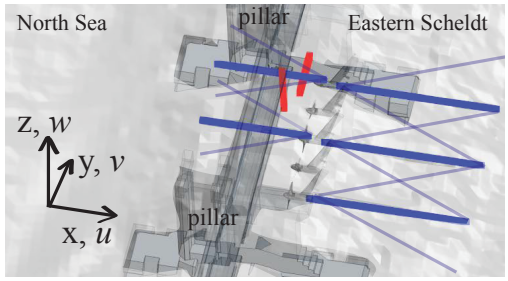

Figure 2.3: A 3D view of the turbine array and the ADCP measurement locations of datasets 1 (horizontal and vertical red lines) and 2 to 5 (horizontal blue lines; three per device), x is the direction along the main flow. Courtesy of Deltares.

flow and the recovery of velocity deficits. *Guerra and Thomson* (2017) have already proven that reliable turbulence characteristics can be obtained from shallow seas with the ADCP transducer of this study.

The integral turbulence length scale, L [m], representing the size of the turbulence eddies present in the flow, is estimated for each ten minutes of velocity data. To this end, a turbulence time scale, obtained from a Fourier transformation of the corresponding dataset, is multiplied by the mean velocity, using Taylor's frozen turbulence hypothesis (*Nieuwstadt et al.*, 2016), although this is not strictly valid in the wake of the turbine. The method was successfully applied to determine turbulence length scales at an offshore site by *Milne et al.* (2016) and *Guerra and Thomson* (2017). The turbulence intensity, I [-], which denotes the turbulence level of the flow - or the strength of the velocity fluctuations - is calculated as the ratio between the 10-min averaged root mean square of the turbulent fluctuations and the mean free stream flow velocity measured three rotor diameters (diameter $D = 5.3$ m) upstream of the turbine.

Poor quality data points and data points during the time span of turbine operation outside of the operational tip speed ratio were flagged and filtered out prior to the analysis. These data were excluded based on low signal amplitude, low signal correlation, and the orientation of the ADCP transducers, in line with the work of *Milne et al.* (2013). The Doppler noise was removed using a low pass filter. The sampling volumes of the seaward-looking transducers were intersected by passing turbine blades two times per blade rotation. The corresponding signal is removed by identifying velocity fluctuations at twice the rotational frequency. Overall, up to 5 percent of the data obtained during neap tides were removed while 60 percent of the data obtained during spring tides were removed. This difference is on account of the higher incidence of large water level differences - for which the turbines had to be lifted out of the water - during spring tide. The interpretation of the data will be done through a simple 1D model.

2.2.3. MODEL APPROACH

A theoretical model is set up in the second part of this chapter. The model aims to quantify how the rotor thrust of a turbine is influenced by a weir, using the 1D balances of mass, momentum and energy. The field data form the basis to schematize the flow fields in the theoretical model, which is validated with thrust data from the turbine in Sec. 2.3.3. The model approach of *Garrett and Cummins* (2007) is extended with the inclusion of an abrupt

step in the bathymetry, representing a weir, for a situation with a turbine upstream of the weir and for a situation with a turbine downstream of the weir. As input the model uses the hydraulic head difference, the deceleration of the flow at the rotor plane, and geometry information, which is in line with the work of *Garrett and Cummins* (2007) and *Nishino and Willden* (2012b). The model may be used as an engineering tool, giving a rapid assessment of both the drag of a barrier and turbine, and the turbine production, which is particularly useful in optimization studies.

2.3. DATA ANALYSES

This section presents the observed hydrodynamics of the flow over a weir at the Eastern Scheldt storm surge barrier, considering representative situations during flood and ebb with the corresponding head differences being defined as positive and negative, respectively. The studied full-scale turbines are located at the lee side of the weir during flood (positive head) and at the upstream side of the weir during ebb (negative head). The turbulence characteristics of the flow are presented in order to interpret the role of the large velocity gradients in the wake flow of the weir, which may converge the flow at the turbine location. This possibly affects turbine blockage and performance. Furthermore, the analysis of turbulence quantities enables a distinction between the respective contributions of the turbine and gate to the flow field, which is relevant to schematise the flow in Sec. 2.4. The data are shown for a time-averaged head over the weir for both an increasing and decreasing water level head, to capture the influence of the tidal stage on the observed profiles. At the end, the hydrodynamics is linked to the performance of the turbine, by relating the observed turbine thrust to the different conditions.

2.3.1. HYDRODYNAMICS OF THE WEIR

The variations in the flow are mainly governed by the tidal cycle, suggesting that the flow at the weir can be assumed quasi-steady, ignoring inertia effects imposed by the tide. In other words, the time variations in the boundary conditions of the flow are slow relative to the travel time of a fluid particle passing the weir. The flow velocity is largest during flood, with a maximum around 4.5 ± 0.5 ms^{-1}. A slightly lower velocity maximum of 3.8 ± 0.2 ms^{-1} is observed during ebb.

Fig. 2.4 presents the flow field along a vertical and a lateral transect at the weir, prior to the installation of the turbines (dataset 1). Two transducers measured the flow velocity: one looking upwards from the weir crest at a lateral position of $y = 9.8$ m and one looking sideways from the pillar at a height of $z = -4.8$ m NAP (Fig. 2.3). The water surface in Figs. 2.4a-c and 2.4g-i is located at approximately a height of $z = 0$ m NAP. The full width of the weir is 39.5 m, of which 8 m is presented in the lateral profiles of Figs. 2.4d-f and 2.4j-l.

Figs. 2.4a-c show the vertical velocity profile at the weir for the flood situation. The along-stream flow velocity is nearly uniform above a depth of -7.5 m NAP. Variations in the velocity, turbulence intensity and integral length scale are only manifest below this depth. Fig. 2.4g-i shows the vertical velocity profile for the ebb situation, which is uniform above a depth of $z = -9$ m NAP. The flow velocity is lower in the ebb situation than in the flood situation. The turbulence intensity has a peak value, namely above 0.2, close to the crest of the weir ($z = -9.5$ m). The lateral velocity profiles, which are presented in Fig. 2.4d and j, are uniform during both the and ebb and flood situation, except from the small peak in

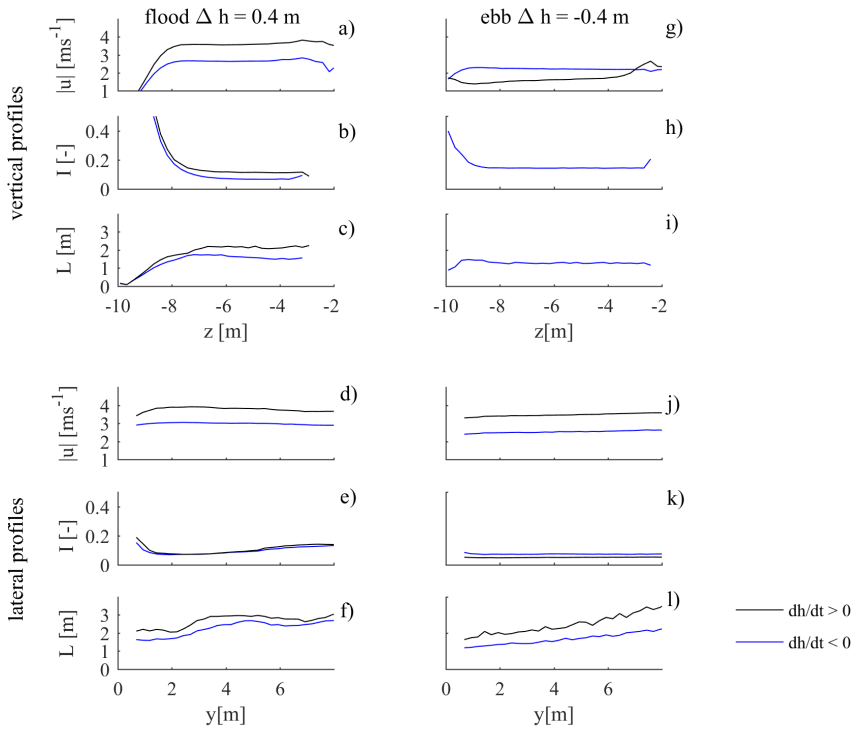

Figure 2.4: The time-averaged flow field in a gate without turbines is displayed for a water level head of 0.4 m (panels a-f, flood) and -0.4 m (panels g-l, ebb) over the barrier based on measurements during a spring-neap cycle in 2011 (dataset 1). The pillar is located at a lateral position of $y = 0$m, the weir crest at a height of $y = -9.5$m. The panels display the vertical (a-c and g-i) and the lateral (d-f and j-l) profiles of the time-averaged streamwise flow velocity u, the streamwise turbulence intensity I, and streamwise turbulence integral length scale L. The dataset is split into conditions for increasing (black) and decreasing (blue) heads.

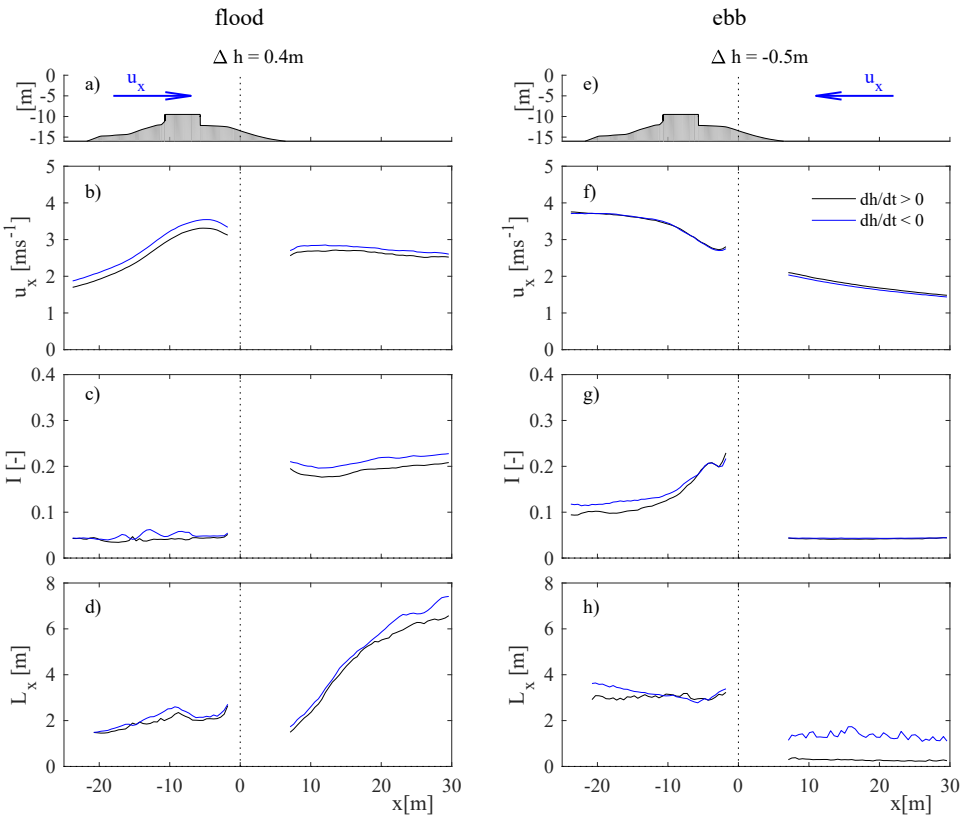

Figure 2.5: The streamwise flow field at the weir at a water depth of approximately -4 m, that is 5.5 m above the weir crest, at the centre of the weir for a water level difference of 0.4 m (a-d) and -0.5 m (e-h). The flow field is obtained, with turbines in idling mode (dataset 3). The panels present a longitudinal transect of the bathymetry over the weir (a,e) and the corresponding along-stream profiles of the flow velocity (b,f), the streamwise turbulence intensity (c,g), and the turbulence integral length scale (d,h). The dataset is split into conditions for increasing (black) and decreasing (blue) heads.

turbulence intensity of 0.2 near the pillar (Fig. 2.4e).

The observations indicate that the flow through the gate is mainly affected by the vertical confinement imposed by the weir. The vertical profile shows a marked decrease in the along-stream velocity close to the crest of the weir, while the flow is largely uniform in the remainder of the profile. The high turbulence intensity near the weir crest indicates that turbulent mixing takes place. The bed level decreases abruptly at the lee side of the weir. Likely, the flow separates downstream of the weir and a recirculation zone develops.

Dataset 3 gives insight in the flow over the weir at a height of 4 m below NAP, that is 5.5 m above the weir crest (Fig. 2.5b and e). The longitudinal flow velocity at this depth accelerates from 1.5-2.0 ms^{-1} to 3.0-3.5 ms^{-1}, over a distance from 10-25 m upstream of the weir to the weir crest. Figure 2.5 shows that the streamwise turbulence intensity of the flow is highest at the lee side of the weir, namely around 0.2. Here, the turbulence integral length scale increases with the downstream distance from the weir from 2 m to approximately 7 m during flood and from 0.5 m to 3 m during ebb (Fig. 2.5d and h). These

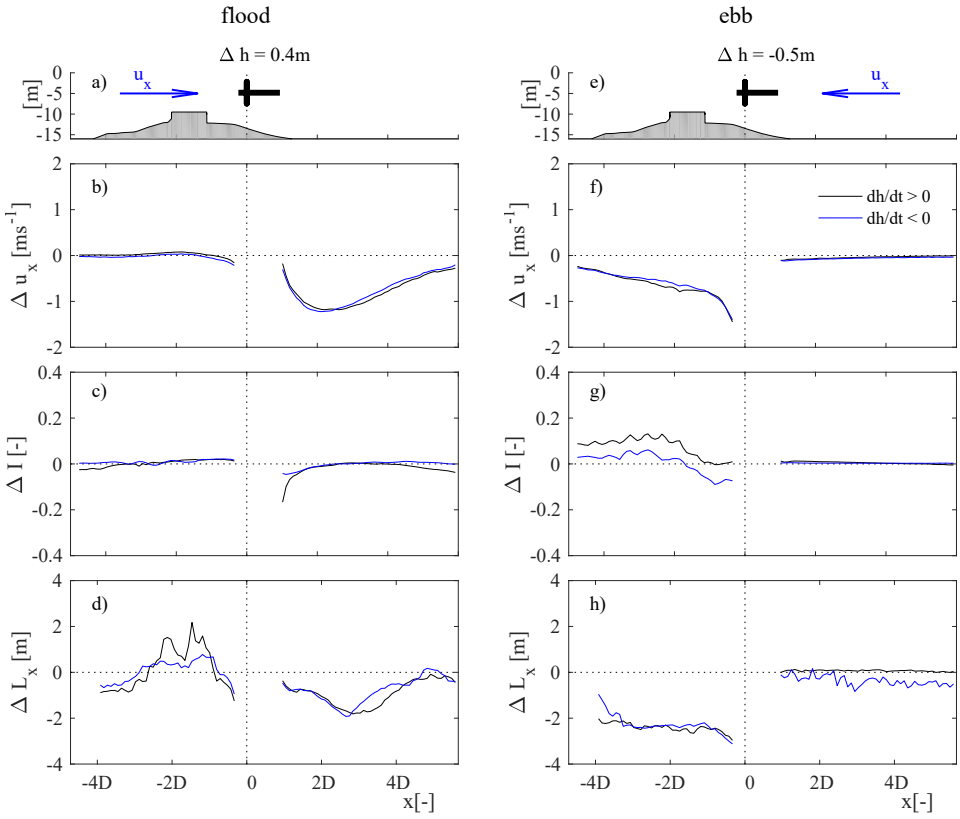

Figure 2.6: The streamwise flow field at the weir at a water depth of approximately -4 m (axis height) for the centre turbine of the array for a water level difference of 0.4 m (a-d) and -0.5 m (e-h) presented as the difference (a deficit) between a turbine in idling mode (dataset 3) and a turbine loaded (dataset 2). The panels display a cross section of the bathymetry over the weir with turbine (a,e) and the corresponding along-stream profiles of the flow velocity deficit (b,f), the turbulence intensity deficit (c,g), and the turbulence integral length scale deficit (d,h). The dataset is split into conditions for increasing (black) and decreasing (blue) heads. The horizontal axis is normalized by the rotor diameter D of 5.3 m.

observations are consistent with the flow field obtained from dataset 1 (pre-installation).

The data suggests that the weir confines the flow vertically (dataset 1), hence the flow accelerates when passing the weir (dataset 3). The flow recirculation downstream of the weir, might cause the observed high values in turbulence intensity and integral turbulence length scale at the lee side of the weir when the turbines do not operate. The turbulence integral length scales, and hence the turbulence eddies in the recirculation zone, are possibly larger at larger distances from the weir where the water depth increases. The influence of inertia on the main flow characteristics, judged from the difference between the blue and black lines in the figures, is limited, though slightly larger during flood when the flow velocity is largest.

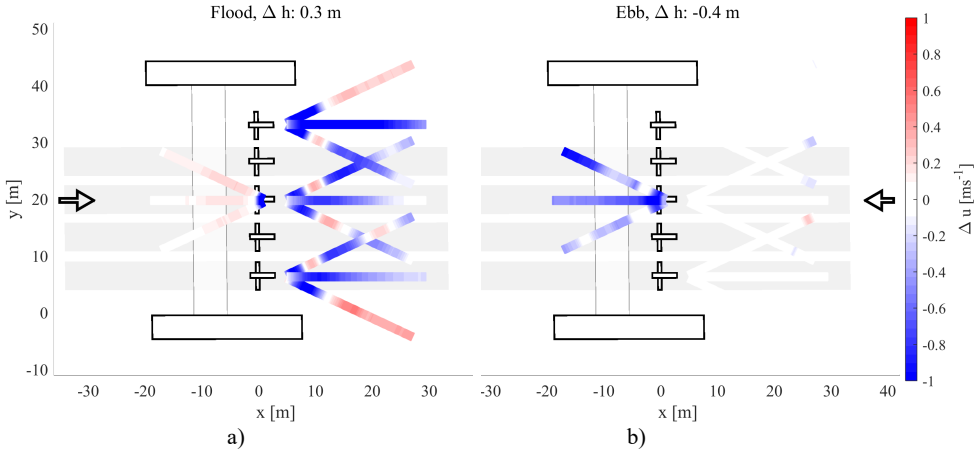

Figure 2.7: A top view of the differential flow field at turbine axis height for a head of 0.3 m during flood a), and -0.4 m during ebb b). The panels display the time-averaged flow velocity when the turbines are loaded minus the flow field when they operate in idling mode (dataset 4 and 5). The flow direction is indicated with the black arrow.

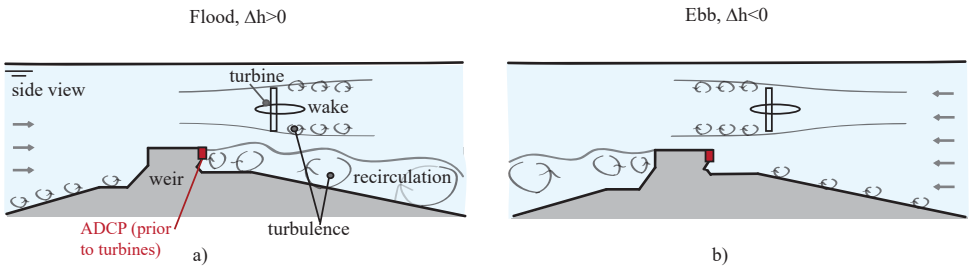

Figure 2.8: Impression of the flow passing the weir and the centre turbine of the installation (in side view); the flow recirculates downstream of the lee side of the weir (indicated with instantaneous turbulence rollers in the flow). The turbine is situated at the lee side of the weir during flood a) ($\Delta h > 0$), and at the leading side of the weir during ebb b) ($\Delta h < 0$). The upward looking ADCP transducer, which measured the flow field prior to installing the turbines in 2011 is indicated in red.

2.3.2. HYDRODYNAMICS OF THE WEIR WITH TURBINES

The flow field at the weir changes significantly when the turbines are loaded. The differences with the flow field when the turbines are in idling mode are presented in Fig. 2.6. The along-stream flow velocity in the centre line of the turbine axis decreases when the turbine extracts energy. This results in a small velocity deficit one rotor diameter upstream of the turbine and a velocity deficit equal to half of the undisturbed velocity in the turbine wake (Fig. 2.6b,f). The velocity deficit is largest at a distance of $2D$ downstream of the turbine during flood and at a distance of $0.5D$ downstream of the turbine during ebb. The ebb wake is rather short and the deceleration mainly occurs upstream of the rotor plane. Possibly, the contraction of the ambient flow at the weir enhanced turbulent mixing and hence the recovery of the ebb wake.

The turbulence intensity did only increase with 0.05 or 0.1 with respect to a situation with the turbines in idling mode (Fig. 2.6c,g). This suggests that most of the observed turbulent fluctuations originate from the ambient flow over the weir, rather than from the turbines. The integral turbulence length scale decreases by 2 m in the turbine wake (Fig. 2.6d,h). The latter may be a consequence of the flow bypassing the turbine along the bed, which is suppressing the height of the recirculation zone downstream of the weir (Fig. 2.8). This suggests that energy, otherwise lost in turbulence, becomes available to the energy harvesting by the turbine.

Fig. 2.7 depicts the turbine-induced changes to the flow in a horizontal plane at approximately the axis height of the turbines. To this end, the flow field for turbines in idling mode is subtracted from the flow field with the turbines loaded. The data is measured with the transducers at the turbines as presented in Fig. 2.3.

There is a velocity deficit downstream of the turbines, in the wakes, while there is a velocity surplus in the area in-between the turbines and their wakes, the so-called bypass area (Fig. 2.7a). The increase of the flow velocity in the bypass area amounts to 0.2 ms^{-1} relative to an ambient velocity of 2.0 ms^{-1} at a head difference of 0.3 m. The relative velocity increase in the bypass was approximately the same for other analyzed water level heads over the barrier up to 0.5 m. The acceleration of the bypass flow was less distinct during the ebb phase (Fig. 2.7b).

The flow may accelerate in the bypass area if the turbine swept area comprises a considerable fraction of the total channel area (*Garrett and Cummins*, 2007). The turbine performance is then likely affected by local blockage, which increases the mass flux through the rotor. The observed increase of the flow velocity adjacent to the wakes suggests that local blockage affects performance of the turbines at the weir. The local blockage is larger during the flood phase (Fig. 2.8a), than during the ebb phase (Fig. 2.8b), which is attributed to the weir and its downstream recirculation zone that vertically converge the flow at the turbine location during flood.

2.3.3. TURBINE THRUST

Fig. 2.9 presents the observed thrust force T on the turbine for the ebb and flood situation, normalized by a theoretical thrust, using

$$T/T_0 = T/(\rho \Delta h g A_D), \tag{2.1}$$

where ρ is the water density, A_D is the rotor swept area (22.1 m^2), and Δh is the available head at the weir. This thrust ratio is higher during flood than during ebb for the same

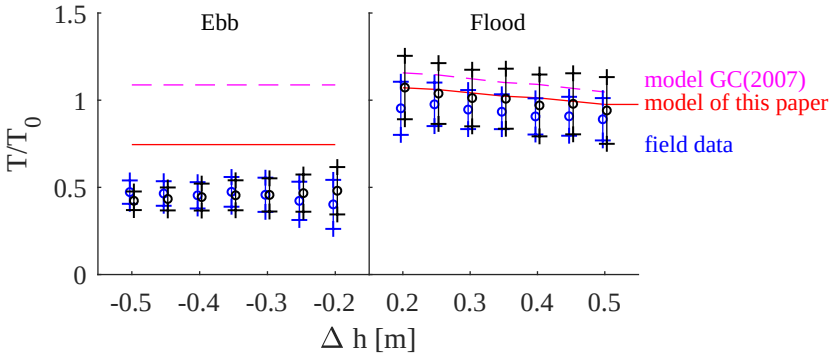

Figure 2.9: A series of box plots of the mean observed thrust coefficient C_T' (∘) and its standard deviation (+) of the centre turbine of the array at different tidal stages, where the dataset is split into conditions for increasing (black) and decreasing (blue) heads. The quantity on the horizontal axis, Δh, is the water level head over the weir; at positive head (flood), the turbine is downstream of the weir. The lines show the thrust coefficient, C_T, calculated with two models using a set of input variables discussed in Appendix C.

water level head, which implies that either the ambient flow velocity or the thrust coefficient of the turbine or both are higher for the flood situation. The standard deviation of the ratio appears larger at a head difference around 0.2 m, which may be a processing artefact. When the local flow velocity reached the cut-in speed of the turbines around this head, the filtering routine could not discern all data from accelerating or decelerating turbine conditions.

The value of the thrust ratio is likely dependent on the geometry only, judging from the fact that similar values are found for different instants during ebb and flood, respectively. The observed thrust ratio slightly decreases for an increasing head during flood which is probably caused by the increase in water depth at the weir. The difference between the ratios for ebb and flood is attributed to the differences in geometry corresponding to each stage. The turbine shape is having a limited contribution to the difference between ebb and flood as it is symmetric.

Garrett and Cummins (2007) postulated how the turbine performance in a rectangular channel with two full-slip rigid lid boundaries is affected by the local blockage. Fig. 2.9 shows the maximum thrust ratio based on the theory of *Garrett and Cummins* (2007), where the blockage is defined as the blade-swept area relative to the conveyance cross section at the weir for the flood situation (giving a blockage of 0.29), and equal to the local channel area at the rotor plane for the ebb situation (0.20). The observed thrust ratio is smaller than the corresponding theoretical value. One of the reasons may be that water can bypass to other gates neighbouring the weir with turbines. However, also the flow separation and expansion downstream of the weir are not included the model schematization of *Garrett and Cummins* (2007).

The next section aims to quantify how rotor thrust is influenced by the weir geometry, by extending the model of *Garrett and Cummins* (2007). Based on the data analyses, two geometrical parameters can be identified having an additional influence on the turbine thrust at a weir, besides the lateral confinement of the flow in a rectangular channel. The first parameter is the size of the recirculation zone downstream of the weir, as the energy

is dissipated in the expansion of the flow downstream of the weir. The second parameter is the vertical confinement or blockage by the weir. While the recirculation is indirectly of importance, affecting mainly the downstream flow field, the local blockage directly increases the local velocity, augmenting the mass flux through the turbine.

2.4. MODELLING TURBINE PERFORMANCE AT A WEIR

In this section a theoretical model is proposed that accounts for the influence of a weir on turbine performance in a single gate or channel. In line with the work of *Garrett and Cummins* (2007) we use a simplified representation of the flow based on the 1D balance equations for mass, momentum and energy. The field study indicated that this approximation can be made as the flow fields observed in the rotor swept area and the bypass, respectively, were largely uniform which also motivates the use of a bulk thrust ratio for the entire rotor plane. Furthermore, the quasi-steady approximation is made since the measured turbine thrust is controlled by stationary processes such as the wake deceleration, bypass acceleration and turbine thrust ratio which were all similar for different tidal stages.

The horizontal-axis turbine is represented by a so-called actuator disk, assuming an homogeneous distribution of the blade influence over the disk and neglecting angular momentum of the flow. The bed is assumed horizontal while the weir is schematized with a horizontal crest, a vertical trailing edge, and a streamlined leading edge. The flow in the channel is schematized via two streamtubes and a recirculation zone. One streamtube passes the disk (indicated D) while the other one follows the bypass (indicated B) (Figs. 2.10 and 2.11). The latter comprises the flow bypassing the rotor at the upper, lower and lateral sides. The recirculation zone extends along the bed between the flow detachment point at the downstream end of the weir and the reattachment point in the far wake of the turbine. The flow velocity in this zone is assumed to have a negligible magnitude, in accordance with the field observations. The presence of the step in the bed with a recirculation zone downstream of it distinguishes this schematization from the one used in the model of *Garrett and Cummins* (2007).

The water passing the weir and turbines is considered an ideal fluid: incompressible, inviscid, and with a constant density. The flow in the model domain is assumed to be steady and normal to the weir and the streamlines are supposed to have a limited curvature only. Owing to the latter, the streamwise pressure gradient is constant within each cross section of a streamtube which - in the absence of shear stress and streamline curvature - leads to laterally uniform velocity distributions in each streamtube. Consistent with this approximation, it is assumed that neither momentum nor energy is transferred between the streamtubes.

The free surface is approximated using a free-slip rigid lid, hence the model is valid for flows with small Froude numbers only. The local variation of the free surface level is then negligible relative to the flow depth. The rigid lid position is based on the water level at the turbine which can vary during the tidal cycle. The flow velocity at the inflow - and outflow boundary (stations 1 and 7, respectively) is assumed to be uniformly distributed and equal in magnitude, as a consequence of the horizontal bottom and free surface. The respective velocities within the domain are expressed as a factor times the inflow velocity u_1 (at station 1), using the velocity factors α in the turbine streamtube and β in the bypass. The velocity factor corresponding to station 2, α_2, is defined as the ratio between velocity

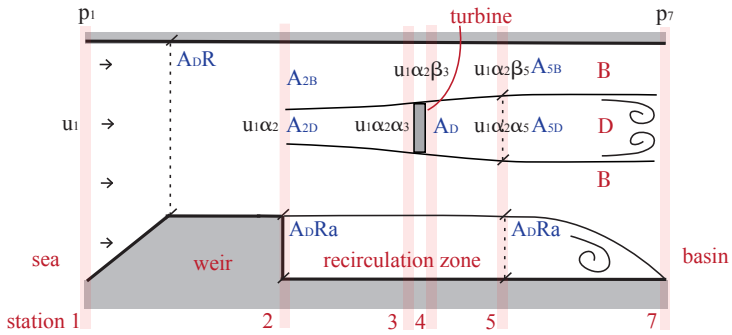

Figure 2.10: A schematic sketch of the flood flow via a streamtube passing the turbine (indicated D), a bypass streamtube (indicated B), and a recirculation zone of the weir. The numbers refer to the stations of the model schematization. The respective velocities within the domain are expressed as a factor times the inflow velocity u_1 (at station 1), using the velocity factors α in the turbine streamtube and β in the bypass. The cross-sectional area of a streamtube at each station is expressed as the product of the rotor-swept area A_D, the relative weir area a, and the blockage $1/R$. An overview of the velocity and cross section of each streamtube is given in Tab. 2.2

at station 2 and 1: $\alpha_2 = u_2/u_1$. The velocity factors of the station 3 to 6 are defined relative to the velocity at station 2 at the weir crest; e.g. the velocity factor at station 3 in the rotor plane is defined as $\alpha_3 = u_{3D}/u_2$. All velocities within the domain are summarized in Fig. 2.10 and Tab. 2.2.

The resulting non-dimensional flow problem is solved when the cross sections of the streamtubes at every station along the channel are known. Additionally, the dimensional problem is solved when the corresponding pressure and velocity distributions are known. The velocity factor at the disk α_3, the weir area relative to the cross section above the weir a, the rotor swept area relative to the cross section above the weir, i.e. the local blockage $1/R$, and the pressure difference between stations 1 and 7, are supposed to be known. Hence, the velocity factors α_5, β_3, β_5 and the undisturbed velocity u_1 are the remaining unknowns. Therefore, to solve the algebraic problem, four equations need to be formulated. These include a mass balance between stations 1 and 2, two mass balances for the streamtubes B and D, respectively, and a balance for horizontal momentum between the start and end of streamtube D. The position of this streamtube relative to the weir differs for the flood and ebb situation, hence two different schematizations are required which is discussed below. The solution procedures for the resulting systems of equations are presented in Appendices A and B.

2.4.1. MODELLING THE FLOOD SITUATION

The schematized flood situation has the disk positioned one rotor diameter downstream of the weir, which is in accordance with the geometry of the field situation (Fig. 2.10). Table 2.2 gives the cross sectional areas of the streamtubes at the respective stations, where A_D denotes the turbine area, $A_D R$ the channel cross section at the crest of the weir, and R the ratio between the channel cross section and the rotor-swept area, also referred to as the inverse of the blockage [-] *Garrett and Cummins* (2007). The frontal area of the

Table 2.2: Definitions of the streamtube cross sections and corresponding flow velocities at stations n for the flood situation; A_{nB} is the cross section of the bypass streamtube, A_{nD} is the cross section of the streamtube passing the turbine, and A_n is the cross section of the entire channel including the recirculation zone. (See also Fig. 2.10 for the corresponding schematization of the flow.)

n	1, 7	2	3,4	5
A_{nB}	-	$A_D(R-\alpha_3)$	$A_D(R-1)$	$A_D(R-\alpha_3/\alpha_5)$
A_{nD}	-	$A_D\alpha_3$	A_D	$A_D\alpha_3/\alpha_5$
A_n	$A_DR(1+a)$	A_DR	$A_DR(1+a)$	$A_DR(1+a)$
u_{nB}	-	$u_1\alpha_2$	$u_1\alpha_2\beta_3$	$u_1\alpha_2\beta_5$
u_{nD}	-	$u_1\alpha_2$	$u_1\alpha_2\alpha_3$	$u_1\alpha_2\alpha_5$
u_n	u_1	-	-	-

weir relative to the channel cross section at the crest of the weir is denoted a [-].

MASS BALANCES

Mass is conserved in the channel between stations 1 and 2 which, using a constant density, results in

$$Q = A_1u_1 = A_2u_1\alpha_2, \tag{2.2}$$

in which Q denotes the discharge in the channel [m^3s^{-1}], α_2 is the flow velocity factor at station 2 [-], u_1 is the inflow velocity [ms^{-1}] at station 1, and A_n is the channel cross section as defined in Tab. 2.2. Likewise, equating the mass fluxes in stations 2 to 5 of the streamtube B (bypass) results in *Garrett and Cummins* (2007)

$$Q_B = u_1\alpha_2A_{2B} = u_1\alpha_2\beta_3A_{3B} = u_1\alpha_2\beta_5A_{5B}, \tag{2.3}$$

where Q_B denotes the discharge in streamtube B [m^3s^{-1}]. Similarly, the mass balance for streamtube D (turbine) gives

$$Q_D = u_1\alpha_2A_{2D} = u_1\alpha_2\alpha_3A_{3D} = u_1\alpha_2\alpha_5A_{5D}, \tag{2.4}$$

in which Q_D denotes the discharge in streamtube D, where it is noted that $Q = Q_B + Q_D$.

ENERGY BALANCES

The energy balance equations for the channel between stations 1 and 2, and for the streamtubes B and D between stations 2 and 5, involve the pressure distributions in stations 2, 4 and 5, respectively. These pressure distributions are needed later on to close a balance for horizontal momentum between stations 2 and 5. Pressure is defined with respect to the hydrostatic states, as the governing equations involve pressure differences due to the dynamics only.

The flow contracts smoothly, with negligible energy dissipation, between stations 1 and 2 resulting in a constant energy head H [m] along this section, which is given by

$$H = u_1^2/(2g) + p_1/(\rho g) = u_1^2\alpha_2^2/(2g) + p_2/(\rho g), \tag{2.5}$$

where g is the gravitational acceleration [ms^{-2}], ρ is the density of water [kgm^{-3}], and p_n [$kgms^{-2}$] is pressure at station n.

The energy head H_B in streamtube B is also approximately constant between stations 2 and 5, due to the weak curvature of the streamlines, which leads to

$$\begin{aligned} H_B = u_1^2\alpha_2^2/(2g) + p_2/(\rho g) &= u_1^2\alpha_2^2\beta_3^2/(2g) + p_{3B}/(\rho g) \\ &= u_1^2\alpha_2^2\beta_5^2/(2g) + p_5/(\rho g). \end{aligned} \tag{2.6}$$

Using similar arguments, the energy head in streamtube D can be assumed piecewise constant - with a discontinuity at the disk - discerning the energy head upstream of the turbine H_{3D}, between stations 2 and 3,

$$H_{3D} = u_1^2\alpha_2^2/(2g) + p_2/(\rho g) = u_1^2\alpha_2^2\alpha_3^2/(2g) + p_{3D}/(\rho g), \tag{2.7}$$

and the energy head downstream of the turbine H_{4D}, between stations 4 and 5,

$$H_{4D} = u_1^2\alpha_2^2\alpha_3^2/(2g) + p_{4D}/(\rho g) = u_1^2\alpha_2^2\alpha_5^2/(2g) + p_5/(\rho g), \tag{2.8}$$

in which p_{3D} and p_{4D} denote the pressure in streamtube D upstream and downstream of the turbine disk, respectively.

MOMENTUM BALANCE

Applying the balance equations for horizontal momentum to the channel section between stations 2 and 5 leads to

$$Qu_1\alpha_2 + A_2p_2/\rho) - F_w/\rho - F_t/\rho = Q_Bu_1\alpha_2\beta_5 + Q_Du_1\alpha_2\alpha_5 + A_5p_5/\rho, \tag{2.9}$$

in which F_w is drag force on the trailing edge of the weir and F_t is the turbine thrust.

Starting with the latter, the turbine thrust is formulated using

$$F_t = \rho u_1^2 C_T A_D/2, \tag{2.10}$$

in which C_T [-] is the thrust coefficient. The thrust results from the net pressure force on the disk (*Burton et al.*, 2002; *Betz*, 1920), which is given by the product of the disk area and the pressure difference between stations 3 and 4 of streamtube D. Therefore, the thrust coefficient C_T [-] can be defined alternatively by combining equations 2.6, 2.7, and 2.8, giving

$$C_T = (p_{3D} - p_{4D})/(1/2\rho u_1^2) = \alpha_2^2(\beta_5^2 - \alpha_5^2), \tag{2.11}$$

which coincides with the definition of Eq. 2.1 of C_T'. The resulting power coefficient C_P, used later on, is simply obtained by multiplying C_T with the local velocity factor $\alpha_2\alpha_3$.

Finally, to close equation 2.9, the drag force F_w on the trailing edge of the weir is formulated. To this end, the pressure distribution in cross section 2 is assumed to be hydrostatic which is a valid approximation as the local streamlines are nearly parallel and the flow velocity in the recirculation zone is relatively small, see Fig. 2.10. The drag force F_w is then given by

$$F_w = -p_2RA_Da. \tag{2.12}$$

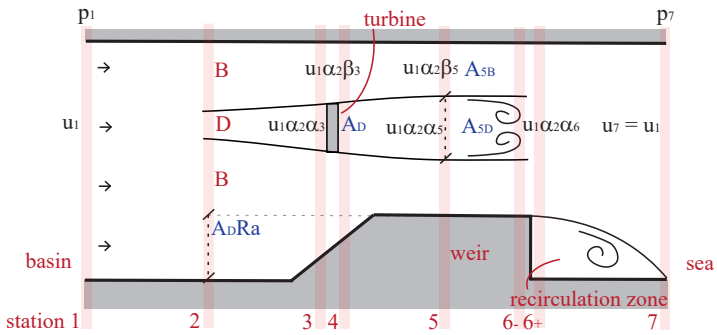

Figure 2.11: A schematic sketch of the ebb flow via a streamtube passing the turbine (indicated D), a bypass streamtube (indicated B), and a recirculation zone of the weir. The numbers refer to the stations of the model schematization. The respective velocities within the domain are expressed as a factor times the inflow velocity u_1 (at station 1), which is equal to the velocity at station 2, using the velocity factors α in the turbine streamtube and β in the bypass. The cross-sectional area of a streamtube at each station is expressed as the product of the rotor-swept area A_D, the relative weir area a, and the blockage $1/R$. An overview of the velocity and cross section of each streamtube is given in Tab. A.3.

Table 2.3: Definitions of the streamtube cross sections and corresponding flow velocities at stations n for the ebb situation; A_{nB} is the cross section of the bypass streamtube, A_{nD} is the cross section of the streamtube passing the turbine, and A_n is the cross section of the entire channel including the recirculation zone. (See also Fig. 2.11 for the corresponding schematization of the flow.)

n	1, 2, 7	3,4	5	6^-	6^+
A_{nB}	$A_D(R+Ra-\alpha_3)$	$A_D(R+1/2Ra-1)$	$A_D(R-\alpha_3/\alpha_5)$	-	-
A_{nD}	$A_D\alpha_3$	A_D	$A_D\alpha_3/\alpha_5$	-	-
A_n	$A_DR(1+a)$	$A_DR(1+1/2a)$	A_DR	A_DR	$A_DR(1+a)$
u_{nB}	-	$u_1\alpha_2\beta_3$	$u_1\alpha_2\beta_5$	-	-
u_{nD}	-	$u_1\alpha_2\alpha_3$	$u_1\alpha_2\alpha_5$	-	-
u_n	u_1	-	-	$u_1\alpha_2\alpha_6$	$u_1\alpha_2\alpha_6$

2.4.2. MODELLING THE EBB SITUATION

Fig. 2.11 shows the flow schematization for the ebb situation with the turbine positioned just upstream of the leading edge of the weir. A few rotor diameters upstream from the turbine the flow is undisturbed (station 2). The wake downstream of the turbine has expanded before it reaches the crest of the weir, leading to parallel streamlines at station 5, while it has largely recovered at the end of the weir (station 6). This reflects the field observations of the velocity deficit during ebb.

The required mass and energy balances are largely similar to those used in the flood model (Eq. 2.3, 2.4, 2.6, 2.7, and 2.8), but the conveyance areas and velocities need to be redefined before applying these equations to the ebb configuration. For convenience, the equations are reformulated below using the modified parameters listed in Tab. A.3. Importantly, the relative velocity α_2 equals 1, because the flow velocity at station 2 of the ebb model is vertically uniform and equal to the velocity in station 1.

MASS BALANCES

Equating the discharge in streamtube B at stations 2, 3 and 5 gives

$$Q_B = u_1 A_{2B} = u_1 \beta_3 A_{3B} = u_1 \beta_5 A_{5B}. \tag{2.13}$$

Similarly, the constant discharge in streamtube D leads to

$$Q_D = u_1 A_{2D} = u_1 \alpha_3 A_{3D} = u_1 \alpha_5 A_{5D}. \tag{2.14}$$

ENERGY BALANCES

Assuming a sufficiently smooth contraction of the bypass, the energy head [m] in streamtube B at stations 2, 3 and 5 are equated to give

$$\begin{aligned} H_B = u_1^2/(2g) + p_2/(\rho g) &= u_1^2 \beta_3^2/(2g) + p_{3B}/(\rho g) \\ &= u_1^2 \beta_5^2/(2g) + p_5/(\rho g). \end{aligned} \tag{2.15}$$

For streamtube D, the energy head upstream of the turbine at stations 2 and 3 is given by

$$H_{3D} = u_1^2/(2g) + p_2/(\rho g) = u_1^2 \alpha_3^2/(2g) + p_{3D}/(\rho g), \tag{2.16}$$

while downstream of the turbine, at stations 4 and 5, the energy head is given by

$$H_{4D} = u_1^2 \alpha_3^2/(2g) + p_{4D}/(\rho g) = u_1^2 \alpha_5^2/(2g) + p_5/(\rho g). \tag{2.17}$$

MOMENTUM BALANCE

Conservation of horizontal momentum in streamtube D between stations 2 and 5 gives

$$Q_D u_1 + A_{2D} p_2/\rho - F_t/\rho + F_l/\rho = Q_D u_1 \alpha_5 + A_{5D} p_5/\rho, \tag{2.18}$$

in which F_t is the turbine thrust, given by Eq. 2.10, and F_l is the horizontal component of the external pressure force on the lateral boundary of streamtube D. The latter is calculated as the product of the increase in the streamtube area and the average pressure between stations 2 and 5,

$$F_l = (A_{5D} - A_{2D})(p_5 + p_2)/2, \tag{2.19}$$

which is a reasonable approximation if the expansion of the wake over the weir is small relative to the weir height, which is in line with the field situation. Though, this schematization of the ebb situation has limited, as the weir drag is not explicitly incorporated, it is the best we can think of for now.

2.4.3. VERIFICATION AND VALIDATION

The set of equations constituting the flood model and ebb model prescribe the streamtube cross sections at the considered stations, the corresponding velocity factors α and β, and the turbine thrust coefficient C_T, as functions of the blockage $1/R$ and the relative weir height a. The algebraic solution procedure is explained in Appendices A and B.

It has been verified that the model results converge to the analytical results of Betz *Betz* (1920) for a vanishing blockage ($1/R \to 0$) and vanishing relative weir height ($a \to 0$). In this situation the bypass velocity factors β approach a uniform value of one, while the

velocity at the turbine converges to the average of the free stream velocity and the velocity in the wake of the turbine, $\alpha_3 = 1/2(1+\alpha_5)$. Furthermore, it has been verified that for arbitrary blockage $1/R$ and vanishing relative weir height a the results converge to those obtained with the model of *Garrett and Cummins* (2007).

Next, the model is validated against the field data using blockage and relative weir height from the observed ebb and flood conditions (see Appendix C). The tidal water level at the weir varies in time. Using the rigid lid approximation, the position of the free surface in the model is varied accordingly. A validation of the calculated thrust coefficients is presented in Fig. 2.9. The calculated thrust coefficients of the flood model fit nicely within the measured range, suggesting that the most important processes influencing the turbine thrust are included. The model predicts thrust coefficients that are higher than those derived from the field observations for the ebb situation, as the current schematization may overestimate the expansion of the wake over the weir, resulting in a higher thrust. Also, the model does not include the effect of the flow bypassing to neighbouring gates. The observed and predicted thrust coefficients in Fig. 2.9 vary with the head, in particular during flood. This is attributed to the tidal water level variation at the turbine, an effect that is reproduced reasonably well by the model.

The model excludes free surface phenomena, besides the water level variation at the turbine due to the tide. The rapid, local variations of the free surface level relative to the water depth scale with the square of the Froude number, which is small for the Froude numbers observed in the field that never exceeded 0.5. Although this justifies the use of a rigid lid, a free surface approximation such as postulated by *Whelan et al.* (2009a), *Houlsby et al.* (2008), or *Vogel et al.* (2016), would be a useful extension to the model when applying it to relatively higher steps in the bathymetry which are associated with higher Froude numbers.

2.4.4. PERFORMANCE ESTIMATE

The performance of the weir-mounted turbine can be quantified with the power coefficient,

$$C_P = \alpha_2 \alpha_3 C_T, \tag{2.20}$$

which gives the fraction of the energy extracted by the turbine compared to the energy available in the flow through to rotor swept area in absence of the turbine. Here, $\alpha_2\alpha_3$ is the velocity factor at the turbine disk and C_T is the turbine thrust coefficient.

However, our main interest is to determine the weir-turbine configuration for which the production is maximal for a given head Δh, hence an additional non-dimensional number is introduced to compare the produced power to the nominal power. The nominal power, P_0, can be defined as the energy available in the flow in the channel, $A_D R$, driven by the head difference Δh,

$$P_0 = u_1 \rho g \Delta h A_D R, \tag{2.21}$$

where Δh is the available head at the weir [m] and g is the gravitational acceleration [ms^{-2}]. Scaling the power P delivered by the turbine with the nominal power P_0 gives the following dimensionless performance measure,

$$\eta = P/P_0 = C_P u_1^2/(2g\Delta h R), \tag{2.22}$$

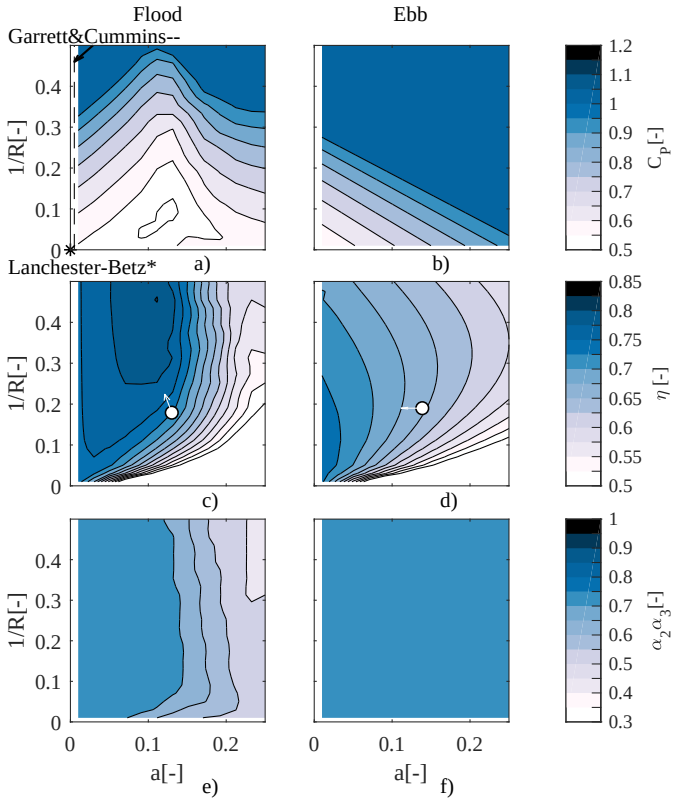

Figure 2.12: The estimated power coefficient, C_P, for flood a) and ebb b) conditions for different relative weir areas (horizontal axis) and blockages (vertical axis). The calculated production, P/P_0, for flood b) and ebb c) as defined in Eq.2.22. The dot 'o' indicates the geometry of the field situation of which C_T was presented in Fig. 2.9. The panels e) and f) give the velocity in the rotor plane relative to the undisturbed flow velocity $\alpha_2\alpha_3$ of the model for flood and ebb conditions respectively. The power coefficients as discussed in *Garrett and Cummins* (2007) ($--$), and *Lanchester* (1915) and *Betz* (1920) ($*$) are indicated in panel a.

which we refer to as the efficiency. Here, C_P is the turbine power coefficient, and u_1 is the undisturbed inflow velocity, which are both calculated by the model.

2.4.5. APPLICATION

The model can be used to calculate how a turbine performs when it is mounted near a weir and how the design can be optimized for a higher production. The control variables of this flow problem include the relative rotor area of the turbine (the blockage), the relative weir area, and the ratio between the flow velocity at the rotor plane and the undisturbed inflow velocity. The resulting turbine performance can be presented with the power coefficient and the efficiency (Eqs. 2.20 and 2.22, respectively).

Here, the validated model is applied to the flow past a schematized weir and turbine. The flow is now forced by a fixed water level difference, as in the observed field situation the turbine operation does not affect the available head. The position of the rigid lid,

which represents the water level at the turbine, is taken constant for clarity. An optimal efficiency is calculated by varying the relative deceleration in the rotor plane, $\alpha_2\alpha_3$, for different values of the blockage, $1/R$, and the relative weir area, a. The resulting power coefficient, the optimal efficiency and the relative deceleration in the rotor are presented in Figs. 2.12a and b, c and d, and e and f, respectively.

The power coefficient gives the fraction of the energy flux extracted by the turbine. It is maximal for a high blockage of the turbine, above 0.4, (Figs. 2.12a,b) and - in the ebb situation - also for a high relative weir area, as the thrust on the rotor is highest in these cases. The power coefficient is minimal for a relative weir area of 0.12 and a blockage of 0.08 in flood situation. Here, the thrust on the rotor is small, as only a small portion of the mass flux passes through the rotor plane. A higher power coefficient can be obtained when reducing the relative velocity in the rotor plane, $\alpha_2\alpha_3$, while increasing the relative weir area (Fig. 2.12e). Below, the efficiency of the configuration is discussed to give insight in the production relative to the total energy loss, including losses in viscous processes - such as in the turbine wake and in the attachment of the flow to the bed.

The efficiency is highest for a large blockage - above 0.23 - and a relative weir area around 0.08 for the flood situation (Fig. 2.12c). This efficiency is higher than for a turbine in a flat-bed channel, where the relative weir area is zero. The efficiency of the channel with a turbine downstream of a weir can exceed the efficiency of a flat-bed channel if energy, which is otherwise lost in the turbine wake or recirculation, is used for energy production. This happens when a larger mass flux is forced through the turbine in presence of the weir, than in a flat bed channel. However, this benefit is lost when the relative weir area is further increased and relatively more energy is lost in the turbine wake and recirculation.

An optimum is found for small blockage and small relative weir area in the ebb situation. When increasing the relative weir area and blockage in the model, the flow stagnates and the momentum flux through the rotor decreases. The optimum of the model of the ebb situation did not exceed the efficiency of a turbine in a flat-bed channel.

The difference between the performance for flood and ebb, respectively, can be linked to the mutual roles of momentum advection and the pressure force in transferring power to the rotor blades. In the flood situation, the turbine is situated downstream of the weir and the momentum advected by the flow past the rotor plane is relatively high. In the ebb situation, with the turbine situated upstream of the weir, advection of momentum through the rotor plane is relatively small in favour of the net pressure force on the turbine, as the pressure distribution at the front of the weir is opposite in sign with respect to the flood situation. This difference likely has an effect on the optimal value of the relative velocity in the rotor plane, $\alpha_2\alpha_3$, at which the turbine should be operated to render the production maximal.

For the range of weir-turbine geometries plotted in Fig. 2.12, the optimal value of $\alpha_2\alpha_3$ varies between $1/3$ and $2/3$ (Figs. 2.12e and f). While in previous work a value of $2/3$ was used to achieve an optimal power coefficient for a turbine in an unconstrained flow or a rectangular channel ((*Betz*, 1920), (*Lanchester*, 1915), and (*Garrett and Cummins*, 2007) respectively), here a smaller value is required to realize an optimal production in some of the considered weir-turbine geometries. A different $\alpha_2\alpha_3$ value may be achieved by changing the turbine design. *Vogel and Willden* (2017) already indicated that a turbine with a higher solidity may be required for a constrained flow than for an unconstrained flow to sustain the higher blade forces. The turbine tip speed ratio can also be changed to

realize the higher rotor thrust.

The blockage and relative step height of the studied turbines in the Dutch storm surge barrier are indicated in Figs. 2.12 c and d with a dot. The production of these turbines can be improved by increasing the blockage, moving up in the domain for the flood situation and by decreasing the relative weir area, moving to the left of the calculated domain for the situation during ebb. The production of a weir-mounted turbine could be further optimized by varying the horizontal distance to the weir, which is however not included as a free variable in the present model. Determining the optimal distance of a turbine to a weir will be part of Chapter 3 using experimental testing of a weir-mounted tidal turbine.

The data analysis and theoretical modelling confirmed that installation of turbines in a hydraulic structure can be attractive, as the local blockage is high and the energy normally lost in the recovery of a velocity deficit downstream of a weir may become available to energy extraction. The latter is particularly encouraging when the impact of tidal turbines to their installed environment should remain small. The field analysis suggested that the production of a turbine benefits from the installation in a weir, which was largely confirmed by the theoretical model. A hydraulic structure is therefore an attractive location to mount your turbine if no other location providing high blockage is available at the tidal site.

2.5. CONCLUSION

This research has extended the 1D turbine performance model of *Garrett and Cummins* (2007) to situations where turbines are installed near a weir or an abrupt expansion of a channel. Data from a monitoring programme at full-scale turbines formed the basis for the modelling. This showed that the weir affected the turbine performance in two ways. Firstly, it increased the local blockage when it was located upstream of the turbine, augmenting the mass flux through the rotor plane. Secondly, the turbine clearly suppressed the dissipation of energy in the recirculation zone downstream of the weir, increasing the extractable fraction of the energy flux of the channel flow. The field data showed that a 1D approach is suited to estimate the performance of full-scale turbines, and the model was verified and validated using the data.

The model provides fundamental insight in the effect of a weir, and particularly of its height, on the performance of a tidal turbine. The extended model serves as a quick design tool or parametrization of turbines in a large scale shallow water model, as it enables the calculation of performance estimates over a range of turbine-weir geometries. The performance could exceed the limit prescribed for turbines in an unbounded channel for specific channel geometries as was demonstrated in previous studies. The chapter demonstrates how turbines perform when they are installed in hydraulic structures, revealing the chance to economically exploit energy from tidal currents at bridges and flood defences.

3

The performance of a weir-mounted tidal turbine: An experimental investigation

This chapter has been published as M. C. Verbeek, R. J. Labeur, and W. S. J. Uijttewaal, 2020 "The performance of a weir-mounted tidal turbine: Experimental investigation. Renewable Energy, 168, 64-75, https://doi.org/10.1016/j.renene.2020.12.013

3. An experimental investigation

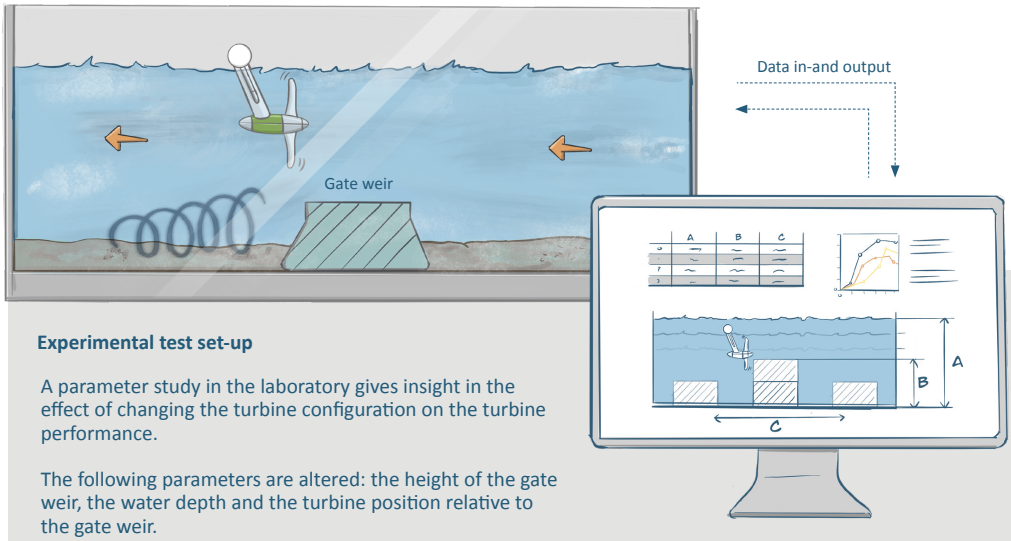

Experimental test set-up

A parameter study in the laboratory gives insight in the effect of changing the turbine configuration on the turbine performance.

The following parameters are altered: the height of the gate weir, the water depth and the turbine position relative to the gate weir.

Different experimental runs

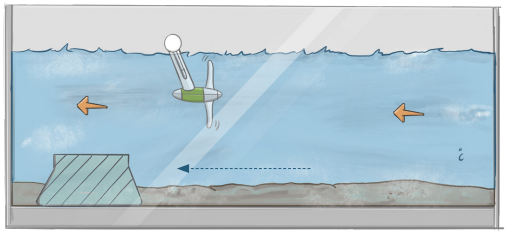

Test set-up with turbine upstream of a weir

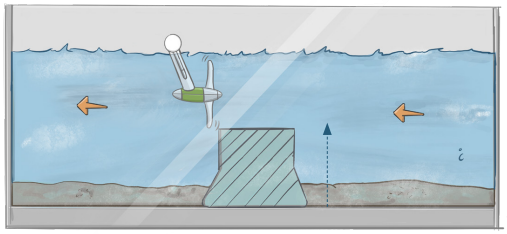

Test set-up with high - and low weir

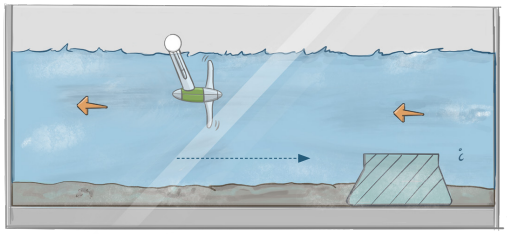

Test set-up with weir downstream of the turbine

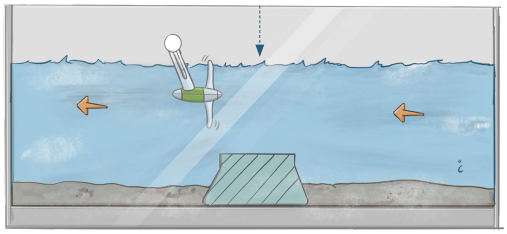

Test set-up with high and low water level

The previous chapter showed that retrofitting turbines in open storm surge barriers is a promising way of harvesting sustainable energy, as the production by the turbines was large compared to situations with an unconstrained flow. A hypothesis, in the form of a analytical model, was proposed to explain this performance covering a range of turbine-weir configurations.

However, the model is validated for two cases only. If we want to apply it for a larger range of turbine-weir geometries to fulfil the thesis objective, more cases are needed. Besides, it remained still unclear whether key assumptions about the distribution of the flow over wake and bypass holds for these different geometries.

Therefore, the aim of this chapter is to further clarify the consequences for the power output of tidal turbines when placing them in a hydraulic structure. To this end, experimental measurements of turbine power and wakes are performed, using a down-scaled turbine mounted at a submerged weir. The analytical model is compared to this dataset, validating its range of application for optimising turbine-weir geometries.

The experimental data show that the power coefficient of the turbine can be increased by optimising the blockage of the channel and the distance between the turbine and the structure, which is related to the wake configuration. In this way, the power coefficient increased by 40 percent when the turbine was re-positioned from the upstream to the downstream end of the structure. The theoretical model could reproduce the measured power within 10 percent accuracy, proving its value as a rapid assessment tool.

3.1. INTRODUCTION

The EU has targeted to increase the share of renewable energy in the electricity sector from 21% in 2014 to at least 45% in 2030 (*European Committee*, 2014). Ocean energy can provide a substantial and reliable contribution to the required energy mix (*Bahaj*, 2011). The tidal flow between bridge pillars and through open barriers is a yet unharvested and promising source of ocean energy, which can be exploited using tidal stream turbines. This technology was demonstrated in a Dutch storm surge barrier, where five 250 kW turbines were installed in a gate opening (*Verbeek et al.*, 2020a; *O'Mahoney et al.*, 2019). This type of existing barrier is a suitable location for tidal energy harvesting, provided that attention is paid to the structural stability of the barrier and the increased resistance by the turbines. However, it is yet unclear how the power output from these turbines should be maximised when they are mounted inside hydraulic structures.

The underlying problem is that the interaction of a turbine with the flow through hydraulic structures is poorly understood. Many researchers investigated either the hydrodynamics of horizontal-axis turbines (e.g. *Garrett and Cummins*, 2007, *Stallard et al.*, 2013) or the flow through a hydraulic structure (*Hofland*, 2005), but until now their combination has not been explored. Even-though, three geometry parameters can be listed that mainly influence the structure - turbine interaction. Firstly, *Verbeek et al.* (2020a) indicated that the streamwise position of a turbine relative to a weir determines the shape of the turbine wake and hence the power output. Secondly, the ratio between the rotor swept area and the local cross section of the channel, the so-called blockage, affects the energy flux that can be harvested by a turbine in a constrained flow (*Garrett and Cummins*, 2007). Lastly,

Wimshurst and Willden (2016) showed, using a CFD study of a turbine at a submarine hill, that a streamwise decrease of the water depth at the turbine location is essential to increase the turbine thrust. A systematic analysis of these parameters could unravel optimal design choices, however, the data required for such investigations are missing.

Theoretical models, such as postulated by *Garrett and Cummins* (2007), *Vennell* (2010) and *Nishino and Willden* (2012b), provide a useful framework to define the type of data that are needed for this purpose. These methods are based on 1D balances of mass, energy, and momentum of the flow passing a turbine that is schematised as an actuator disk (*Betz*, 1920, *Lanchester*, 1915). Recently, this approach was extended to include a turbine in a hydraulic structure, where the latter is schematised as a step in the bed (*Verbeek et al.*, 2020a). From this model, we infer principal indicators of turbine performance that should be measured: e.g., the power coefficient of the turbine, the distribution of the flow in the wake and bypass, and the associated pressure recovery in the wake. Besides, these measurements can be compared with the corresponding model predictions, thus verifying the application of these models to complex geometries. This may allow a selection of the associated design parameters using theoretical models which, unlike advanced computational fluid dynamics (CFD), can evaluate the turbine performance for a wide range of input variables using limited computational resources only.

The aim of this chapter is to clarify the consequences of placing a tidal turbine in a hydraulic structure, using experimental observations. To meet this aim, an experimental turbine with a 1-in-8.6 scale is tested in a flume, in combination with different weir geometries, for which the observed performance characteristics have been related to the observed wake properties. To this end, the influence of three geometrical parameters on the power coefficient and hydrodynamics are evaluated: the weir height, the local blockage, and the streamwise distance between turbine and weir. The results from the model of *Verbeek et al.* (2020a) are compared with the measurements in order to validate the range of application of the model for optimising design parameters in more complex turbine-structure geometries. In this way, this study facilitates an optimal placing and operation of tidal stream turbines in hydraulic structures in order to harvest more power from the ocean, which contributes to the knowledge needed to meet targets on renewable energy production.

This chapter has the following structure. First, it is discussed how the experiments are set-up to obtain specific information concerning the turbine power and wake configuration. Subsequently, the experimental data are presented and differences in power output for the different turbine-weir combinations are discussed, in particular how this relates to the wake configuration. Thereafter, the obtained experimental results are compared to the theoretical prediction of the model of *Verbeek et al.* (2020a). The range of application of this type of theoretical models is discussed and possibilities for optimising the geometry to harvest more power from the flow are explored. The discussion section addresses the implications of mounting a turbine in a barrier, considering the increased resistance of the structure. Finally, conclusions are drawn regarding the power output consequences of placing a turbine in a hydraulic structure.

3.2. METHODS

The experimental set-up is inspired by the hydrodynamics of a weir-mounted turbine in the Eastern Scheldt barrier, The Netherlands, as described by *Verbeek et al.* (2020a) (Fig. 3.1a). However, the aim of the experiments is to gain insight in the most important processes

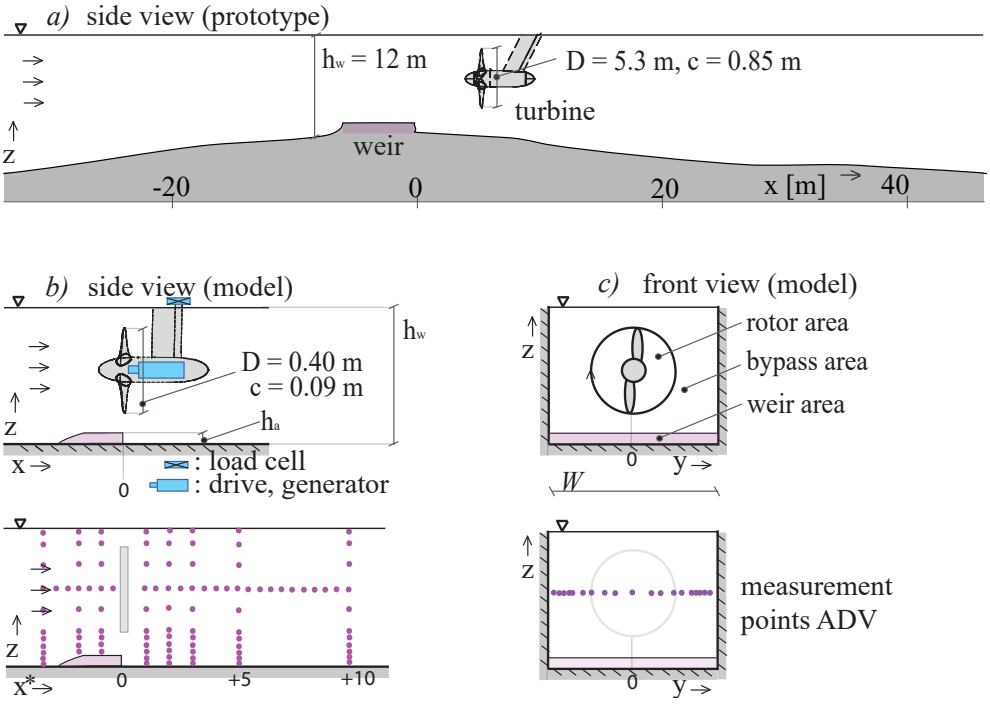

Figure 3.1: A schematic drawing of a) the prototype turbine in the Eastern Scheldt, b) the laboratory set-up of a turbine downstream of a broad crested weir in a side view c) and in a front view; the dimensions of the set-up are indicated in the figure; for panel a) and b): D is the rotor diameter, c is the blade chord, h_a is the height of the weir, and h_w is the water depth in the flume; for panel c): W is the flume width; the lower panels show the measurement locations of the velocimeters in side and top view, respectively. Lateral transects are taken at $x^* = -2, 3$, and 10 for each test. Vertical profiles are taken at the flume centreline.

rather than accurately reproducing the flow at the test site in the Eastern Scheldt barrier.

To this end the experiments provide information about turbine power and wake configuration when placing a turbine in different hydraulic structure geometries in order to improve our understanding of the relevant physics and to facilitate comparison with theoretical models. The required tests are done with a down-scaled turbine in an experimental flume. The design of the experimental set-up, the data processing, and scaling analysis are explained in this section.

3.2.1. EXPERIMENTAL SET UP

A 1-in-8.6 geometrically-scaled T1 turbine from the company Tocardo Power Turbines BV is used (Fig. 3.2b). The design of the T1 is similar to the prototype T2, which is deployed in the Eastern Scheldt barrier and has a rotor diameter of 5.3 m, except for the relatively thicker hub. The rotor diameter of the T1 equals 3.4 m at full scale and 0.4 m at model scale. The electrical system and mount of the model turbine are especially manufactured for the tests; the blades and hub are provided by Tocardo. The torque is applied by an AC Servo motor and drive, while controlling the turbine at a constant tip speed.

The turbine is mounted in a horizontal, recirculating flume with a length of 40 m, a

Figure 3.2: Photos from the experimental set up: a) the recirculating current flume in the Laboratory of Environmental Fluid Mechanics of Delft University of Technology, The Netherlands, b) the turbine and weir; the turbine is positioned two rotor diameters upstream of the weir end in the picture ($x/D = -2$)

width of 0.78 m, and a height of 0.85 m in the Laboratory of Environmental Fluid Mechanics of Delft University of Technology, The Netherlands (Fig. 3.2a). The investigated hydraulic structure concerns a long-crested weir which can be installed at the bed of the flume (details will be given in Sec. 3.2.3). The discharge in the flume amounted to 0.4 $m^3\ s^{-1}$, and the water level in the flume was 0.65 m or 0.70 m relative to the bed level, depending on the experimental case. This corresponds to an undisturbed flow velocity in the flume of 0.73-0.79 m s^{-1}. The inflow section of the flume features a honeycomb structure, consisting of horizontal parallel pipes to straighten the inflow. All tests are performed for a single streamwise turbulence intensity at the inflow of around 5-7 %, which is consistent with a typical offshore site value at hub height (*Milne et al.*, 2016) and in line with earlier scale tests of e.g. *Batten et al.* (2012) and *Stallard et al.* (2013).

Three series of tests are conducted in which three geometrical parameters are systematically varied: blockage by the turbine, height of the weir, and streamwise distance between the weir and the turbine, which are defined in Sec. 3.2.3. In particular, attention is payed to the weir-turbine distance as this had a major influence on wake configuration and turbine performance and was not investigated before (*Verbeek et al.*, 2020a). Consequently, the turbine is placed at five distances from the weir within each test series. Additionally, two weir heights and two blockages are considered. One reference test without turbine is conducted for each series. The resulting test cases are summarized in Table 3.1 and one configuration is illustrated as an example in Fig. 3.1.

Flow data are obtained at vertical transects in the centre line of the flume, for a range of streamwise distances, including - but not limited to - the transects defined in the theoretical model of *Verbeek et al.* (2020a). Consequently, the profiles at the following streamwise locations are (at least) sampled in each test: the inflow section of the flume, the crest of the hydraulic structure, and the turbine wake at, respectively, three and ten rotor diameters downstream of the turbine, where at the latter location the wake has almost fully recovered (*Stallard et al.*, 2013). In between these locations, additional velocity transects are obtained at streamwise intervals of one rotor diameter to gain detailed insight on the configuration of the wake (Fig. 3.1d). Lateral transects at axis height are measured at the inflow section and in the wake at three and ten rotor diameters downstream of the blades for each test. Fig. 3.1e indicates the locations of these measurements.

Table 3.1: Overview of dimensions and scaling parameters of the three series of tests and corresponding values of the prototype of the Eastern Scheldt, The Netherlands; D is the rotor diameter, h_a is the weir height, h_w is the (flume or field) water depth; the definitions of the parameters, B^*, a^*, and x^* are given in Eqs. 3.8-3.10 and the dynamical parameters Fr, Re, Re_c, and λ are defined in Eq. 3.2, 3.3, 3.4, and 3.5, respectively; tests are conducted at a discharge of 0.4 m^3s^{-1}

Parameter	Symbol	Unit	Series 1	Series 2	Series 3	Prototype
Geometry	D	[m]	0.40	0.40	0.40	5.3
	h_a	[m]	0.05	0.10	0.10	3.0
	h_w	[m]	0.65	0.65	0.70	12
	a^*	-	0.08	0.15	0.14	0.25
	B^*	-	0.25	0.25	0.23	0.24
	x^*	-	$-2,-1,0,1,2$	$-2,0,1$	$-2,0,1$	1
Dynamics	λ	-	$[0,10]$	4	4	4
	Fr	-	0.36	0.36	0.31	0.28
	Re	-	$5.0\cdot10^5$	$5.0\cdot10^5$	$5.0\cdot10^5$	$2.4\cdot10^7$
	Re_c	-	$0.6\cdot10^5$	$0.6\cdot10^5$	$0.6\cdot10^5$	$0.2\cdot10^7$

3.2.2. DATA PROCESSING

Flow velocities are measured with Nortek Vectrino side-looking and down-looking transducers (*Nortek AS*, 2019). The device sampling frequency was 25 Hz at an acoustic frequency of 10 MHz. The cylindrical sampling volume had a width and height of 6 mm, and each location was sampled for 3-minute intervals. A central data-acquisition system recorded water levels, turbine thrust, turbine torque, turbine tip speed and the flume discharge at 200 Hz during the tests for 3-minute up to 15-minute intervals. Three minutes is sufficiently long to obtain stationary mean values of flow velocity, turbulence intensity, and turbine load. This is verified with an auto-correlation analysis of the time series and converge check with available longer time series. Water levels are measured with six conductivity meters along the flume centre line. Turbine thrust [N] is measured with a bending beam load cell (version: LSH-100KG, precision class: C3) connected to the turbine strut (Fig 3.1b). The turbine torque Q [Nm] and angular frequency Ω [min^{-1}] are recorded in the turbine generator. All devices are calibrated to get physical units.

Amongst others, the data are used to determine the ratio α between the velocity in the wake and the inflow of the flume, which is defined by

$$\alpha = u_w/u_1, \tag{3.1}$$

in which u_1 [m s^{-1}] is the inflow velocity of the flume and u_w [m s^{-1}] is the flow velocity in the wake. The latter is obtained by interpolating the velocity field at three rotor diameters downstream of the rotor swept plane, using the measured vertical and horizontal transects for each test. The ratio α quantifies the amount of kinetic energy extracted from the flow (the so-called velocity deficit) and, together with the wake area, provides the mass flux in the wake. This ratio is therefore a principal indicator of turbine performance in confined channels (*Garrett and Cummins*, 2007). In Sec. A.3.1 this parameter will be used as an input to the theoretical model of *Verbeek et al.* (2020a) in order to compare this model to the experimental data.

3.2.3. SCALING ANALYSIS

Although it is not the intent of the experiments to reproduce exactly the flow at the test site, the Eastern Scheldt turbine will nevertheless be referred to as the prototype. In this section, the corresponding model scaling and particular choices made for the test set-up will be explained.

The most important physical processes that should be reproduced in the experimental tests are the flow separation downstream of a hydraulic structure, and the turbine wake and bypass. Their interaction largely determines the power output of a turbine mounted in a hydraulic structure. Therefore, both the flow in the hydraulic structure and at the turbine should be scaled correctly.

HYDRAULIC STRUCTURE

A weir is chosen to represent the hydraulic structure, which suffices to represent the flow separation and reattachment of the mean flow (*Hofland*, 2005). The weir was scaled assuming Froude similitude with the sill-beam of the prototype, for which the flow is sub-critical and surface undulations are negligible. Besides, the experimental flow is turbulent, with Reynolds numbers in excess of $\mathcal{O}(10^5)$, such that the results are representative for a full-scale situation (*Bahaj and Myers*, 2013).

The Froude-number Fr is defined as the ratio between inertia and gravitational forces, and the Reynolds-number Re gives the ratio between inertia and viscous forces in the prototype and model. They are defined, respectively, as

$$Fr = u_1/\sqrt{g h_w}, \tag{3.2}$$

$$Re = u_1 h_w \rho/\mu, \tag{3.3}$$

in which u_1 [m s^{-1}] is the inflow velocity of the flume, g [m s^{-2}] is the gravitational acceleration, h_w [m] is the water depth, ρ [kg m^{-3}] the water density, and μ [kg m^{-1}s^{-1}] the dynamic viscosity of water. The undisturbed flow velocity, u_1, at full scale is typically 2 m s^{-1}, and the water depth away from the weir amounts to 12 m. The resulting Froude and Reynolds numbers of the flow in the model and prototype are presented in Table 3.1, demonstrating Froude-similitude and turbulent flow conditions in the flume ($Re > 10^5$) - in accordance with the flow in prototype.

At full scale, the water depth at the weir equals 9 m giving a weir height of 3 m (see Fig. 3.1c). To assess the influence of the relative weir height on the flow field and power output, weir heights of 0.05 m and 0.10 m were chosen, with corresponding flume depths of 0.65 m and 0.70 m, respectively. Both weirs have a 1:5 upstream slope and a 0.80 m long horizontal crest.

TURBINE

The second aspect of the analysis – the flow physics of the horizontal-axis turbine – also involves scaling arguments. To this end, the scaling parameters representing the power output and wake, e.g. chord Reynolds number, the turbine tip-speed ratio and the performance coefficients, should be respected when transforming the flow from prototype scale to the experimental scale (*Bahaj and Myers*, 2013).

First, the chord Reynolds number needs to be considered, indicating the character (turbulence) of the flow over the blade chord. It is defined as

$$Re_c = u_1 c \rho/\mu, \tag{3.4}$$

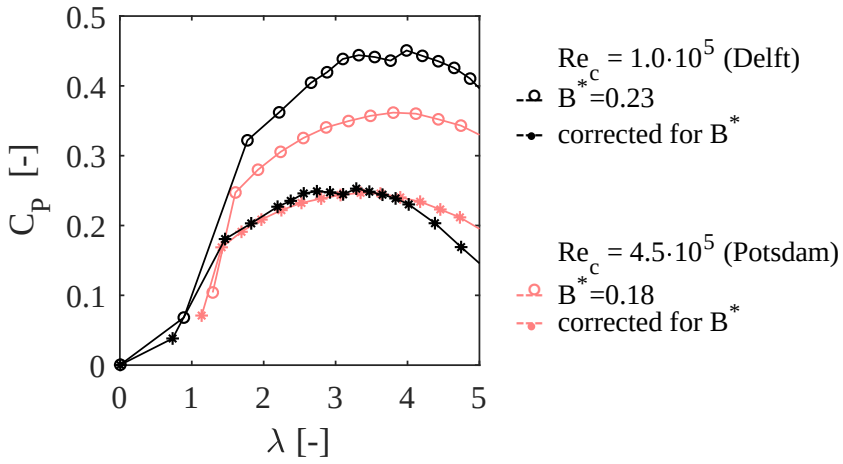

Figure 3.3: The measured power coefficient of the experimental turbine at different tip speed ratios in two experimental flumes with different geometry and inflow speed. The power coefficients of the different flumes agree after correction for the flume blockage using *Garrett and Cummins* (2007).

in which c [m] the width of the blade chord. The values in Table 3.1 are calculated for a blade chord of 0.85 m for the prototype and 0.09 m for the experimental turbine, showing that the experimental flow conditions around the blades are well in the turbulent regime, as is the corresponding flow in prototype. Perfect agreement between Reynolds numbers of model and prototype is not needed to reproduce the hydraulics and often impossible at experimental scale (*Myers and Bahaj*, 2012).

Second, in order to achieve a realistic reproduction of the turbine wake, the so-called tip speed ratio must be considered. The tip speed ratio, λ, is the tangential velocity of the rotor tip divided by the inflow velocity, defined by

$$\lambda = \left(\frac{2\pi\,\Omega}{60}\,\frac{\mathrm{D}}{2}\right) / u_1, \tag{3.5}$$

where Ω is the angular frequency [min^{-1}] of the rotor, and u_1 [m s^{-1}] is the inflow velocity. The latter is defined as the depth-averaged velocity at the centre of the inflow section of the flume, where the weir and turbine do not affect the flow. The bed boundary layer is fully developed at this location such that the velocity profile is logarithmic, which is taken into account when determining u_1 from the measurements. Using these definitions, the model turbine is controlled at $\lambda = 4$ which is the same value as in the prototype.

Third, to scale the power production of the turbine properly, the power coefficient and the thrust coefficient of the turbine must be considered. The power coefficient C_P is the turbine power output P [W] relative to the energy flux P_0 [W] of the inflow over the rotor swept area (A_D) which is defined as

$$C_P = P/P_0 = \left(\mathrm{Q}\,\frac{2\pi\,\Omega}{60}\right) / \left(\frac{1}{2}\rho u_1^3 A_D\right), \tag{3.6}$$

in which Q is the torque [N m] exerted on the rotor. Furthermore, the thrust coefficient

C_T relates the horizontal force exerted on the turbine T [N] to the momentum flux of the inflow T_0 [N] over the rotor swept area, as follows,

$$C_T = T/T_0 = T/\left(\frac{1}{2}\rho u_1^2 A_D\right). \tag{3.7}$$

The power and thrust coefficients of the model turbine have been determined by SVA Schiffbau Versuchs Anstalt (Potsdam, Germany) in a cavitation tunnel using a Reynolds number, which was five times higher than the Reynolds number used in our tests, for a range of tip speed ratios (see Fig. 3.3). These power coefficients have been corrected to account for the blockage of the flume walls using the formulation of *Garrett and Cummins* (2007) for a comparison with our tests. The agreement of the curves is excellent indicating both tests operate in the turbulence regime sufficiently far from the drag crisis around $Re = 2 \cdot 10^3$ (*Myers and Bahaj*, 2012). Scaling of the hydraulics in hence acceptable to represent the full-scale conditions (*Myers and Bahaj*, 2012).

The blockage corrected power curves of Fig. 3.3 peak at 0.25, which is at the relative low-end of the spectrum for horizontal axis turbines. The strong blade design, with a large blade solidity as inspired by marine propellors, is designed especially for high-blockage conditions and this comes at cost of efficiency when installing them in an unbounded flow.

THE COMBINED GEOMETRY

Three parameters are used to describe and scale the combined geometry of the flume, weir, and turbine: the relative blockage of the turbine, the relative weir area and the relative streamwise distance of the turbine to the weir.

The swept area of the turbine relative to the channel cross section, the blockage B^* [-], is defined as

$$B^* = A_D/(h_w W), \tag{3.8}$$

where h_w [m] and W [m] are the depth and width of the flume, respectively. Accordingly, the relative weir height a^* [-] is defined as

$$a^* = h_a/h_w, \tag{3.9}$$

where h_a [m] is the crest height of the weir. The streamwise distance of the turbine to the weir is scaled with the rotor diameter, using the dimensionless distance x^* [-], defined as

$$x^* = x/D, \tag{3.10}$$

where D [m] is the rotor diameter. The location $x^* = 0$ is at 10.6 m away from the inflow section of the flume, and corresponds to the trailing edge of the weir (for tests where a weir was present, see Fig. 3.1b).

The dimensionless blockage and weir height are varied around the prototype values of $B^* = 0.25$ and $a^* = 0.1$, in order to evaluate the effect of these parameters on the power output. In each test series the turbine is mounted at half the water depth locally above the crest of the weir. In a similar fashion the dimensionless rotor distance x^*, which in prototype ranges between -1 during ebb and 1 during flood, is varied between -2 and $+2$ (see also Table 3.1).

Concluding, the dimensionless scaling parameters of both components of the experimental set-up, the weir and turbine, as well as their combination, are equal to those of the prototype. This implies that the processes reproduced in the experiments are representative for field conditions.

3.3. RESULTS OF THE EXPERIMENTS

The generally observed flow pattern is as follows. The flow accelerates towards the weir crest and subsequently expands and slows down over a distance of approximately 7 weir heights downstream. The turbine creates a wake typically extending up to 10 rotor diameters downstream, where the streamwise flow velocities are lower and the turbulence intensities are higher than in the corresponding ambient flow. Overall, the data confirm that the wake configuration is affected by the relative weir area, the blockage, and the turbine position relative to the weir.

Next, we discuss the performance of the turbine in the different test configurations, after which the details of the corresponding flow fields and their influence on the power output are analysed.

3.3.1. OBSERVED TURBINE PERFORMANCE

First, as a reference case, the turbine is positioned in a flat-bed flume without a weir. The turbine is operated at a range of tip speed ratios, λ, while its power and thrust are measured. The corresponding power and thrust coefficients are given by the black lines in Fig. 3.4a and b, respectively. The power curve has a parabolic shape with a maximum around $\lambda \approx 4$. Power output is smaller for higher λ, which is a result of extra drag, as well as for lower λ, which is due to extra stall (*Burton et al.*, 2002). These observations confirm the general characteristics of a horizontal-axis turbine.

VARYING THE ROTOR DISTANCE

Next, for the same water depth and a weir height of 5 cm, the turbine is placed at successive distances x^* from the weir (series 1 of Table 3.1). Fig. 3.4 shows that, with a constant tip speed ratio, the power and thrust coefficients generally increase up to 40 percent with increasing x^*. These coefficients are also larger than for the corresponding reference values (flat bed) for $x^* \geq -1$. The extreme values for the power and thrust coefficient occurred at the limits of the considered range of distances, that is, the observed coefficients are smallest for $x^* = -2$ and largest for $x^* = 2$. Moreover, the optimal tip speed ratio increases from $\lambda \approx 3.5$ for $x^* = -2$ to $\lambda \approx 5$ for $x^* = 2$, with a corresponding increase of the power coefficient C_P from 0.45 to 0.70 (indicated by the black line in Fig. 3.4).

These effects are partly explained by the additional blockage of the weir, giving an effective, local blockage at the turbine equal to $B^*/(1-a^*)$, which is larger than the flume blockage B^*. *Bahaj et al.* (2007) proposed corrections of the tip speed ratio and the power coefficient to account for the corresponding increase of the flow velocity, in the bypass as well as in the wake. This is confirmed by our measurements for $-1 \leq x^* \leq 1$ if the deformation of the free surface at the weir – another effect influencing blockage – is also taken into account. For $x^* = -2$ and $x^* = 2$ the situation is more complex. Since these turbine locations involve flow contraction and flow expansion, respectively, the associated streamwise gradients of the background flow velocity and pressure fields likely play a role here too in the turbine performance.

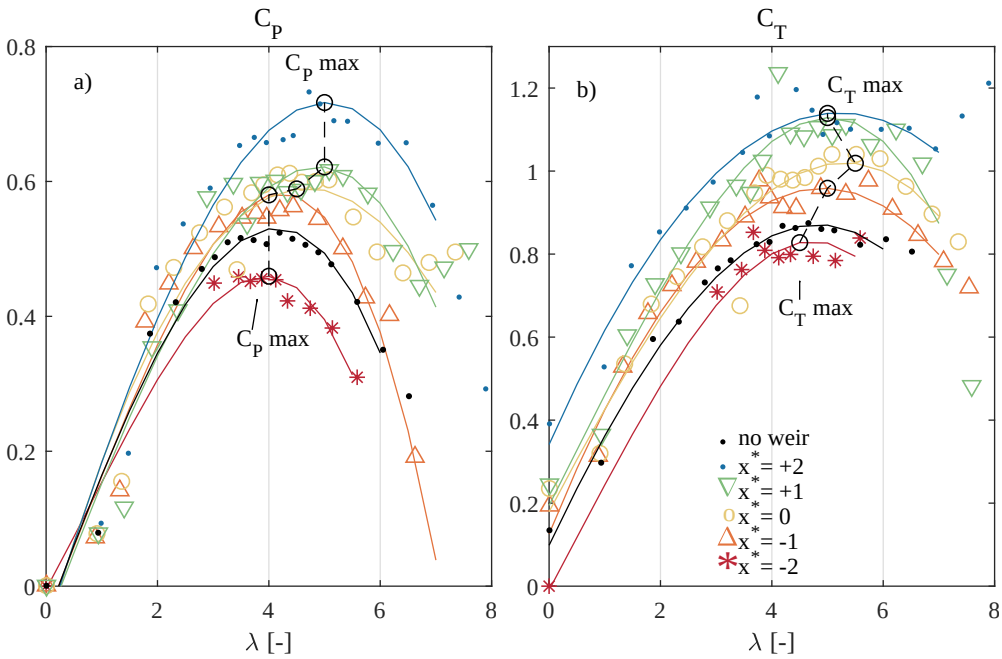

Figure 3.4: The measured power coefficient, C_P a) and thrust coefficient, C_T b) of test series 1, $B^* = 0.25$ and $a^* = 0.08$, presented for different tip speed ratios, λ, and for five relative distances of the turbine to the weir end ($-2 \leq x^* \leq 2$). Drawn lines are for illustrative purposes only. They are calculated using a root-mean-square interpolation of the data with a third degree polynomial, a typical shape of a performance curve (*Burton et al.*, 2002).

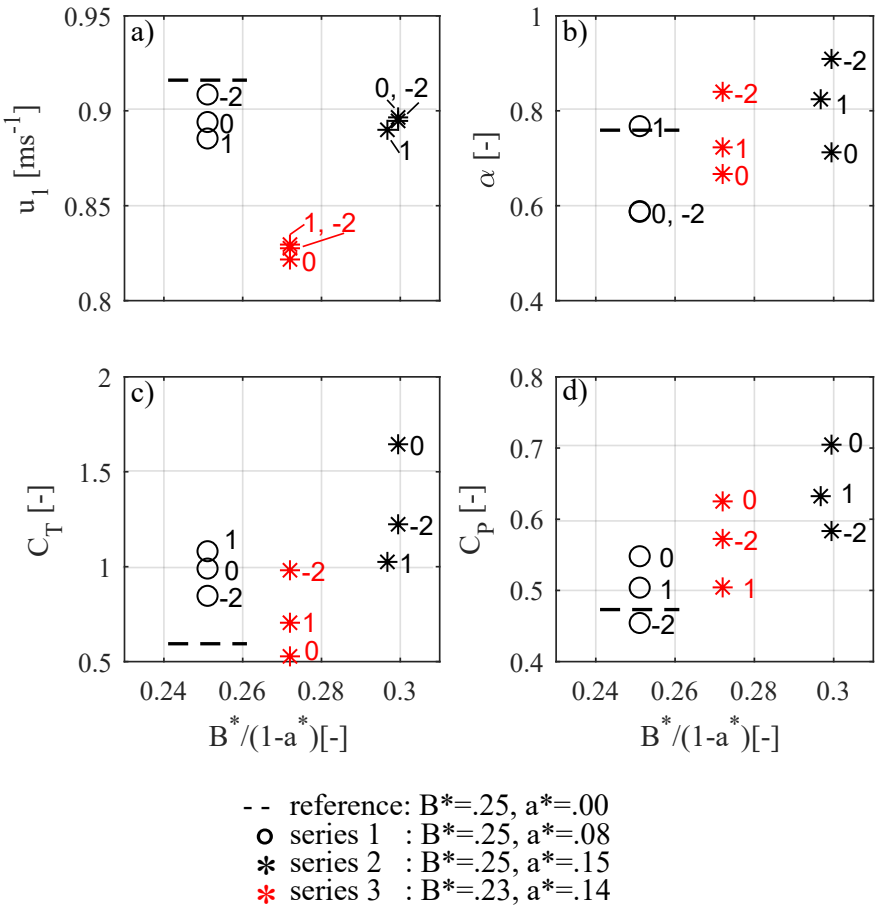

Figure 3.5: Time-averaged velocity and performance parameters presented as a function of the effective blockage, $B^*/(1-a^*)$, between the turbine and the weir end. The distance x^* is displayed to the right of each data point. The panels display a) the depth-averaged velocity at the upstream end of the flume and corresponding standard deviation is indicated with an errorbar (symbol "+"), b) the local velocity coefficient in the wake, c) the thrust coefficient, and d) the power coefficient at $\lambda = 4$. The figure presents the subset of the data for which effective blockage was varied.

VARYING THE BLOCKAGE AND WEIR HEIGHT

In order to investigate the simultaneous effects of blockage and weir height in more detail, the turbine performance is also determined for a larger weir height of 10 cm, giving $a^* = 0.15$ and $a^* = 0.14$, in combination with blockages B^* of 0.25 (series 2) and 0.23 (series 3), respectively. We consider cases where the turbine was operated at $\lambda = 4$ to only study the effect of local blockage and not of tip speed ratio. The corresponding depth-averaged inflow velocities, u_1, velocity coefficients, α, and the power and thrust coefficients, C_T and C_P, are plotted in Fig. 3.5 as functions of the effective, local blockage $B^*/(1-a^*)$, as suggested by the results in Section 3.3.1. Only the data of which effective blockage was varied is displayed to isolate its effect.

The reference velocity u_1 is smaller for series 3 than it is for series 1 and 2, which is a direct consequence of the larger water depth in series 3 to obtain the smaller blockage while the discharge remained unaffected. This difference does not compromise our analysis, since dimensionless quantities are used to characterize turbine performance (i.e., α, C_P and C_T). The relative velocity at the rotor plane, α, is highest for the cases with the largest effective blockage and the highest weir (series 2), moreover if the turbine is situated upstream of the weir. The velocity coefficient is generally smallest if the turbine is positioned at the weir end. Importantly, these results are already corrected to account for the increased local velocity, in other words, they concern effects additional to those caused by the effective blockage only.

As with the variable turbine distance, a larger C_P is generally observed if the effective local blockage is large. The tests with the largest blockage (series 1 and 2) show an increase of the power and thrust coefficients with the turbine distance x^* too, although the effect is comparatively weak for the higher weir (series 2). This trend is not observed for the smaller blockage (series 3). The smallest coefficients occur for the low weir of series 1 and - on average - the highest values for the series with highest effective blockage (series 2). Variation within each series may be explained from the non-uniformity of the flow field at the weir (contraction and expansion), which is examined in the next section.

3.3.2. OBSERVED FLOW FIELDS

In the experiments, particular attention is payed to the wake behind the rotor plane as it influences the flow bypassing the turbine and the associated pressure recovery. The latter are principal indicators of turbine performance in confined channels (*Garrett and Cummins*, 2007). The wake is here defined as the region downstream of the rotor where the flow velocity amounts to less than ninety percent of the flume inflow velocity, u_1. Important characteristics in this respect are: the horizontal extent and vertical expansion of the wake, and its (a)symmetry. To this end, Fig. 3.6 shows the observed velocity magnitude, turbulence kinetic energy, and lateral velocity of the flow in a cross section along the centre line of the flume for turbine positions $x^* = -2$ and $x^* = 1$, for constant $\lambda = 4$. The complete data set for all the series of Table 3.1 and the reference cases are given in the Appendix.

The presence of a weir generally increases the horizontal extent of the turbine wake. The longest wake is observed for $a^* = 0.15$ and $x^* = -2$, in which case it is five rotor diameters longer than in the case of the turbine without a weir (Fig. 3.6b). For cases with $a^* = 0.14$ and $a^* = 0.15$, the wake generally extends three to five rotor diameters further downstream than for the cases with $a^* = 0.08$ (see Fig. 3.6b,c,e, and f).

The vertical expansion of the wake, on the other hand, is reduced if a weir is present,

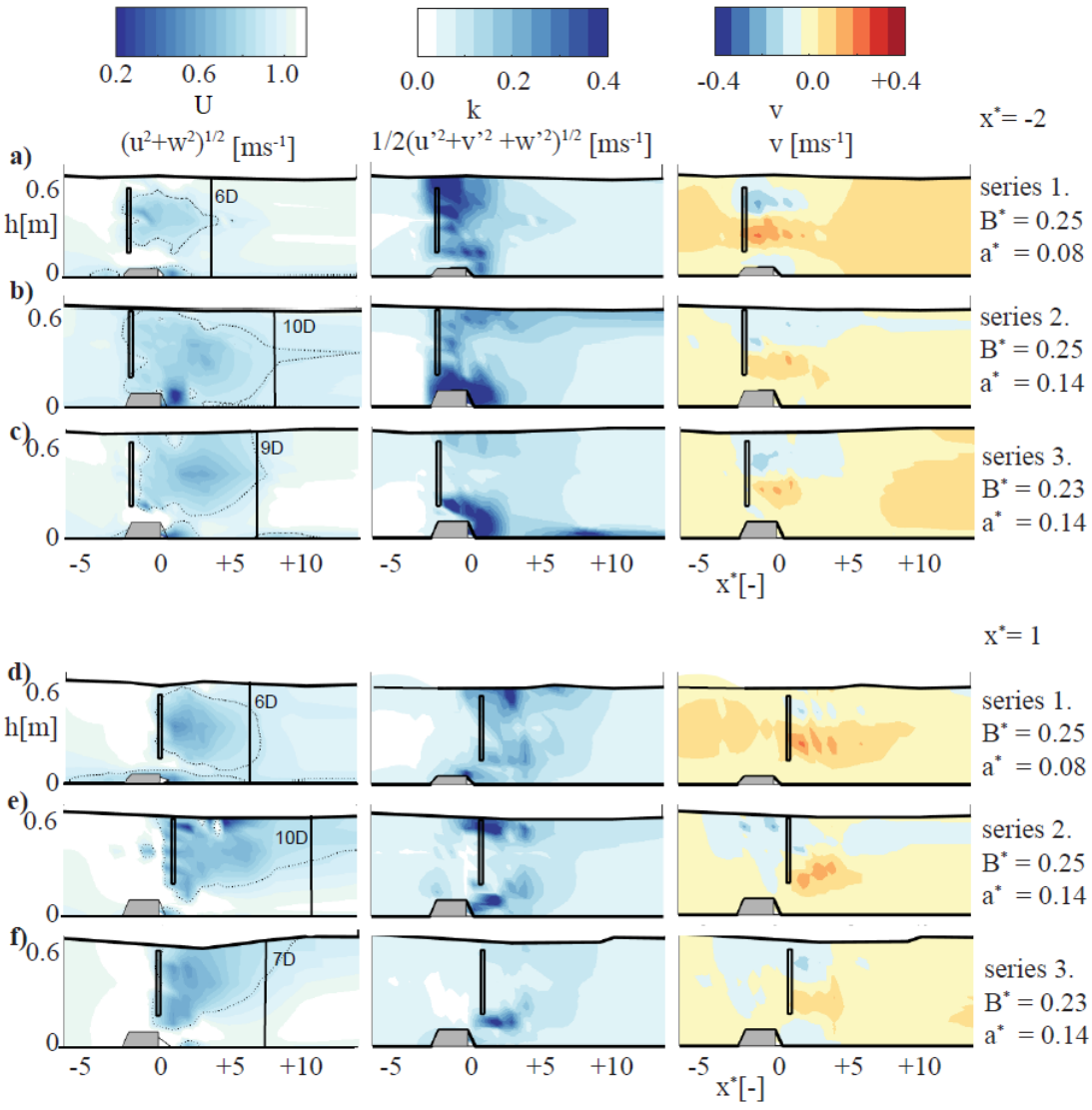

Figure 3.6: Measured flow velocity in a streamwise plane at the flume centre line, U, the turbulence kinetic energy, k, in the same plane and the lateral velocity v for all tests. The wake contour (dotted line) in the left-most panels corresponds to a streamwise flow velocity of 90 % of the inflow and the vertical line with label indicates the mean wake length. The free surface level displayed is interpolated from the water level data.

moreover if the turbine is situated upstream of the weir (Fig. A.1). Furthermore, the weir enhances the flow beneath the turbine where velocities are approximately 0.5 m s^{-1} larger than in the flow above the turbine. Especially for the smaller blockage (series 2), this asymmetry of the bypass flow is related to the confinement of the wake by the free surface.

In some configurations the horizontal extent and the vertical expansion of the wake influence each other. Recovery of the wake involves a larger downstream distance if the flow is vertically more confined, or if the wake interferes with the flow bypassing the turbine. It is possible that the wake cannot fully expand in these cases due to the flow contraction by the weir (for $x^* = -2$), the high bypass velocity, or the nearby free surface (for $x^* = 1$). The turbulence kinetic energy is particularly high in these situations (center panels of Fig. 3.6a,b and d), which suggests a strongly sheared wake flow.

The observed lateral velocity, which is a measure for wake rotation along the streamwise axis, is shown in the right panels of Fig. 3.6. The rotation in the wake is largest for situations without a weir or when the turbine is situated downstream of the low weir. The confinement of the flow by the weir reduces the wake rotation, possibly due to the increased shear at the interface of the wake and the bypass area. This is substantiated by the observation of a small torque load, which gives the wake its swirling motion.

3.3.3. INTERPRETATION: INFLOW AND WAKE EFFECTS

In Sec. 3.3.1 we described that local flow characteristics affected the power coefficient. The power coefficient was generally larger when the turbine was placed at the crest of the weir or downstream thereof, as a result of blockage and a high relative flow velocity at the rotor plane. However, it follows that the power coefficient not only depends on these local characteristics, but also on the upstream and downstream flow pattern as induced by a particular weir-turbine geometry. This flow is e.g. featured by a non-uniform inflow velocity profile for a turbine downstream of the weir (Fig. 3.6d-f) and a relatively long wake for a turbine upstream of the weir (Fig. 3.6a-c). The implications of the upstream and downstream flow pattern for the turbine performance will be discussed below.

The characteristics of the flow *upstream* of the turbine affect the power coefficient through its distribution and its streamwise gradients. The flow experiences the largest blockage for an incoming flow, which is uniformly distributed over the cross section (*Draper et al.*, 2016). Consequently, the alteration of the vertical velocity profile by an upstream weir can slightly reduce the power coefficient of a downstream turbine. This is relevant for the studied cases for which $x^* > 0$ where we observed a higher velocity below than above the turbine (Fig. 3.6d-f). Furthermore, streamwise gradients in the incoming flow velocity, as a result of contraction or expansion, may affect the power coefficient. The observed acceleration of the inflow for a turbine at the weir crest likely favoured the power coefficient due to the associated negative streamwise pressure gradient which increases the turbine thrust, such as postulated by *Wimshurst and Willden* (2016).

The flow pattern *downstream* of the turbine also influences the power coefficient, where especially wake expansion plays an important role. A wake with a large vertical (or lateral) extent is associated with a large streamwise pressure difference over the turbine. This follows directly from a theoretical analysis of the flow: if the wake cross-section is larger, the flow velocity in the wake is smaller, hence the resulting pressure difference over the turbine is larger. This explains the comparatively large power output of turbines placed at the trailing edge or downstream of a weir, as the backward-facing step of the weir forces

an abrupt expansion of the bypass flow behind the turbine. Furthermore, a long horizontal extent of a confined wake involves smaller gradients in the ambient pressure and hence a smaller pressure drop over the turbine, limiting turbine performance. The ambient pressure gradient is here associated with acceleration of the bypass flow, such as e.g. discussed by *Vogel et al.* (2016). This explains the non-optimal power output when the turbine is situated upstream of the weir.

While not directly relevant for the power coefficient, the bypass flow may also affect the hydraulic resistance of the turbine-weir combination, and hence the energy yield of the turbine if the flow is controlled by the hydraulic head difference across the structure. This is a consequence of the interaction of the bypass flow with the flow separation downstream of the weir. We observed that the main flow attached at shorter distances to the bed when the turbine is located at the weir end or further downstream ($x^* \geq 0$), compared to situations without a turbine or with a turbine upstream of the weir ($x^* < 0$) (Fig. 3.6). This substantiates the hypothesis of *Verbeek et al.* (2019) on the interaction between a weir and a turbine, i.e., the high velocity in the bypass area reduces the length of the recirculation zone downstream of the weir if the turbine is placed at $x^* \geq 0$. *Verbeek et al.* (2019) suggested that, as a consequence, a larger portion of the kinetic energy of the inflow can be harvested by turbines for these configurations.

From the analysed cases, it is concluded that the power coefficient not only depends on the local geometrical parameters at the turbine but also on upstream flow properties and downstream wake properties, sometimes even in a counter-intuitive way. For instance, the power coefficient may still be optimised by adapting the weir as a means of controlling the wake for cases where vertical wake expansion is limited. Theoretical models could provide the necessary framework for analysing the relationship between hydrodynamics and power output for simple turbine-weir geometries.

3.4. THEORETICAL MODELLING

A validation of the theoretical model of *Verbeek et al.* (2020a) against the obtained data set reveals the application range of the model, proving whether or not it can be applied to optimise the geometry of turbine-weir configurations comparable to those considered in the experiments.

3.4.1. MODEL DESCRIPTION

In the theoretical model the flow is described using one-dimensional balances of mass, energy and momentum postulated by *Garrett and Cummins* (2007). Using a momentum-extracting (actuator) disk to describe the action of the turbine, all geometrical information is integrated over the channel width and depth. Additionally, the model schematization of *Verbeek et al.* (2020a) includes an instantaneous step of arbitrary height in the bed as a weir, with downstream a separating flow, and a turbine either upstream or downstream of the weir. The latter determines the configuration of the bypass streamtubes. For the turbine streamtube, the velocity factor, α, is prescribed in the current study (referred to as α_5 in *Verbeek et al.* (2020a)). The water surface is approximated by means of a stress-free rigid lid.

3.4.2. VALIDATION RESULTS

The power output computed by the model is compared to the experimentally obtained values for a range of λ values ($0 < \lambda < 6$). In Fig. 3.7 and Tab. 3.2 the computed power for the first test series ($B^* = 0.25, a^* = 0.08$) is compared to the corresponding experimentally obtained values. To this end, the results of the analytical model with a turbine upstream of the weir are compared to the experimental results for $x^* = -2, -1$, while the model results with the turbine downstream of the weir are compared with the experiments for $x^* = 1, 2$. Results for $x^* = 0$ are not compared to the model, as no model schematization is available of this situation. However, given the dataset, the validation will be comparable to the situation for $x^* = 1, 2$. The value α in the analytical model is taken as an input as it could be easily obtained from the velocity data.

Table 3.2 shows that the model performance is generally good for optimal values of the tip speed ratio, $\lambda \approx 4$, with the predicted power output deviating less than 10 percent from the corresponding experimental results. For $-1 < x^* < 1$ the model also performs well for sub-optimal tip speed ratios, $3 < \lambda < 5$, while for $x^* = -2$ and $x^* = 2$ model results are acceptable only if the tip speed ratio is optimal. The latter is attributed to flow contraction and wake expansion, respectively, that influence the performance of the turbine when it is placed at larger distances from the weir (see section 3.3.3). These secondary effects are not included in the analytical model which compromises its performance for these turbine positions, especially if the tip speed ratio is sub-optimal. Overall, regardless of the value of x^*, the model performance is poor for tip speed ratios $\lambda <$ ca. 3. In these cases the experimental results are influenced by flow separation and the associated energy losses at the blades, a process which is ignored in the theoretical model, leading to smaller power values. Similarly, for λ slightly larger than 4, where increased drag in the experiments leads to a lower relative wake velocity (α), a process which is not part of the theoretical model. We therefore continue our analysis by considering the model accuracy at optimal tip speed ratio, which is also the more relevant case in practice.

Regarding the turbine, the tip speed ratio and blade shape are not specified directly in the model, but represented by an energy-extracting disk lumping all design and operational information into velocity coefficients. This approach assumes uniformity of the flow velocity and turbine properties over the turbine swept area, which generally leads to an overestimation of the power output as compared to the non-uniformity of the actual situation (*Draper and Nishino*, 2014). Similarly, the blockage by the turbine has been assumed uniform in the model, while in the experiments it is larger in the vertical than in the horizontal direction. We may speculate that the flow in the experiment may therefore experiences slightly less blockage, resulting in a lower power output (*Draper et al.*, 2016).

Regarding the wake flow, in particular the streamwise distance between the turbine and weir affects power output since this influences the wake expansion and flow redistribution in the wake and bypass. By varying this distance the observed power output could change by 40 percent, as shown in Fig. 3.4. This effect is not explicitly accounted for in the theoretical model, as it is assumed that the turbine wake does not interfere with the recirculation zone behind the weir. This is a reasonable assumption if the turbine-weir distance is relatively small. To increase the application range of the model to larger values of x^*, however, a more precise schematization of the wake based on the actual distance x^* would be necessary. Another model limitation related to wake expansion concerns the schematization of the free surface by means of a rigid lid. While the position of the rigid lid is chosen with care,

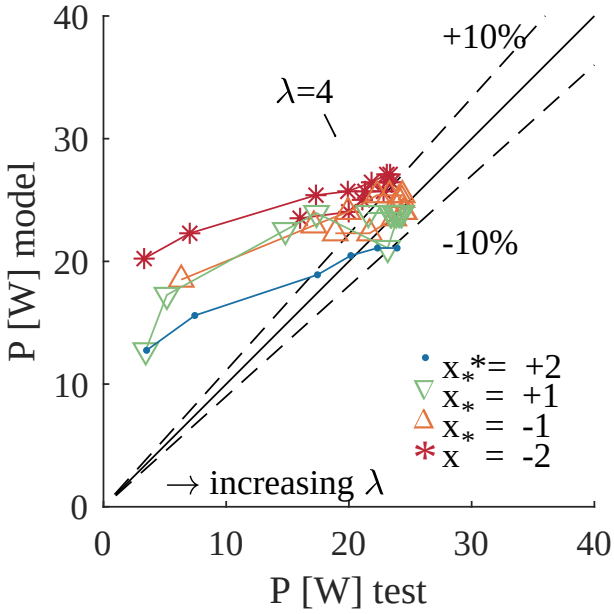

Figure 3.7: The power estimations from the model of *Verbeek et al.* (2020a) for a turbine downstream of a weir and upstream of a weir compared to experimental data.

3

Table 3.2: The tip speed ratio λ and wake velocity coefficient α_5 corresponding to the power estimates presented in Fig. 3.7. The table shows that the model is most accurate (within ten percent) for the test situations with $-2 < x^* < 2$ and $\lambda \approx 4$.

x^* [-]	λ [-]	α_5 [-]	P_{test} [W]	P_{model} [W]	relative error power [%]
-2	-	0.82	3.3	20.2	511
-2	2.3	0.77	7.0	22.3	217
-2	3.0	0.58	23.1	27.1	17
-2	4.1	0.61	22.8	25.7	13
-2	5.1	0.68	20.0	24.0	20
-1	1.3	0.79	6.3	18.5	192
-1	2.2	0.61	19.9	24.0	21
-1	3.1	0.56	23.3	25.4	**9**
-1	4.2	0.61	24.5	24.0	**-2**
-1	5.3	0.67	21.7	22.3	**3**
+1	0.9	0.98	3.4	12.8	270
+1	2.4	0.76	17.4	23.9	38
+1	2.9	0.81	23.2	21.1	**-9**
+1	4.1	0.77	23.7	23.9	**1**
+1	5.1	0.77	24.3	23.9	**-1**
+2	1.0	1.10	3.5	12.8	263
+2	2.5	0.95	20.2	20.5	**2**
+2	2.9	0.91	22.3	21.1	**-6**
+2	4.3	0.90	23.6	21.1	-11
+2	5.2	0.90	25.9	21.1	-18

based on the mean water level measured, undulations of the free surface near the turbine, as observed in the experiments, are absent in the model. This implies that while the first order effect of the free surface, the blockage, is included in the theoretical model, second order influence of undulations is not. The latter refers to the ambiguous influence of the free surface, which may either constrain the expansion of the wake and thereby reduce the power output, such as discussed by *Bahaj et al.* (2007), or increase the blockage and efficiency due to flow contraction at the turbine position as described by *Whelan et al.* (2009b). Depending on which of these processes dominates, the model is too optimistic or too pessimistic a this point respectively.

Despite all these simplifications, the model results are reasonably accurate for operational values of λ. We therefore conclude that the current model is valid for a well-defined set of practical cases. A first condition is that that the horizontal and vertical blockage should be approximately the same, to ensure that local blockage at the turbine is equal to the prescribed geometric blockage in the model. Next, the model should only be used to predict the power output near the maximum of the power curve, which in this case is at $\lambda = 4$. The user of the model should also be aware that the prescribed velocity coefficient in the rotor plane or wake, α, may apply to a specific turbine design. Depending on the application, it can hence be useful to prescribe the velocity factor in the bypass or thrust coefficient (referred to as β_5 and C_T respectively in *Verbeek et al.* (2020a)) to the theoretical model instead of the α. Lastly, the current model assumes a simple shape of the wake to predict the performance, limiting its use to the turbine-structure distances considered in this work. Three-dimensional computational fluid dynamics must be considered if more accurate performance estimates are required.

3.5. DISCUSSION

The presented experimental and theoretical analysis applies to hydro-kinetic turbines in a geometry consisting of a channel, which is narrow relative to the turbine diameter, combined with an abrupt step of small height in the bed. This geometry represents the case of a river passing a sluice gate with a weir. We argue that in such situations the local flow condition, governed by the effective blockage and the wake velocity coefficient, is the main factor influencing the turbine performance. The associated geometry range targeted in this study is characterised by a blockage, B^*, between 0.1 and 0.7, a relative step height, a^*, between 0.1 and 0.3, and a distance of the rotor swept plane to the step in the bed of at most two rotor diameters, corresponding to $-2 < x^* < 2$. Beyond this range other processes affect the power coefficient as well, in particular the streamwise and vertical flow velocity gradients, for which the accuracy of the proposed theoretical model is limited.

In large-scale applications of this technology, multi-turbine systems can be installed in multi-gate barriers. Noteworthy is that the power coefficient of a single gate with turbines, as presented in this chapter, is then affected by the flow through the neighbouring gates as well. For this reason, optimizing the lateral distribution of turbines in a barrier is a direction of explored in Chapter 4. As a first step, *Verbeek et al.* (2020a) already proved the validity of the theoretical model for arrayed deployments of turbines upstream or downstream of a weir, based on detailed information of the flow in the rotor plane and wake from field measurements. For comparable geometries, the predictive capability of the theoretical model can likely be improved to an accuracy of 10% if the flow distribution in the neighbouring wakes and bypasses is schematised explicitly in the theoretical model,

such as in the work of *Nishino and Willden* (2012b).

Where this chapter focused on clarifying influences of the geometry on the power coefficient, the practical implementation of hydro-turbines involves the optimisation of the energy yield and the induced flow resistance as well. With regard to the latter, the optimal turbine configuration in a hydraulic structure may differ from the optimal position presented in this work. This can be explained as follows. The energy yield is the product of both the power coefficient and the ambient flow velocity cubed. If the ambient flow is driven by external water level differences, as for instance caused by the tide, the ambient flow velocity is also influenced by the resistance of the turbine-weir geometry. A high power coefficient will then reduce the ambient flow velocity if the overall resistance experienced by the flow is increased, which is referred to as 'channel-choking' by *Nishino and Willden* (2012b). The additional resistance is associated with expansion losses in, respectively, the turbine wake and in the flow separation zone downstream of the weir. Streamlining the flow in these regions could minimize the added resistance, bearing in mind that this will only lead to a larger energy yield if the power coefficient is not significantly reduced. Future research should indicate how such considerations would affect the optimum turbine position and velocity induction regarding energy yield.

Interestingly, the experimental results already point at the existence of a geometry where both the power coefficient and energy yield are high and the added flow resistance is limited. In particular, flow separation and expansion downstream of the weir are suppressed if the turbine is placed at the weir end, while the power coefficient was close to optimal for this position. This offers the opportunity to optimize the design achieving both a high energy yield and a limited additional resistance. The latter is also relevant if the environmental impact of turbine arrays should be minimized. The turbines in the Eastern Scheldt barrier - which were an inspiration for the presented experiments of this work - already benefit from this phenomenon during the tidal flood phase, as discussed in the work of *Verbeek et al.* (2019).

3.6. CONCLUSION

The aim of this study was to clarify the consequences of placing a tidal turbine in a hydraulic structure with regard to the turbine performance. Unique experimental measurements of turbine power and wakes were performed to meet this aim. The influence of weir height, blockage, and streamwise distance between turbine and weir on the power coefficient and associated hydrodynamics was evaluated. Besides, the measurements were used to validate an analytical model for predicting the power output, which is based on a simplified representation of the flow. Combining experiments and theoretical modelling gave insight into the processes that affect the power output of turbines in hydraulic structures, and into the application range of the proposed analytical model.

The power coefficient generally increases if a turbine is placed in a hydraulic structure, which is a result of the increased local blockage. The data reveal a close link between the power coefficient and the observed flow patterns. Upstream, local, as well as downstream flow effects determine the performance. Local effects concern the effective blockage and relative flow velocity in the rotor plane. Effects resulting from the flow upstream and downstream of the rotor concern the velocity distribution in the inflow, bypass and wake, and the streamwise velocity gradients of the background flow. Depending on the position of the turbine relative to the weir, one or a combination of these processes affects its

performance.

The power coefficient increased with up to 40 percent when the turbine was repositioned from two rotor diameters upstream of the weir to two diameters downstream of the weir. Over this range, in successive order, flow contraction, local effective blockage and flow expansion dominated the physics at the turbine. Most power could be harvested if the local blockage was highest, that is, when the turbine was placed at the structure crest, but only when allowing space for a favourable wake configuration.

The influence of local effects on the power coefficient could be well predicted with the theoretical model, within 10 percent accuracy, making it a promising tool to maximise power for the different control variables within this range. The model has limitations for geometries beyond the studied range of $x^* = \pm 2$, in which processes of flow contraction and expansion become increasingly important. By including more information, particularly on the wake configuration, the application range of the model could be extended to include these configurations. In this way this work advances the knowledge needed to meet targets on renewable energy.

4

Optimizing the configuration of tidal turbines in a storm-surge barrier

This chapter is written by M.C. Verbeek, H. Talstra, R.J. Labeur and W.S.J. Uijttewaal and submitted for publication in December 2022.

4. Optimizing the configuration of tidal turbines in a storm barrier

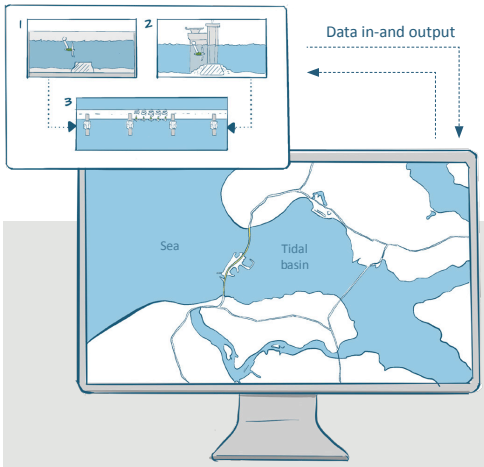

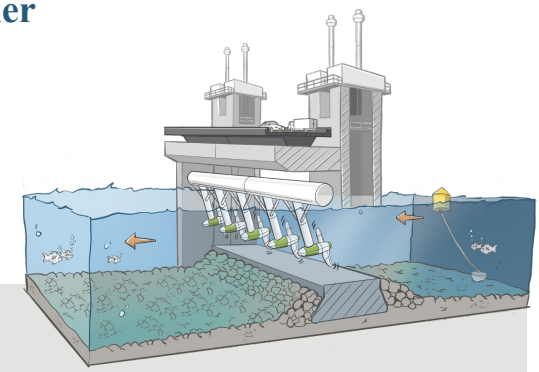

A tool is developed to calculate the optimum configuration of tidal turbines in a barrier.

Several scenarios are run with the tool with different numbers of turbines to find an optimum configuration.

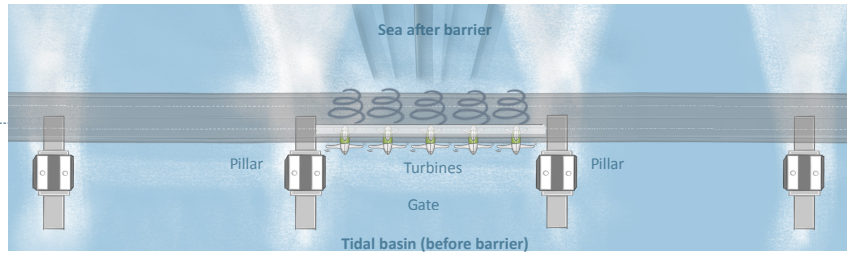

An example: a configuration of three parallel gates (one gate with five tidal turbines)

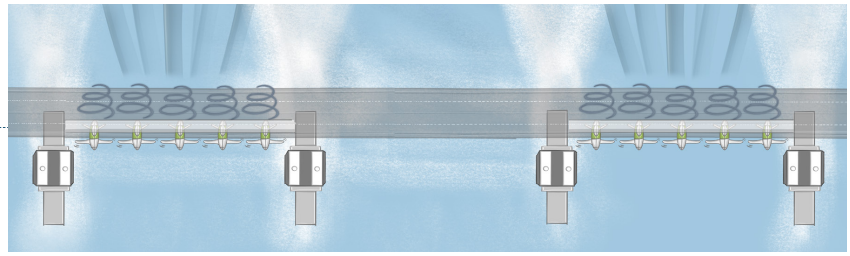

Configuration with parallel gates (two gates with turbines)

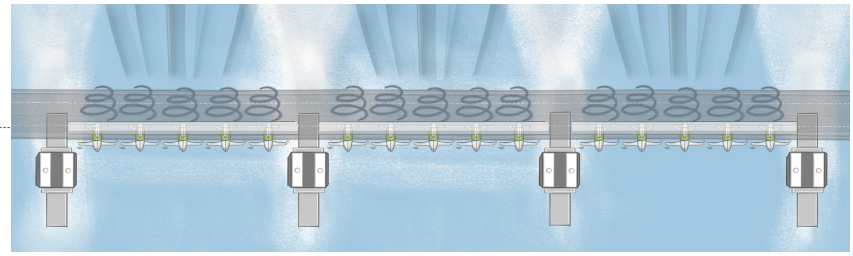

Configuration with parallel gates (three gates with turbines)

The previous chapter clarified how power output of tidal turbines can increase when they are placed in a tidal barrage, bridge or hydraulic structure, using a down-scaled turbine mounted at a submerged weir. Experimental measurements of turbine power and wakes were presented and the theoretical model of Chapter 2 was successfully validated with a 10% accuracy for the thrust.

However, if we want to harvest more energy from the tidal flow, more turbine fences should be retrofitted in barrages or open barriers, providing an integral solution for flood protection and emission-free power generation, within environmental constraints. To optimize the turbine-barrage configuration with respect to these objectives, simulation tools are needed to predict the efficiency of the turbines as well as their impact on the adjacent tidal system. These tools should be based on an accurate representation of the underlying flow processes, which cover a wide range of spatial scales - from meters at the barrier and turbines to tenths of kilometers in the tidal basin.

This chapter presents the development of such a tool by linking an analytical model for turbines in barrier gates (developed in Chapter 2) to a regional flow model. The turbine model is validated with experimental data from Chapter 3, and data from a thoroughly monitored tidal energy pilot project (Chapter 2).

Simulations reveal how clustering the turbines in small arrays (fences) can increase their efficiency, owing to array blockage effects, with only little effect on the tidal exchange. We also demonstrate the potential of using turbines to manipulate the tidal jet, issued from the barrier, with benefits for coastal - and nature protection in the basin. The presented research helps understanding how turbines in open barriers can be configured with high energy yield and calculated impact to the environment.

4.1. INTRODUCTION

The EU targets to further decarbonise the energy system, as this is critical to reach climate objectives in 2030 and 2050 (*EU*, 2019). Tidal stream turbines, which are a promising technology in a development stage, are becoming an affordable option for sustainable energy harvesting in coastal areas, and, in this way, contribute to this target (*Borthwick*, 2016). Besides, the EU aims to conserve its natural capital and protect its citizens from environment-related hazards, such as coastal floods. However, these objectives are complex and interlinked, which makes it non-trivial to develop and optimize tidal energy projects in practice. In the research described in this chapter we develop a modelling tool specifically for this purpose and apply it to an existing pilot project to shed light on the possible trade-offs and compromises of the above objectives.

In the tidal energy pilot under consideration (in the Eastern Scheldt tidal basin, The Netherlands) the above objectives could actually be combined. Five horizontal-axis tidal turbines were retrofitted in a single gate of an open storm surge barrier or tidal barrage, in order to harvest sustainable energy from the passing tidal current. Hereby, the flood protection function and estuary ecosystem value were warranted over the span of the pilot, between 2015 and 2019 (and later between 2021 and 2023) (*Leopold and Scholl*, 2019; *Verbeek et al.*, 2020a,b). In order to understand how energy yield as well as flood protection within environmental constraints can still be served simultaneously while retrofitting more

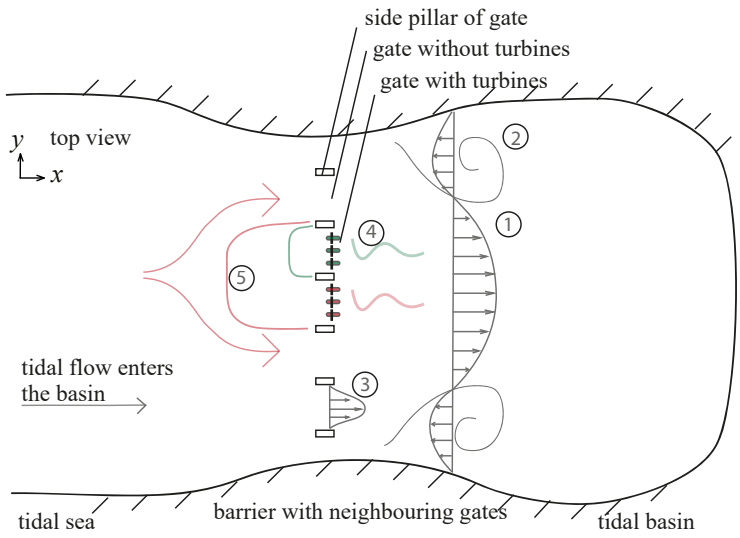

Figure 4.1: Schematic overview (top) of turbine-barrier flow interaction at the basin scale, of $\mathcal{O}$(1-10) km, illustrating the relevant processes: 1. flow contraction in the tidal channel, 2. large-scale turbulence structures, 3. flow contraction in barrier gates, 4. turbine added resistance, 5. turbine-turbine and gate-gate interactions.

turbines in neighbouring gates of a barrier, a modelling tool is needed that can predict turbine power production as well as the impact of the barrier and turbines on the adjacent tidal system. By incorporating the main physical processes, such a tool should also be instrumental in applying lessons learned to other tidal sites.

Specifically, the desired tool must be able to predict how small-scale flow processes associated with the turbines affect larger-scale flow processes in a tidal basin, and vice versa (see Figs. 4.1 and 4.2). At small scales, an individual turbine device influences the blockage of its neighbour turbine through bypass flow and wakes (*Nishino and Willden*, 2013; *Cooke et al.*, 2016). Besides, the flow through the barrier itself also interacts with the turbine (*Verbeek et al.*, 2020a). At larger scales, the distribution and amplitude of the tidal current over the barrier is affected by the sum of these processes, and vice versa. In turn, these large-scale processes have impact on e.g. discharge distribution and sediment transport (*Leopold and Scholl*, 2019), which are important to flood- and nature protection of a basin. Due to this interaction of scales, an important requirement of the desired tool is the dynamic coupling of flow phenomena at both scale levels: from flow patterns at the scale of a single turbine device, of $\mathcal{O}$(1-10) m, up to flow patterns at the scale of a barrier and the wider tidal basin, of $\mathcal{O}$(1-10) km.

The described coupling of scales usually comes at the cost of an increased computational effort. Obviously, it is desirable to minimize this effort where possible. This can be achieved in two ways. Firstly, by modelling small-scale turbine processes (such as the flow through and bypassing a turbine device) in a sub-grid manner, using a parametriza-

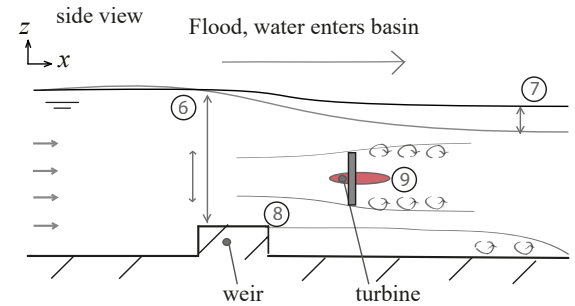

(a)

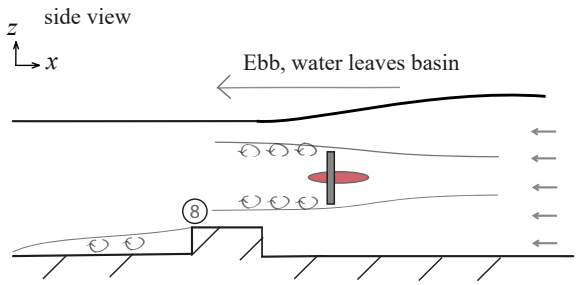

(b)

Figure 4.2: Schematic overview (side) of turbine-barrier flow interaction at device scale, of $\mathcal{O}$(1-10) m, during flood flow (a) and ebb flow (b), illustrating the relevant processes: 6. flow contraction by local blockage, 7. free-surface level variation, 8. flow expansion downstream of the weir, 9. flow expansion in the turbine wake.

tion which accounts for the relevant physical processes, and coupling this to a larger-scale numerical flow model. And secondly, by applying local mesh refinement in the larger scale model near the barrier and turbine devices (to accurately and efficiently resolve the coupling of scales), while using a coarser mesh resolution in the far field. In this study, this is achieved by employing an unstructured triangular mesh combined with a numerical flow model based on the finite element method.

With this in mind, the aim of the research described in this chapter is twofold. Firstly, to establish the elementary dynamics of a single turbine-gate configuration, in order to develop and validate an efficient sub-grid parametrization which describes the energy yield and head-discharge relation of turbine devices mounted in a barrier with gates. Secondly, to couple this sub-grid parametrization with a larger-scale numerical flow model and applying it to a tidal power pilot project in order to assess the effects of alternative turbine configurations on energy yield, discharge distribution, tidal prism, and system functions related to natural capital and coastal protection. The findings will help understanding how to optimally combine complex EU ambitions on coastal protection, energy generation and nature conservation in a tidal energy project.

In view of both aims above, this chapter is structured as follows. Sec. 4.2 describes the developed sub-grid turbine-weir parametrization, as well as its coupling with a larger-scale numerical model solving the two-dimensional (2D) shallow water equations. The resulting modelling tool is validated using (successively) field data and experimental data of turbines in hydraulic structures (*Verbeek et al.*, 2020a,b). In Sec. 4.3, this tool is applied to the above mentioned pilot project in the Eastern Scheldt storm surge barrier. Site-specific as well as general results are presented in Sec. 4.3.4. The discussion in Sec. 4.4 integrates findings from both parts of the scope: the applicability range of the developed sub-grid tool, and the ensuing design considerations for tidal energy sites. Besides, some trade-offs and compromises between the various (complex and interlinked) design objectives are considered. Conclusions are formulated in Sec. 4.5.

4.2. SUB-GRID TURBINE MODEL AND ITS COUPLING TO LARGER SCALES

This section describes the development of the sub-grid turbine model and its coupling to a larger-scale model for computing tidal flows. To this end, we will first identify the physical processes relevant to each scale in Sec. 4.2.1. Concerning the turbines, we next derive a theoretical formulation aggragating the elementary dynamics of a turbine array mounted in a barrier gate with a weir (Sec. 4.2.2). For an individual turbine, this provides a relation between the local discharge, the head difference over the turbine and the power production. The resulting parameterization is implemented in a tidal flow model, using interior boundary conditions, thereby achieving the desired coupling of scales. The overall approach is validated in Sec. A.4.3.

4.2.1. GOVERNING PHYSICAL PROCESSES

We consider a semi-enclosed tidal basin, having a open barrier in its inlet; see Figure 4.1 for a conceptual lay-out of the system. Here, a tidal inlet refers to the sea body between two islands or headlands, where the tidal exchange flow locally contracts. In this work, the barrier (or barrage) consists of parallel gates, spanning the width of the tidal inlet. Each of the gates is in fact a small channel formed by side pillars and a bottom beam (weir). In the gate an array of tidal turbines can be installed, see Figure 4.2. An array (often referred to as a fence) consists of tidal devices placed next to each other, perpendicular to the flow. The performance and impact of these arrays of turbines are the result of a superposition of processes. Next, we introduce them in order of their associated length scale, which is roughly 1-10 km for the channels (horizontal length or width), and typically 1-10 m for the gates and devices (diameter of the turbine blade swept area).

CHANNEL SCALE

Figure 4.1 distinguishes five channel-scale processes, which need to be resolved with sufficient detail when when using a numerical flow model for turbine-barrier interaction. With reference to the figure, these processes are discussed briefly below.

The tidal flow towards the barrier (1) contracts in the tidal inlet. In *Broekema* (2020) it was shown that this process is associated with large horizontal gradients of the flow velocity, and can be typified as a (tidal) jet. The flow further contracts (3) within the barrier gate (horizontally) and over the weir (vertically). The corresponding acceleration of

the flow velocity enhances turbine thrust and power coefficients, mainly as a result of an additional pressure difference over the turbines (*Nishino and Willden*, 2013; *Vennell et al.*, 2015). The subsequent expansion of the flow behind the barrier (2) leads to large-scale, quasi-horizontal turbulence driving large gyres along the side slopes of the inlet channels.

The turbines themselves decelerate the flow locally through their so-called added resistance (4), as energy head of the flow is lost in turbine power extraction and energy dissipation in the turbulent wakes (*Vennell et al.*, 2015). As a result of this resistance, single turbine devices and arrays of turbines interact with each other (5) through water level set-up and bypass flows. In *Nishino and Willden* (2012a) and *Cooke et al.* (2016) it was postulated that there exists an optimal intra-turbine spacing (referred to as local blockage) and inter-array spacing (array blockage) maximizing the power coefficient of a single turbine. The power extraction of the tidal farm as a whole can therefore be optimized by altering the intra-turbine and intra-array spacing, depending on the total number of devices (farm blockage). The optimum strikes a balance between the higher efficiency of a single device, when operated in clusters of devices, and the added resistance of the overall farm to the flow, in conjunction with the response of the adjacent tidal basin (basin efficiency).

GATE-TURBINE SCALE

Figure 4.2 illustrates four device-scale processes, which will be included in a sub-grid model and coupled to the aforementioned large-scale flow model. With reference to the figure these processes are discussed below.

In a free, unbounded flow, a turbine can capture at most a fraction of $16/27$ of the incoming energy flux through a plane with the same size as the rotor swept area. This famous result was derived analytically by Betz (*Betz*, 1920), and is due to the flow bypassing the turbine because of the higher local resistance. In a constrained flow however, such as in the barrier gate (6), the bypass flow is suppressed leading to a higher limit of power extraction. This effect is governed by the local blockage B (or occupation ratio) of the turbine, which is defined as the ratio of the streamwise projection of the rotor swept area and the channel cross section. It was shown in (*Garrett and Cummins*, 2007) that the limit of power extraction increases with a factor of $(1-B)^{-2}$. In a similar way, spatial and temporal variations of the free surface level (7) influence the power extraction, by altering the local blockage, an effect that is characterized by the local Froude number *Whelan et al.* (2009b).

Turbine performance is furthermore dependent on the local flow patterns and the pressure field within the gate. In particular, these are affected by the crest of the weir (8). The weir causes an additional contraction of the flow, which also involves a negative pressure gradient. Moreover, the recirculation zone behind the weir (9) interacts with the wake flow of the turbine, slowing down its recovery. All this will further enhance the performance of the turbine, depending also on the position of the turbine with respect to the weir. In *Verbeek et al.* (2020a) an analytical model was postulated and validated, accounting for the effects of the weir on the turbine performance and added resistance.

4.2.2. MODELLING APPROACH

The channel-scale processes (1-5) are basically governed by the two-dimensional shallow water equations (SWE) where the equations of motion of the flow are averaged over the

depth (*Battjes and Labeur*, 2017). This averaging relies on the pressure being hydrostatic in the vertical direction, which is obviously not the case around the gates and turbines. Therefore, the small-scale processes (6-9) have to be taken into account by means of a sub-grid model, treating the non-hydrostatic effects in a semi-analytical manner. In our approach, we express the discharge through a gate - with or without turbines - in terms of the head difference over the gate and the device properties. The resulting discharge relation will be coupled to the large-scale model by means of an interior boundary condition. Details of the approach are described below.

SHALLOW-WATER FLOW MODEL

The shallow water equations that govern the channel-scale flow are discretized using a finite element method based on a numerical approach that was introduced in (*Labeur*, 2009) and further developed in (*Labeur and Wells*, 2009, 2012), see also (*Steenman*, 2020; *Talstra et al.*, 2019). The method employs a computational mesh consisting of triangles, that can have arbitrary size and shape, which conveniently accommodates to irregular geometries and allows for a flexible local mesh refinement in the domain of interest.

Importantly, near the barrier a sufficient mesh resolution is required in order to warrant a correct reproduction of the intra-turbine and inter-array interactions. Also the wakes from arrays of turbines and the adjoining lateral recirculation zones need to be resolved with sufficient detail (combined with a horizontal turbulence model) in order to predict the overall efficiency of the tidal farm correctly. A maximum triangle size of $\mathcal{O}(10)$ m (turbine spacing) is considered necessary here, which can be furnished by refining the triangles locally, keeping the total number of triangles in the mesh acceptable for computational efficiency.

Along the exterior boundaries of the model domain, either the water level or the flow velocity must be prescribed. The actual boundary conditions to be imposed depend on the situation at hand which, for our case, will be specified in Sec. 4.3.2.

In addition, we introduce interior boundaries in order to implement the sub-grid turbine model. These boundaries are located at and aligned with the barrier gates and turbines, and are created by locally disconnecting the mesh, see Fig. 4.3. The action of the turbines and/or barrier gates is simulated by expressing the volume flux between the resulting pairs of opposite points in terms of the water level difference between these points. The corresponding head-discharge relation is used to prescribe the flow velocity at interior boundaries, which provides the desired dynamic coupling between water levels at neighbouring nodes on both sides of the barrier location. It now remains to quantify this relation for the various gate-turbine configurations.

SUB-GRID TURBINE MODEL

The basis of the head-discharge relation used for the sub-grid turbine parameterization is the analytical model given in *Verbeek et al.* (2020a). In this model, the device-scale processes are quantified by combining two existing approaches, a head-discharge relation describing the flow over a long-crested weir (*Battjes and Labeur*, 2017), and an actuator disk model to calculate the performance of a single turbine in a channel (*Garrett and Cummins*, 2007). The resulting head-discharge relation for the turbines/gates takes the following generic form,

$$q = d_c u_c = (\zeta - b_c)\sqrt{\frac{2g\,\Delta h}{f}} \tag{4.1}$$

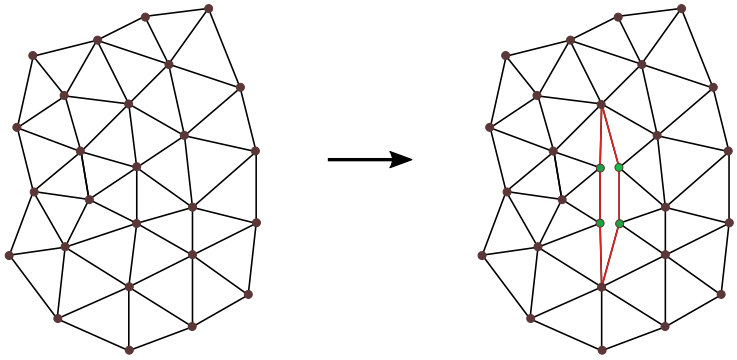

Figure 4.3: Creation of an interior boundary (indicated red) by duplication of associated nodes (indicated green)

in which q is the volume flux at the gate per unit width, $d_c = \zeta - b_c$ is the water depth at the weir crest, ζ and b_c are, respectively, the water level and bed level at the weir crest, u_c is the depth-averaged flow velocity at the crest, g is the gravitational constant, Δh is the head difference over the gate, and f is a dimensionless head loss coefficient

The geometrical parameters ζ and b_c depend directly on the dimensions of the gate and the adjoining water level. To account for the influence of the free surface height on the blockage, we use a time-variable, uniform water level ζ by averaging the water levels upstream and downstream of the gate obtained from the shallow-water model. This is allowed if the head difference Δh is small relative to the water depth, and only acts as a pressure force driving the flow.

The discharge coefficient f emulates all device-scale processes, and depends on the specific turbine-weir configuration. We distinguish turbines on a flat bed, turbines upstream of a weir, turbines downstream of a weir, and a weir only. The different cases are characterized by the distance between the turbine rotor and weir crest, the rotor diameter, and the deceleration of the flow velocity behind the turbine. The latter is specified as the dimensionless ratio of the initial velocity in the turbine wake and the undisturbed ambient velocity. This parameter, referred to as α_5, depends on the turbine operation and is to be obtained from experiments and/or field tests.

To derive closed algebraic expressions for f, the flow passing the weir and turbines is schematized by means of two streamtubes, a streamtube passing the rotor disk, and a streamtube following the entire bypass flow (see Fig. A.2). Assuming quasi-steady flow (inertia terms and local mass storage can be neglected), one-dimensional balances of mass, momentum and energy apply to both streamtubes. The tubes interact via pressure forces, that depend on their spatial configuration, leading to a set of coupled equations. This can be solved analytically to give the distribution of the flow over both streamtubes, the head-loss coefficient f, and the turbine thrust and power coefficients, see A.3.1 and the supporting material in Sec.A.4.

The derived head-discharge relation is applied to the flow component normal to the interior boundary. This is in accordance with the physics of turbines, as horizontal-axis turbines extract streamwise momentum from the flow. However, it also requires that the mesh contours within the model are aligned with the turbine-swept planes, which is easily

accomplished when using an unstructured mesh. Provided this condition is met, our sub-grid turbine parametrization can be coupled to other types of spatial discretization as well, for which computer source code is available in the supporting material in Sec.A.4.

4.2.3. MODEL VALIDATION

The coupled model has been validated elaborately with field - and experimental data, which is described in detail in the supporting material in Sec.A.4. In essence, the validation showed that the model predicts the magnitudes of the head loss and discharge through a gate with turbines quite well, with a relative accuracy of more than 80%, which is close to the accuracy of the measurements. Furthermore, the model very accurately predicts the turbine thrust and power coefficients. However, for a turbine placed upstream of a weir the power was overestimated by approximately 60% in the field situation. With a view to the results below, the latter implies that for this particular turbine-weir configuration the computed added resistance of the tidal farm may be on the conservative side.

There remain a few points of attention when applying the coupled model. First, the wake recovery downstream of the turbine arrays and the barrier (which influences the performance of the tidal farm) is simulated by using a Smagorinsky turbulence closure model (*Talstra*, 2011), an approach that should be refined however if wake development need to be resolved with greater accuracy. Furthermore, the bed level used in the mesh at the sub-grid location must be based on the nearby bottom bathymetry, excluding the weir-gate geometry, as the later is already accounted for in the sub-grid model. Lastly, the wake velocity factor α_5 is used as a calibration parameter for which the turbine characteristics must be known beforehand in order to predetermine a realistic range of values (see Sec. 4.3.2 for the calibration of α_5).

4.3. CASE STUDY EASTERN SCHELDT TIDAL BASIN

This section describes how the developed tool is used in a case study. We determine an optimal configuration of turbines in the storm surge barrier of the Eastern Scheldt by varying the number of turbines and their spacing. First, the study area and the tidal energy pilot project are introduced after which the tidal model for the Eastern Scheldt and the sub-grid model for the adopted turbines are calibrated. Thereafter, the results of the optimization study are analysed, considering the performance as well as the environmental impact of the tidal farm.

4.3.1. TIDAL DYNAMICS

The Eastern Scheldt is a tidal basin located in the southern part of the North Sea, with a large semi-open storm surge barrier in its inlet (see Fig. 4.4). The barrier has a total length of 8 km, spanning the three tidal channels (from North to South) Schaar, Hammen and Roompot, and also includes two barrier islands separating the channels. The construction of the barrier consists of a submarine dam, with sixty-two parallel open gates on top distributed evenly over the three channels. The gates, which are 40 m in width, are formed by concrete piers with a bed beam - or weir. Bed protection, consisting of boulders and asphalt mastic , extends to six hundred meters up- and downstream of the barrier to protect the local seabed against the impact of the high current velocities near the barrier.

A pilot project that started in 2015, involved the deployment of five horizontal-axis

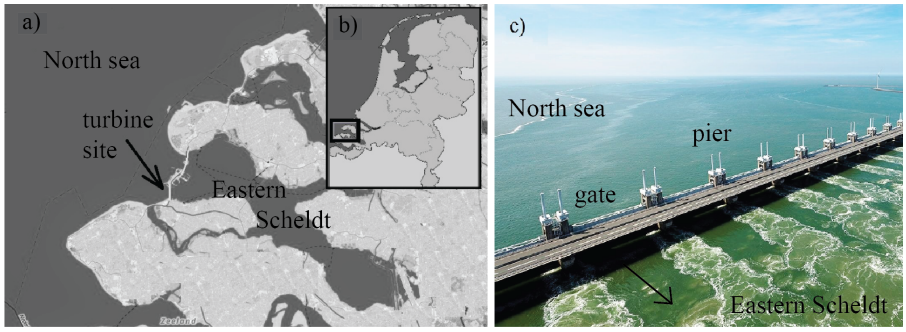

Figure 4.4: The Eastern Scheldt estuary; horizontal planform showing turbine site (a), location in the Netherlands (b), aerial photograph of the storm surge barrier and its gates (source: Rijkswaterstaat)

tidal turbines which were retrofitted in one gate of this barrier to harness energy from the passing tidal current (*Leopold and Scholl*, 2019; *Verbeek et al.*, 2020a,b). The flow velocity inside the barrier gates amounts up to 5 ms^{-1}, which makes this form of energy generation attractive at this location. Interestingly, the storm surge barrier has room for retrofitting many more turbines. However, it is unclear how the different functions of the barrier structure are warranted when up-scaling the energy yield. The two most important conditions are discussed below and reflected upon in the results.

The storm surge barrier's main objective is flood protection. In particular, the gates of the dam can be closed to protect the south-western part of the Netherlands from coastal flooding. For the integrity of this structure it is imperative that the scour holes, which are forming at either side of the barrier by the strongly contracting flow at the tidal inlet (*Broekema et al.*, 2018), are not further deepened. In *Broekema* (2020) a mitigation strategy for this erosion was proposed where the lateral non-uniformity of the flow upstream of the scour hole is reduced. Interestingly, this is what the tidal turbines could possibly realize, when positioned in the centre of the tidal jet.

Another objective of the barrier is to preserve the nature capital of the Eastern Scheldt basin. The barrier is left partly open to allow tides to pass, thereby sustaining the ecosystem of the area. The sandy inter-tidal flats, which are the most biodiverse locations of the area, need sufficient sediment supply by the tide. Hence, an optimal configuration of turbines involves a minimal reduction of the tidal volume (discharge) and maintains a maximal tidal asymmetry. This is crucial as the construction of the open barrier itself already lowered the so-called tidal volume by 30 percent (*Louters et al.*, 1998). Hence, an optimal turbine configuration in terms of energy yield can compromise the ecological objectives of a site, and vice versa.

4.3.2. MODEL SET-UP AND CALIBRATION

This section summarizes the main issues of the application and calibration of the coupled model to the Eastern Scheldt case study. An extensive overview and discussion of the calibration and the resulting model settings is given in the supporting material in Sec.A.4.

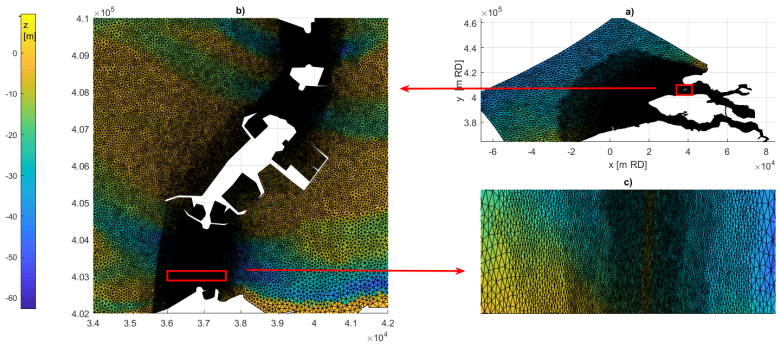

Figure 4.5: Spatial discretization shallow-water flow model, colorbar indicates depth [m] with respect to mean sea level; overall mesh including Eastern Scheldt, Western Scheldt and adjacent North Sea (a), mesh refinement at the barrier (b); mesh refinement near the gates (c)

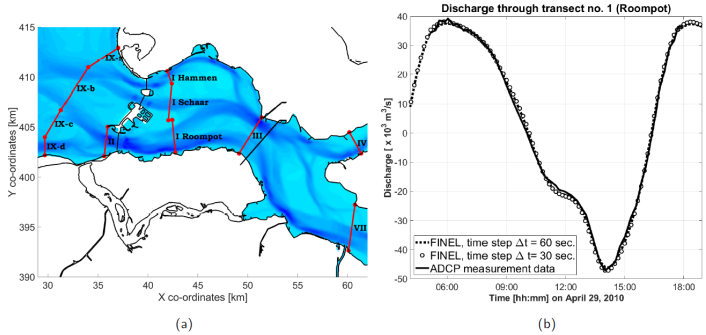

Figure 4.6: Calibration of shallow-water flow model; locations of ADCP transects across the Eastern Scheldt basin used for model calibration (a), computed and observed discharge past transect no. I in the Roompot inlet (b)

SHALLOW-WATER FLOW MODEL

The shallow-water flow model encompasses the Eastern - and Western Scheldt tidal basins, and the adjacent part of the North Sea (Fig.4.5). The size of the triangular elements roughly varies from 5 m at the barrier, via 50 m at the edge of the bed protection and 100 m in the tidal basin, to 2 km in the far field at open sea, which results in about 340,000 elements. The bathymetry is based on data sets of Rijkswaterstaat (Dutch Ministry of Infrastructure), with a high level of detail near the barrier (Fig. 4.6). The tidal water level is prescribed along the seaward boundary of the model, using 95 harmonic constituents obtained from a continental shelf model (*van Leeuwen*, 2016).

The model has been calibrated in *van Leeuwen* (2016) in terms of water levels and discharges; the former using fixed gauges across the region, the latter using Acoustic Doppler Current Profiler (ADCP) transects sailed with a ship (observed velocities have been integrated over various cross sections within the basin to obtain the discharges in the tidal channels, see Fig. 4.6a). As an example, Fig. 4.6b demonstrates the correspondance between the observed and computed discharge in the Roompot inlet (transect no. I).

SUB-GRID TURBINE MODEL

At the barrier, interior boundaries are used in combination with the sub-grid turbine model, in such a way that many different configurations of gates with or without turbines can be chosen. The pillars of the storm surge barrier have been included in this boundary by accounting for their respective blockage widths, which amounts to 12% of the total barrier width.

The velocity coefficient α_5 in the turbine model is calibrated using field data from the pilot project at the Eastern Scheldt barrier (*Verbeek et al.*, 2020a). Based on in-situ velocity measurements along the wake centerline of one of the installed turbines, a velocity coefficient of 0.65 was derived, which conforms to the range of values (0.56 - 0.95) found in experiments (*Verbeek et al.*, 2020a). However, this result relies on the velocity profile that was adopted to relate the measured velocity in the wake centerline to an average value characterizing the entire turbine wake streamtube[1]. We therefore perform a sensitivity analysis by applying the coupled model to the pilot project, for a full neap-spring tidal cycle, using values for α_5 between 0.55 and 0.75.

Fig. 4.7 shows computed and measured thrust, power and velocity data versus the water level difference over the barrier. For the considered range of α_5, the computed turbine power and thrust are almost similar, but the computed local velocity at the turbine shows a better agreement for a velocity factor of 0.65, confirming the value proposed in (*Verbeek et al.*, 2020a), and which is adopted here. At the same time, the computed thrust and power agree well with the measured values during the flood phase, while during ebb these are overestimated by approximately 60%. This overestimation is caused both by the decelerating effect of the turbine strut, which in front of the swept plane during ebb - a factor which is not incorporated in the model, and an overestimation of the wake expansion during the ebb phase (see Chapter 2). In line with the observations, the computed added resistance of the turbines is larger during ebb (turbine upstream of the weir) than during flood (turbines downstream of the weir), where the latter is also slightly underestimated in the computations.

Finally, it should be noticed that the adopted value for α_5 is not necessarily the optimal value regarding power extraction, rather it is a value that corresponds to the observed turbine performance parameters and that we wish to reproduce here.

4.3.3. SCENARIOS

The trade-off between lowering the tidal volume (discharge) through the structure and increasing energy yield is studied by varying the turbine configurations in a systematic way. As a guiding principle we use the concept of multi-scale dynamics introduced in (*Nishino and Willden*, 2013). Turbine configurations are thus characterized in terms of their local blockage, array blockage and farm blockage, relating the respective areas of obstruction to the total flow cross section for a turbine or group(s) of turbines (*Cooke et al.*, 2016). The local blockage (B_L) is defined as,

$$B_L = \frac{\frac{1}{4}\pi D^2}{d(D + s_L)} \tag{4.2}$$

[1]The measured velocity deficit in the wake centerline equals half the undisturbed incoming flow velocity which, by assuming a parabolic velocity profile over the wake cross section, corresponds to an average velocity factor of 0.65 for the wake streamtube.

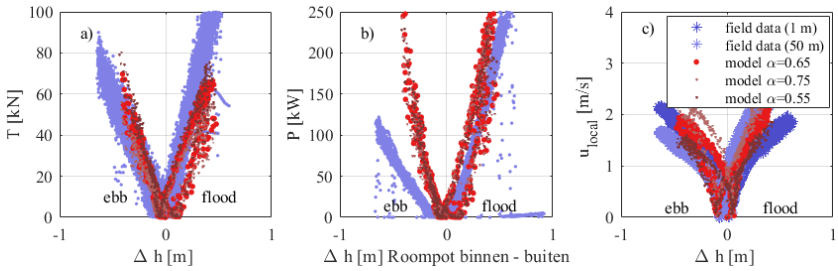

Figure 4.7: Calibration of the sub-grid turbine model; turbine thrust (a), turbine power (b), and flow velocity at turbine (c) versus corresponding water level difference (Δh) over the barrier.

4

Table 4.1: Cross-table indicating the different model scenarios, varying the number of gates filled with turbines (n, farm blockage B_F) and the number of gates left empty in between (s, array blockage B_A); number of turbines per gate (m) equals 5 (local blockage $B_L = 0.3$).

n	0	1	2	5	8	10	15	30
B_F	0	0.03	0.05	0.13	0.21	0.27	0.4	0.8
$s=0,\ B_A=1$	X	X	X	X	X	X	X	X
$s=1,\ B_A=0.5$			X	X	X	X	X	
$s=2,\ B_A=0.3$			X	X	X	X		

where D is the turbine diameter, d is the water depth and s_L is the intra-turbine spacing. Referring to a cluster of turbines in a single gate as an array, the array blockage (B_A) is defined as,

$$B_A = \frac{m(D+s_L)}{m(D+s_L)+s_A} \tag{4.3}$$

where m is the number turbines in a gate, and s_A is the horizontal distance between gates with turbines. In a similar way, the farm blockage (B_F) is defined as,

$$B_F = \frac{n(m(D+s_L)+s_A)}{W} \tag{4.4}$$

where n is the number of gates with turbines and W is the total width of the barrier or inlet.

Our scenarios consider the souternmost inlet of the basin (Roompot) which has 30 gates spanning a total width of 1.5 km. Corresponding to the situation of the pilot study, the number of turbines in a gate (m) is set to 5, giving a local blockage B_L of 0.3. In order to generate independent combinations of farm - and array blockage, we vary the total number of gates with turbines (n), and the number of open gates alternately left open (s). This results in scenarios with 0, 1, 2, 5, 8, 10, 15 and 30 gates with turbines, where - starting at the 8th gate from the south - turbines are placed in neighbouring gates ($s=0$), in every 2$^{\text{nd}}$ gate ($s=1$), or in every 3$^{\text{rd}}$ gate ($s=2$). The resulting combinations of farm - and array blockage are summarized in Tab. 4.1.

In the simulations, overall discharge (tidal volume), power output and power coefficient of the turbines are monitored, while keeping the overall tidal forcing (mean neap-spring tidal cycle) and turbine performance parameters constant.

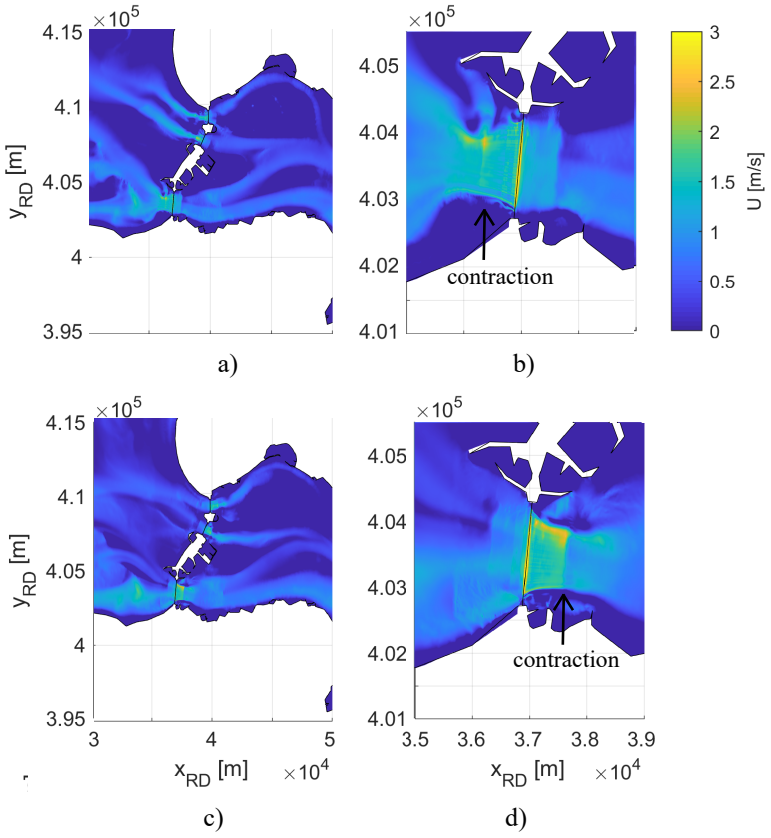

Figure 4.8: Computed flow fields at the inlet of the Eastern Scheldt; western basin, maximum ebb (a), Roompot, maximum ebb (b), western basin, maximum flood (c), Roompot, maximum flood (d); colorbar indicates the depth-mean flow velocity magnitude

4.3.4. RESULTS

This section presents the modelling results of the considered scenarios. First, the general characteristics of the ambient tidal flow in the inlets of the Eastern Scheldt are described. Thereafter, the power output from the turbines and the ways in which turbines affect the tidal exchange are considered.

REFERENCE SCENARIO

For the reference scenario ($n = 0$), the flow towards the barrier contracts horizontally and vertically due to, respectively, the horizontal planform of the tidal inlets of the Eastern Scheldt and the presence of a bottom sill at the barrier *Broekema* (2020). This is illustrated in Fig. 4.8, showing computed flow fields in the inlet during the maximum ebb and flood stages. In every inlet a tidal jet forms that varies periodically in time in response to the tide, with a pronounced asymmetry between ebb and flood as described in *Valle-Levinson and Guo* (2009). A free shear layer with two counter rotating vortices is developing on either side

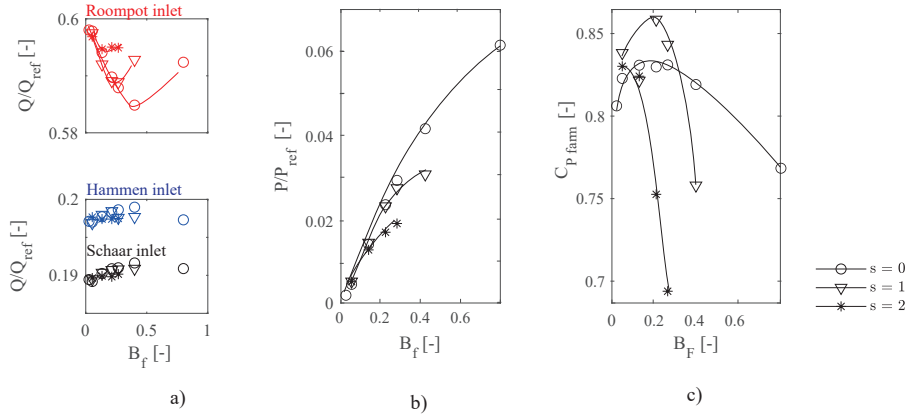

Figure 4.9: Scenarios for turbine placement in the Roompot inlet: computed tidal volume and turbine performance characteristics versus farm blockage (B_F); tidal volume (Q) passing the respective inlets (Roompot, Schaar and Hammen), normalised by the tidal volume (Q_{ref}) in the reference scenario (a), total power output of turbines (P) normalised by a theoretical maximum given by $P_{\text{ref}} = \rho g \int \Delta H Q \, \mathrm{d}t$, where ΔH is the available water level head and Q the corresponding discharge through the barrier in the reference scenario (b), mean power coefficient of the installed turbines (c); all panels present data for one model day, interpolation splines are added as visual aid only.

of the jet directly downstream of the barrier. Paradoxically, the velocity in the jet increases in downstream direction, where also the depth increases due to the presence of scour holes. This effect is due to further contraction of the jet by the downward bed slope, a phenomenon that causes ongoing erosion of the scour holes *Broekema* (2020). Superimposed on the tidal jet, narrow neighbouring jets are present in the flow pattern, associated with the individual barrier gates. This general flow pattern confirms the schematization of the flow and the associated processes as outlined in Sec. 4.2.1.

TURBINE SCENARIOS: TIDAL DISCHARGE AND POWER OUTPUT

The results for the considered scenarios are summarized in Fig. 4.9, in terms of the tidal volume passing the tidal inlets, the power delivered by the turbines, and the associated power coefficient, which are plotted versus the farm blockage (B_F).

For an increasing farm blockage, the tidal volume passing the Roompot inlet initially decreases until a certain minimum - depending on the array blockage the reduction amounts upto 1.5 % of the reference volume (Fig. 4.9a). This tidal reduction results from the additional resistance by the turbines, which increases with the total turbine area and also depends on the array spacing. Remarkably, the tidal volume partly recovers when turbines are distributed evenly over the full span of the barrier, instead of being placed in the mid sections only. The former is the case for low farm blockage with high inter-array spacing, as well as for higher farm blockage with lower inter-array spacing, where arrays of turbines also occupy the gates nearest to the shore lines. This involves a more uniform distribution of the resistance over the barrier width, which reduces the lateral velocity gradient and the associated expansion losses in the wake flow. In any case, the loss of tidal volume in the Roompot is almost completely compensated by a corresponding increase in the other two

inlets, Hammen and Schaar, the overall impact of the turbines on the tidal exchange being less than 1%.

Fig. 4.9b presents the overall power output of the turbines for the considered scenarios normalized with the total power available in the flow passing the inlet. Generally, the power output increases with the number of turbines. For a given farm blockage, the output is highest when turbines are placed in neighbouring gates ($s = 0$) and lowest when arrays are separated by two empty gates ($s = 2$). The latter is the result of the increased inter-array bypass flow when the array blockage decreases. At the same time, the marginal output decreases when installing more turbines, moreover when the farm blockage is large. This is attributed to the deployment of less effective arrays in the nearshore gates of the barrier where the depth and flow velocities are relatively small.

Fig. 4.9c displays the power coefficient, which is a widely used variable to express the efficiency of turbines for harvesting energy from the flow. Interestingly, the scenarios with an inter-array spacing of one gate ($s = 1, B_A = 0.5$) have the highest power coefficient, which peaks at 0.86. This confirms the analytical prediction in *Cooke et al.* (2016), who found a peak value of 0.865 for an optimal array blockage of 0.4. For $s = 1$, the power coefficient decreases to about 0.75 if the farm blockage exceeds 0.3, which is equivalent to more than ten gates being filled with turbines. As similar decline occurs for both the other inter-array spacings ($s = 0, s = 2$), albeit for a different total number of turbines. The inclusion of gates near the sides of the tidal inlet channel when the number of turbines approaches its maximum limit is the most important factor explaining this effect.

TURBINE SCENARIOS: AMBIENT FLOW EFFECTS

The effects of the turbines on the ambient flow patterns in the Roompot tidal inlet are discussed by considering two moments during ebb and flood, respectively, for which the head difference over the barrier and the correspoding flow velocities are maximum. As an example, Fig. 4.10 shows spatial patterns of the flow velocity deviation, relative to the reference situation, for all scenarios with 10 gates being filled with turbines. This number is chosen since it translates to a farm blockage that is close to the theoretical optimum for energy extraction (*Cooke et al.*, 2016).

Downstream of the barrier, the flow velocity decreases *behind* the gates with turbines (the wake), and increases *between* gates with turbines (the bypass). A similar pattern can be recognized at the scale of the tidal farm as a whole, where downstream of the farm the flow is generally decelerating, while in the large-scale bypass around the farm the flow is mostly accelerating. The farm thus redistributes the discharge in the tidal channel, which is characterized by a reduction of the flow contraction behind the barrier.

Upstream of the barrier, the ebb flow decelerates towards the tidal farm over a rather uniform zone, while during flood the deceleration occurs over confined areas just upstream of individual turbine arrays. This indicates that during ebb the gate-gate interaction is governed by the farm blockage while during flood the array blockage is more prominent in this respect. This stems from the deployment of the turbines on the landward side of the barrier gates, which implies a larger added resistance during ebb, and a more pronounced effect on the flow fields, compared to the flood situation. For the same reason (results not shown here), a larger impact occurs when either more gates are filled with turbines (increasing the farm blockage), or when turbine arrays are placed closer to each other (decreasing the array blockage), moreover so during ebb.

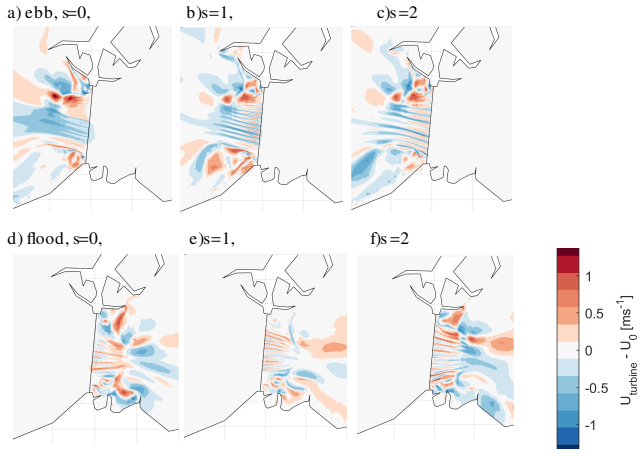

Figure 4.10: Ambient flow effects: velocity deviation in the southern channel inlet (Roompot), relative to the reference scenario, for scenarios with ten arrays of turbines; upper panels: maximum ebb flow for $s = 0$ (a), $s = 1$ (b) and $s = 2$ (c); lower panels: maximum flood flow for $s = 0$ (d), $s = 1$ (e) and $s = 2$ (f)

At basin scale, the influence of the turbines on the flow pattern extends beyond the Roompot tidal inlet, by means of their added resistance. The latter depends on the farm blockage and the position of the turbines with respect to the flow direction (i.e., ebb or flood). The added resistance increases the head difference over the barrier, compared to the reference situation, and causes a small time lag of the tidal water level variation in the entire basin. This increases the discharge in the two northern inlets Hammen and Schaar, where the additional resistance is absent, which alsmost compensates for the decreased discharge in the Roompot inlet.

The above analysis reveals a clear relation between the added resistance and the redistribution of the flow over the barrier across a range of scales, from a single array of turbines to one tidal inlet and even the entire basin entrance. This may be utilized to manipulate the tidal jet, mitigating its scouring potential that presently causes ongoing erosion downstream of the barrier.

4.4. DISCUSSION

The discussion will first address the application range of the proposed model and its further development steps. Thereafter, different turbine configurations and their trade offs and compromises are discussed.

4.4.1. MODEL APPLICATION RANGE

This article proposes a model for optimising the configuration of turbines over a barrier with parallel gates, in order to harvest energy from the flow while sustaining the ecological value of the hinter-lying basin. The model can be applied during both the start-up and

the realization of a tidal energy project. In both phases, changes in hydrodynamic patterns and energy yield need to be explored for alternative turbine configurations, as this is key to balance multiple criteria regarding harvesting energy, sustaining barrier integrity and preserving ecological value.

We are not alone in pursuing such a modelling tool; some other numerical models have been proposed in literature for simulating the performance of free stream turbines in different (farm) configurations (*Nishino and Willden*, 2012a; *Funke et al.*, 2014, 2016; *Angeloudis et al.*, 2016). Unlike these efforts, our model is validated against elaborate sets of both experimental and full-scale turbine data, also capturing the turbine-barrier interaction. The latter involves an unstructured mesh for the shallow-water flow model in order to resolve the interaction of the turbines with a barrier as well as with a complex basin bathymetry, over a wide range of scales, an approach that is also favoured in (*Angeloudis et al.*, 2016).

The article presents an application of the model to a thoroughly monitored field case. In the analysis of this pilot, it was suggested that certain turbine configurations can solve local issues in the hydrodynamics by using a dedicated turbine-configuration. In particular, the lateral velocity profile in the adjacent tidal channel can be manipulated, decreasing the contraction of the tidal jets, which reduces the scouring potential of the flow downstream of the barrier.

As a first step, the present work intended to investigate the flow processes in the basin driving the turbines, using fixed turbine - and configuration settings. For applying the developed tool to future tidal energy projects, a useful extension of the model would be an automatic optimization of these settings with regard to the underlying project goals. For our target application of barrier mounted turbines, different tresholds or weights would be needed, reflecting the project criteria, in order to make an automatic optimisation feasible.

4.4.2. TRADE-OFFS AND COMPROMISES OF FARM CONFIGURATIONS

The optimal configuration of turbines in a barrier is not simply dictated by a numerical result only. In particular, the configuration yielding a maximum energy extraction, when all gates are filled, may involve compromises regarding the structural integrity of a barrier and the ecological impact, the latter being expressed as a reduction of the tidal volume. All trade-offs and compromises have to be put into perspective before adopting a particular alternative. We therefore reconsider the implications for the Eastern Scheldt case, followed by a short discussion of other tidal farm locations, arriving finally at the broader implementation of the EU targets.

Our analysis shows that, accepting a change of the tidal volume of at most 1 percent of the reference situation, room for at least 10 gates with turbines is present. They harvest most energy from the from the flow (highest power output per turbine area, and highest degree of gate-gate enhancement) when configured directly neighboring each other in the centre of the inlet, where the flow velocity is highest. An additional advantage of this choice, regarding the structural integrity of the barrier, is that the contraction of the tidal jet in the inlet is suppressed by this configuration. The latter may decrease the scour potential of the flow at either side of the barrier, as was discussed in Sec. 4.3.1. Besides, the flow asymmetry enforced with a turbine deployment in only one of the three tidal inlets, may induce more sediment transport into the basin than a more symmetric arrangement where turbines are spread evenly over the three inlets (*Gatto et al.*, 2022, submitted). This

is considered favourable for sustaining the biodiverse tidal flats in the area, as discussed in Sec. 4.3.1.

In other turbine–barrage projects around the world, finding the right balance between environmental (flow) effects and turbine energy yield is also a prerequisite. For example, in the Larantuka Strait, Indonesia, where a so-called tidal bridge is planned, both energy yield and the far field flow effects are crucial for its realization (*Ahmad M. Firdaus*, 2020). In this respect it is noteworthy that the presented research shows that the far-field flow effects of turbines inside barriers are relatively small. In particular, the added resistance of turbines in an open barrier appears to be lower than estimated before (*Gatto et al.*, 2022, submitted; *Ouro and Stoesser*, 2019), rendering the estimates less conservative. This enables projects to combine a relatively high energy yield (trade-off) with a limited enviromental impact, provided the proper choices are made. The proposed model can help in finding this balance.

4.5. CONCLUSION

The twofold aim of the research described in this chapter was, first, to develop an accurate and efficient model to study an optimal configuration of turbines in a barrier, and second, to apply it to a realistic tidal site for investigating the energy yield of a tidal farm, and its impact on the tidal volume and flow distribution.

In order to achieve the first aim, the relevant effects of barrier mounted turbines were parameterized, in terms of head-discharge relations, which reduces the computational effort. This parametrization was then coupled to a shallow water flow model which is based on the finite element method. The turbines are implemented by means of interior boundaries along which the head-discharge relations for weir-mounted turbines are prescribed. The latter are derived from a theoretical model which was validated using field and experimental data.

To achieve the second aim, the model is applied to a thoroughly monitored tidal energy pilot project in the Eastern Scheldt basin. The analysis shows that energy is most efficiently harvested from the flow if the turbine arrays are configured with an array blockage of about one half (leaving one gate empty between gates with turbines). In this configuration, inter-array interaction increases turbine efficiency, while the added resistance is still limited. When the farm blockage exceeds 0.3 the latter is more substantial, extending the influence of the turbines to the other tidal inlets as well. The results furthermore show the potential to use turbines to manipulate the tidal jet issued from the barrier, in favour of coastal protection and nature preservation. In particular, this may reduce the ongoing scour of the tidal channels near a storm surge barrier, and increase the tidal asymmetry of the flow to enhance sediment import into the basin.

In essence, choosing an optimum tidal farm configuration is far more complex than achieving the largest power output only. The findings of this chapter, and the developed modelling tool, can be used to understand how complex EU ambitions on coastal protection, energy generation and nature preservation can be combined in a tidal energy project.

5

SYNTHESIS

5. Synthesis

Achieving the aim

The aim: Optimizing the configuration of tidal turbines in storm surge barriers

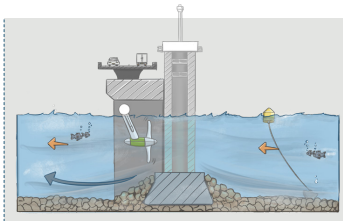

1) Monitoring in the field (small scale processes)

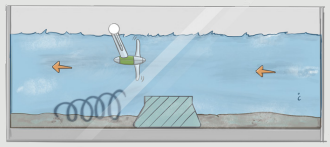

2) Parameter study in the laboratory (small scale processes)

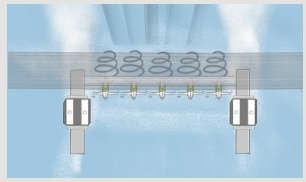

3) Modelling the flow effect (small and large scale)

Three aspects were instrumental to achieve the aim:

1) Study of worlds first array of commercial-scale turbines
2) Study of scaled tidal turbine in the laboratory in different configurations
3) The development of a coupled tool that can calculate small scale turbine influence at larger scale flow in the tidal basin

Finding an optimal balance

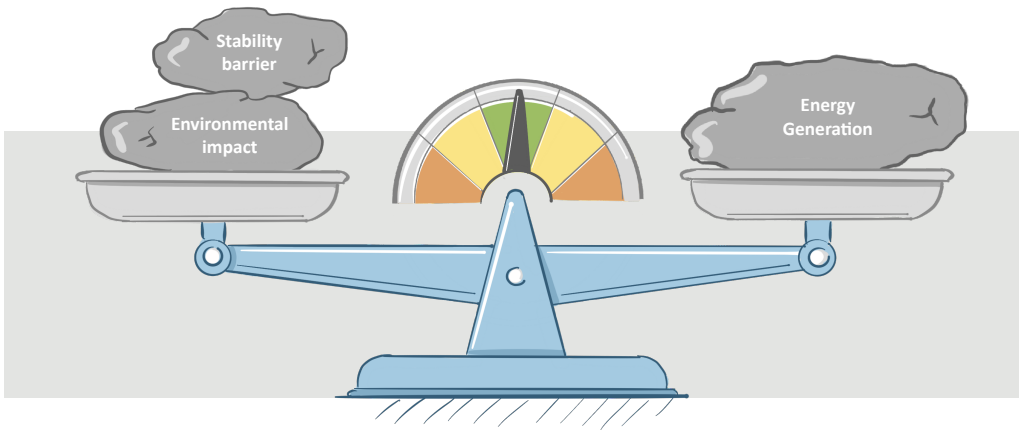

Tool can calculate the complex interaction between tidal turbine, barrier and tidal basin to find an optimal balance between energy generation, barrier stability and environmental impact.

A changing climate and increasing world population brings major challenges to low-lying deltas in the coming decades. CO_2 levels are rising, flood risk is increasing and pressure on nature capital is increasing. EU and NWO ask joint solutions for these challenges. Retrofitting turbines in storm surge barriers is an upcoming and interesting way to generate emission-free power, protect against flooding and stay within environmental constraints. The present research investigated how turbine fences can be optimally placed in barrages (barriers) with regard to these challenges. Correspondingly, the aim of this research was as follows:

> *To develop a physics-based modelling tool to determine an optimal placing of horizontal-axis turbines mounted in a storm surge barrier, with regard to their energy yield and hydrodynamic effects.*

This chapter synthesizes the aspects that were important to meet this aim, gives an outlook for future research and provides implications. Consequently, this chapter is structured as following. Answers to questions underlying the research aim are given in Sec. 5.1. Research outcome that were most important to meet the overall aim are synthesized in Sec. 5.2. And successively the application range of the resulting calculation tool is given in Sec. 5.3. Thereafter, directions for future research are explored in Sec. 5.4. And lastly, implications for the research field are discussed in Sec. 5.5.

5.1. ANSWERING QUESTIONS

In this section the research questions underlying the dissertation aim are answered. Five questions were formulated in Chapter 1. The questions relate to the physics of turbines in barriers, their schematization in hydrodynamic models and their simulation. The questions and their answers are summarized below.

1. What are the main processes governing energy yield and flow effects of commercial-scale tidal stream turbines inside storm surge barriers?

The analysis of high resolution data of the flow through the barrier and around commercial-scale turbines enabled determining the effect of horizontal axis tidal turbines on the water flow on site, in which the power could also be taken into account (Chapter 2). The data showed that local blockage, turbine operation variables (tip speed, blade shape), and contraction and expansion of the ambient flow field governed the energy yield and hydrodynamics of turbines inside a gate of a storm surge barrier. The analysis of Chapter 4 added to this that at the inlet scale also gate-gate interaction and added resistance of the total array of turbines are important, in particular, if multiple turbines are configured in parallel gates of a barrier inside a tidal inlet.

2. How to predict the energy yield of turbines in barriers using an analytical flow model that can serve as a sub-grid formulation in a regional flow model?

The insights from the flow field surrounding the commercial-scale turbines in the Eastern Scheldt (Chapter 2) provided the fundamental basis for an analytical model, which can predict both the energy yield of turbines mounted close to a weir in a barrier gate and the combined resistance of turbine and barrier. The information was used to extend the model of *Garrett and Cummins* (2007) and *Nishino and Willden* (2012b) to include a turbine in a

hydraulic structure, where the latter was schematized as a step in the bed. This model is based on 1D balances of mass, energy, and momentum of the flow passing a turbine that is schematised as an actuator disk (in line with the work of *Betz*, 1920, *Lanchester*, 1915).

3. How does the geometry of a gate of a storm surge barrier affect energy yield and hydrodynamics of turbines mounted inside this gate?

The generated power was strongly dependent on the position of the turbine relative to the gate weir of a storm surge barrier. Surprisingly, the combined resistance of a weir plus turbine is lower than the sum of the individual resistances. The suppression of the wake behind the weir by the accelerating flow around the turbine is responsible for this.

In other words, the geometry of the gate forces the flow to contract (upstream the gate) and expand (downstream) when passing. As a result of the flow contraction, the power coefficient generally increases if a turbine is placed in a gate compared to an unconstrained situation. The energy yield of the turbine in the gate was largest if the local blockage was highest, that is, when the turbine was placed at the gate center above the weir crest, but only when allowing space for a favourable wake configuration.

4. How to develop a model for storm surge barriers with turbines, from the turbine device to the estuary scale, for the purpose of optimizing turbine configuration in barriers based on their energy yield and their hydrodynamic effects?

In order to develop the desired model, turbine effects in barriers are parametrized in Chapter 4, including relevant processes and reducing computational effort. The analytical model resulting from Chapter 2 was used as basis for this parametrization. The parametrization was coupled to the large scale flow by imposing head-discharge relations as internal boundary conditions locally, where turbines were present. The larger scale flow is solved using a Finite Element discretization of the depth-averaged Shallow Water Equations and elaborately validated using data from the physical model and field study. This makes it possible to optimize existing or new tidal power stations based on their energy yield and to determine the impact on the environment (in particular the hydrodynamic aspects).

5. What are effects of multiple turbine configurations on energy yield, nature capital and flood protection in a tidal pilot (case study)?

Thereafter, the model is applied to the thoroughly monitored pilot project for tidal energy in the Eastern Scheldt tidal basin in Chapter 4. The analysis shows that most energy is harvested with largest turbine area. However, this has significant impact on the tidal volume passing the barrier. Therefore, it would be more interesting to chose a configuration where the reduction of tidal volume is less and energy is most efficiently harvested from the flow, e.g. if turbine arrays are fitted with one gate left empty between gates with turbines (array blockage of a half). The efficiency peaks at a total number of ten arrays in this configuration. For the Eastern Scheldt barrier, this gives a total number of fifty turbines when assuming similar turbines as currently in the pilot. This turbine placing is beneficial as inter-array interaction is present, but added resistance of the turbines is limited. In particular, the limited added resistance results in a tidal volume decrease through the storm surge barrier of less than 1.5% for this case. The latter is a

promising result, comparing with a decrease of 30% for construction of the storm surge barrier (*Louters et al.*, 1998).

The results furthermore show the potential to use turbines to manipulate the flow through the barrier (tidal jet) in a certain direction as benefit for coastal protection and nature capital. In particular, to reduce the ongoing scour at the sides of the storm surge barrier and to increase asymmetry of the tide in the basin to increase sediment transport locally.

The above answers are a first step towards answering the overarching question of this research: how to configure turbines optimally with regard to the different challenges in (a particular delta). Below we elaborate on which aspects particularly contributed to this answer.

5.2. SYNTHESIZING RELEVANT ASPECTS

Three aspects of the presented research are of main importance to achieving the aim of this dissertation: the data obtained in the field study, the parameter study and the larger scale model. The data were essential to make a valid representation of the small scale processes, the parameter study validated its range of application and the larger scale model enabled calculating effects of alternative configurations of turbine installations. All were important to optimize turbine placing in and over a barrier.

The first aspect, the data obtained in the field study of Chapter 2, enabled an accurate and physics based schematization of the flow through a gate with weir-mounted turbines. It was accurate, because assumptions on the flow field and turbine performance were directly based on the data of the full scale turbines, which do not have the burden of scale effects; and because measurements were done up and downstream of these turbines over a full spring-neap cycle. The resulting schematization was physics based, because the data allowed identifying the processes driving the performance of turbines inside barriers (e.g. blockage effects and influence of a recirculation zone), which were directly schematised in an analytical model for processes of the so-called 'small scale'. The model estimated power deviated approximately 10% from the data from the laboratory tests in operational conditions. At the same time, the computed thrust and power agree well with the measured values in the field for the situation where at turbine is upstream a gate weir, while when it is downstream these are overestimated by approximately 60%.

The second aspect, the parameter study of Chapter 3, supported the assumptions made for this analytical model on the small scale and proved its range of application. It showed how the performance and resistance of a turbine evolved for alternative geometries, whereas in the field study only two weir-turbine configurations could be assessed. The analytical model was coupled to the so called 'larger scale' model.

The third aspect, the larger scale model itself, enabled quantifying the energy yield and hydrodynamic effects of turbines mounted in parallel gates of a barrier in different configurations. It allows a user to optimally configure tidal stream turbines in barriers at two scale levels: inside the storm surge barrier gates (small scale) and over the parallel gates of the storm surge barrier (large scale). As such, a configuration can be chosen with high energy yield and calculated impact on the surrounding, exploiting the link between the smaller and larger scale processes. The output of the large scale model is the resulting flow pattern within the estuary surrounding the turbines, incorporating interactions between gates with turbines, effects of gates on the flow in the tidal inlet, and on the overall flow

in the basin.

The application of this model to the case of the Eastern Scheldt shows that smartly optimizing the placing of turbines can lead to a 50% increase of the harvested power, with only a 1.5% decrease of tidal volume, at an example of ten gates filled with turbines. The latter is important at this location as the tidal volume transports nutrients and sediment to biodiverse tidal flats in the hinter-lying basin. And in this way, nature capital can be sustained in this location. For the Eastern Scheldt this optimum may lie at 10 gates filled in the barrier center, given the above considerations. However, the optimum depends on how you quantify the implications for each discipline (energy yield, nature capital and flood protection) in a particular tidal site.

5.3. MODEL APPLICATION RANGE

The developed model tool can be applied to other sites as well. However, the user should note that it is valid for a well-defined set of practical cases.

These cases can be characterized as following: a range of barrier geometries with a local blockage (turbine occupation ratio) between 0.1 and 0.7, a relative gate weir height between 0.1 and 0.3 (which imply low Froude numbers) and a distance of the rotor swept plane to the gate weir of at most two rotor diameters. For these cases, the model thrust estimate was approximately 10% deviating from the data points from the laboratory experiment as a result of assumptions underlying the model and measurement accuracy in the tests (see Chapter 3). Three-dimensional computational fluid dynamics must be considered in other cases where more accurate results are required. One should also consider that the presented model is calibrated for a limited set of cases.

In the presented research the model is calibrated for a horizontal axis tidal turbine in a barrier with high blockage conditions. This requires attention when applying the model to for example a vertical axis turbine in lower blockage conditions or to a different type of hydraulic structure (e.g. a bridge with vertical piers instead of a horizontal weir). At least the velocity coefficient in the rotor plane or wake, α, should be re-calibrated for these new cases, as it may apply to a specific turbine-structure design and blockage conditions. The reason these situations can potentially be studied with the presented model is that tip speed ratio and blade shape are not specified directly in the model, but represented by an energy-extracting disk lumping all design and operational information into velocity coefficients. And because flow is schematized as a channel with three streamtubes: one through the rotor, one bypassing the turbine and one in the recirculation zone (downstream the piers or a weir). However, there are also cases for which the current model formulation needs to be adjusted or further validated. This can be part of future research.

5.4. FUTURE RESEARCH

For example, the model may become more accurate for the case where a turbine is upstream a step in the bed by improving the schematization of the wake expansion over the gate weir for this case. Also, the effects of free-surface deformation and inter-array interaction could be integrated in the model, using the work of *Whelan et al.* (2009a) and *Nishino and Willden* (2012b), respectively, making the model applicable to higher Froude numbers and more accurate in situations with larger arrays of individual turbines. Besides, it may be interesting to validate the existing model further with attention to processes in between the

small and large scale, as this will increase the trust in the results for the current application.

In particular, the interaction between gates with turbines was not validated in the field situation nor in the laboratory study, while this was shown to be important in the larger scale model study. The flow effects of two neighbouring gates with turbines can be validated in future research with a field survey of a new full scale pilot study. Another possibility would be to model the scale interaction using Large Eddy Simulation (LES) (e.g. using the work of *Guinée* (2021)), which better capture the mid-scale processes than a depth-averaged modelling approach which was followed in this work. Or to validate modelling results (e.g. wake length and flow velocity distribution) with data from physical model studies of turbine-turbine interaction without barrier influence (e.g *Stallard et al.* (2015)). Though, currently the model is already accurate enough to give good view on processes related to the environmental impact of turbines in barriers.

Therefore, it would be valuable to the turbine sector to further apply the developed model to answer questions on the environmental impact of turbines in barriers. A good example, which is currently of interest to turbine manufacturer Tocardo, is to investigate the impact of turbine operation on the locally applied bed protection surrounding a storm surge barrier. Changes of bed shear stresses in a 3D simulation of our model could provide a good basis to address this question. This application of the developed method brings us to the broader implications of this work.

5.5. IMPLICATIONS

Important assets of this research are the integral approach taken and the coupling of spatial scales. It integrates insights on turbine hydrodynamics from commercial-scale turbine operation with theoretical, numerical, and physical models and applies it to questions from science, turbine engineers, ecologists and infrastructure owners at different scale levels. Consequently, there are implications of this work in different domains: fundamental, practical and societal. First two fundamental implications are discussed, one for the analytical and one for the numerical modelling field.

Firstly, we empirically determined that in a tide-dominated system the turbine performance model of *Betz* (1920) and *Garrett and Cummins* (2007) is valid regardless of the tidal stage. This means that this model may be more robust than previously assumed. Important variables in this type of analytical models, such as: the wake deceleration, bypass acceleration and thrust coefficient, were similar for different tidal stages in a commercial-scale tidal turbine array. This is important as most analytical turbine performance models use a quasi-steady approximation of the flow to model turbine performance.

Secondly, we have introduced an efficient and elegant way to couple two models of different scales by applying an internal boundary condition locally where turbines are present in line with the work of *Angeloudis et al.* (2016). This method may be more accurate than using a momentum sink approach, as no undisturbed inflow velocity is needed in our calculation. But, more importantly, our approach is elaborately validated using laboratory and field measurements. The latter enables making more accurate estimations of energy yield and environmental effects of tidal energy initiatives (in barriers).

Three research outcomes in have more practical implications. They particular contribute to our understanding of flow effects of tidal energy and can thus facilitate tidal energy projects with calculated environmental impact and limited impact to the barrier structure stability in the future.

Firstly, our research shows that disturbances in the flow caused by the presence of turbines inside barriers are smaller in the far field than estimated with conservative model tools. This implies that more turbines can be installed in tidal energy projects than previously thought based on conservative models. An example of a conservative method is from *Gatto et al.* (2022, submitted) who calculated turbine influence in barriers as momentum-sinks using porous disks, excluding beneficial effects of turbine-weir interaction on flow resistance. The small flow effects of turbines in barriers in the far field, incorporated in our calculation tool, is a result of suppression of turbulence generated at the irregular bathymetry at a barrier by the turbine presence.

Secondly, our results show that every configuration of turbines results in a unique net resistance to the flow. This means that placing multiple turbines is more complicated than previously thought. However, it also shows that it is worthwhile to model the effects of alternative configurations to find an optimum. In particular, we argue that every configuration of turbines has its own unique relation between upstream water levels and local velocity. This means that simply calculating discharge factors for gates in barriers does not suffice to estimate the impact accurately. This may also apply to parallel-gated structures not operating in tidal environments, such as the discharge control structures Pannerden and Hondsbroekse Pleij in the floodplains of the Dutch Rhine river.

Thirdly, the analysis in *Verbeek et al.* (2020c) has shown how retrofitting turbines in barriers can alter shear stress values at the sea bed locally and further downstream the structure compared to a situation without turbines. This has implications for the stability of hydraulic structures with turbines and thus the required bed protection in and downstream of the structure. In particular, the shear stress at the barrier can be slightly increased when the turbines are placed just downstream the barrier weir (*Verbeek et al.*, 2020c). This is currently no issue in the storm surge barrier of the Eastern Scheldt, as large boulders are applied at this location. However, when placing turbines laterally in the barrier centre (e.g. in the gates with highest velocities) the shear velocity and corresponding shear stresses in the far field can be decreased. The latter may reduce the scouring potential of the tidal jet further downstream the structure in the case of the Eastern Scheldt (The Netherlands).

Together, these three research outcomes show how renewable energy is optimally harvested from the flow through bridges and open barriers with calculated environmental impact and limited impact to the structure stability. These implications are not limited to future projects but may also be relevant for already operational projects. Recalculating the optimal configuration of turbines may be useful if moving turbines is realistic. Examples of projects where this could be relevant are in the so-called 'tidal bridge', planned in Larantuka Strait, Indonesia. In this project, both energy yield and the far field flow effects are of importance to the realization (*Ahmad M. Firdaus*, 2020).

Lastly, there is a more societal implication of this work. There are many locations worldwide where this technology (hydraulic structures with tidal energy) can be applied in response to the demand for sustainable energy, flood protection and conservation of natural values. In the Netherlands, the knowledge from the project has been incorporated into a multi-disciplinary study into the expansion of the tidal power plant in the Eastern Scheldt, which represents an important step towards further up-scaling of this form of energy production. Our research contributed to the trust in the economic and technical viability of tidal energy in barriers in the Dutch Delta. The tool is freely available and can be used in engineering applications to further investigate energy yield and environmental

effects of tidal energy projects worldwide.

References

Ahmad M. Firdaus, T. A. A. A., Guy T. Houlsby (2020), Tidal energy resource in larantuka strait, indonesia, *Proceedings of the Institution of Civil Engineers - Energy*, *173*(2), 81–92, doi:10.1680/jener.19.00042.

Angeloudis, A., R. A. Falconer, S. Bray, and R. Ahmadian (2016), Representation and operation of tidal energy impoundments in a coastal hydrodynamic model, *Renewable Energy*, *99*, 1103–1115, doi:https://doi.org/10.1016/j.renene.2016.08.004.

Bahaj, A., and L. Myers (2013), Shaping array design of marine current energy converters through scaled experimental analysis, *Energy*, *59*, 83–94, doi:10.1016/j.energy.2013.07.023.

Bahaj, A., A. Molland, J. Chaplin, and W. Batten (2007), Power and thrust measurements of marine current turbines under various hydrodynamic flow conditions in a cavitation tunnel and a towing tank, *Renewable Energy*, *32*(3), 407 – 426.

Bahaj, A. S. (2011), Generating electricity from the oceans, *Renewable and Sustainable Energy Reviews*, *15*(7), 3399–3416.

Batten, W., M. Harrison, and A. Bahaj (2012), Accuracy of the actuator disc-rans approach for predicting the performance and wake of tidal turbines, *Philosophical Transactions of the Royal Society A: Mathematical, Physical and Engineering Sciences*, *371*(1985), doi:10.1098/rsta.2012.0293, cited By 18.

Battjes, J. A., and R. J. Labeur (2017), *Unsteady Flow in Open Channels*, Cambridge University Press, doi:10.1017/9781316576878.

Betz, A. (1920), Das maximum der theoretisch möglichen ausnützung des windes durch windmotoren„ *Zeitschrift für das Gesamte Turbinenwesen*, *Heft 26*, Seiten 307 bis 309.

Borthwick, A. G. L. (2016), Marine renewable energy seascape, *Engineering*, *2*(1), 69 – 78, doi:10.1016/J.ENG.2016.01.011.

Bray, S., R. Ahmadian, and R. Falconer (2016), Impact of representation of hydraulic structures in modelling a severn barrage, *Computers and Geosciences*, *89*, 96–106, doi:10.1016/j.cageo.2016.01.010.

Broekema, Y. B. (2020), Horizontal shear flows over a streamwise varying bathymetry, Ph.D. thesis, Delft University of Technology, doi:10.4233/uuid:016ee80a-fba2-4534-a578-94e7b35022a9.

Broekema, Y. B., R. J. Labeur, and W. S. J. Uijttewaal (2018), Observations and analysis of the horizontal structure of a tidal jet at deep scour holes, *Journal of Geophysical Research: Earth Surface*, *123*(12), 3162–3189, doi:10.1029/2018JF004754.

Burton, T., D. Sharpe, N. Jenkins, and E. Bossanyi (2002), *Aerodynamics of Horizontal-Axis Wind Turbines*, chap. 3, pp. 41–172, Wiley-Blackwell, doi:10.1002/0470846062.ch3.

Cooke, S., R. Willden, and B. Byrne (2016), The potential of cross-stream aligned sub-arrays to increase tidal turbine efficiency, *Renewable Energy*, *97*(Supplement C), 284 – 292, doi:https://doi.org/10.1016/j.renene.2016.05.087.

Draper, S., and T. Nishino (2014), Centred and staggered arrangements of tidal turbines, *Journal of Fluid Mechanics*, *739*, 72–93, doi:10.1017/jfm.2013.593.

Draper, S., T. Nishino, T. A. A. Adcock, and P. H. Taylor (2016), Performance of an ideal turbine in an inviscid shear flow, *Journal of Fluid Mechanics*, *796*, 86–112, doi:10.1017/jfm.2016.247.

EU (2019), The european green deal, *Tech. Rep. 640*, European Commission.

Europe, O. E. (2023), Ocean energy key trends and statistics 2022, www.oceanenergy-europe.eu/wp-content/uploads/2023/03/ocean-energy-key-trends-and-statistics-2022.pdf, *Tech. rep.*

European Committee (2014), A policy framework for climate and energy in the period from 2020 to 2030, *Tech. Rep. COM(2014) 15*, Communication from the commission to the parlement, Brussels, p. 6.

Fallon, D., M. Hartnett, A. Olbert, and S. Nash (2014), The effects of array configuration on the hydro-environmental impacts of tidal turbines, *Renewable Energy*, *64*, 10–25, doi:10.1016/j.renene.2013.10.035.

Funke, S., P. Farrell, and M. Piggott (2014), Tidal turbine array optimisation using the adjoint approach, *Renewable Energy*, *63*, 658–673, doi:https://doi.org/10.1016/j.renene.2013.09.031.

Funke, S., S. Kramer, and M. Piggott (2016), Design optimisation and resource assessment for tidal-stream renewable energy farms using a new continuous turbine approach, *Renewable Energy*, *99*, 1046–1061, doi:https://doi.org/10.1016/j.renene.2016.07.039.

Garrett, C., and P. Cummins (2005), The power potential of tidal currents in channels, *Proceedings of the Royal Society of London A: Mathematical, Physical and Engineering Sciences*, *461*(2060), 2563–2572, doi:10.1098/rspa.2005.1494.

Garrett, C., and P. Cummins (2007), The efficiency of a turbine in a tidal channel, *Journal of Fluid Mechanics*, *588*, 243–251, doi:10.1017/S0022112007007781.

Gatto, V. M., R. J. Labeur, B. C. van Prooijen, and Z. B. Wang (2022, submitted), Rapid assessment of (small) morphological impacts in intertidal systems: methodology and application to tidal energy, *Coastal Engineering*.

Guerra, M., and J. Thomson (2017), Turbulence measurements from five-beam acoustic doppler current profilers, *Journal of Atmospheric and Oceanic Technology*, *34*(6), 1267–1284, doi:10.1175/JTECH-D-16-0148.1.

Guinée, B. (2021), Numerical modelling of tidal turbines in the vicinity of a weir: Application to the eastern scheldt barrier, Master's thesis, Delft University of Technology, Faculty of Civil Engineering and Geosciences.

Hartsuiker, G., R. Thabet, J. Dijkzeul, and H. Klatter (1989), The storm surge barrier eastern scheldt - evaluation of water movement studies for design and construction of the barrier, *Tech. Rep. Z88; PEGESS-N-89011*, Delft Hydraulics and Rijkswaterstaat, 8300 AD Emmeloord, 4330 KA Middelburg, The Netherlands.

Hofland, B. (2005), Rock and roll turbulence-induced damage to granular bed protections, Ph.D. thesis, Delft University of Technology.

Hoitink, A. J. F., Z. B. Wang, B. Vermeulen, Y. Huismans, and K. Kästner (2017), Tidal controls on river delta morphology, *Nature Geoscience*, *10*, 637–645, doi:10.1038/NGEO3000.

Houlsby, G., S. Draper, and M. Oldfield (2008), Application of linear momentum actuator disc theory to open channel flow, *OUEL Report 2297/08*, Department of Engineering Science, University of Oxford.

Jeffcoate, P., R. Starzmann, B. Elsaesser, S. Scholl, and S. Bischoff (2015), Field measurements of a full scale tidal turbine, *International Journal of Marine Energy*, *12*, 3 – 20, doi:10.1016/j.ijome.2015.04.002, special Issue on Marine Renewables Infrastructure Network.

Joukowsky, N. (1920), Windmill of the nej type, *Transactions of the Central Institute for Aero-Hydrodynamics of Moscow*.

Kramer, S., and M. Piggott (2016), A correction to the enhanced bottom drag parameterisation of tidal turbines, *Renewable Energy*, *92*, 385–396, doi:10.1016/j.renene.2016.02.022.

Labeur, R. (2009), Finite element modelling of transport and non-hydrostatic flow in environmental fluid mechanics, *TU Delft Repository*, pp. 1–235, doi:resolver.tudelft.nl/uuid:7b2d7144-4ea8-4bba-9a05-14ec761b43c3.

Labeur, R., and G. Wells (2009), Interface stabilised finite element method for moving domains and free surface flows, *Computer Methods in Applied Mechanics and Engineering*, *198*(5-8), 615–630, doi:10.1016/j.cma.2008.09.014.

Labeur, R., and G. Wells (2012), Energy stable and momentum conservative interface stabilised finite element method for the incompressible Navier-Stokes equations, *SIAM Journal on Scientific Computing*, *34*(2), A889–A913.

Lanchester, F. (1915), A contribution to the theory of propulsion and the screw propeller., *Transactions of the Institution of Naval Architects*, *57*, 98–116.

Leopold, M., and M. e. Scholl (2019), Monitoring getijdenturbines oosterscheldekering jaarrapportage 2018, *Tech. Rep. C010/19*, Wageningen Marine Research Den Helder, Wageningen UR (University and Research centre), doi:10.18174/470409, pp. 1-58.

Louters, T., J. H. van den Berg, and J. P. M. Mulder (1998), Geomorphological changes of the oosterschelde tidal system during and after the implementation of the delta project, *Journal of Coastal Research*, *14*, 1134–1151.

Milne, I., R. Sharma, R. Flay, and S. Bickerton (2013), Characteristics of the turbulence in the flow at a tidal stream power site, *Philosophical Transactions of the Royal Society A: Mathematical, Physical and Engineering Sciences*, *371*(1985), doi:10.1098/rsta.2012.0196.

Milne, I., A. Day, R. Sharma, and R. Flay (2016), The characterisation of the hydrodynamic loads on tidal turbines due to turbulence, *Renewable and Sustainable Energy Reviews*, *56*, 851–864, doi:10.1016/j.rser.2015.11.095.

Myers, L., and A. Bahaj (2010), Experimental analysis of the flow field around horizontal axis tidal turbines by use of scale mesh disk rotor simulators, *Ocean Engineering*, *37*(2-3), 218–227, doi:10.1016/j.oceaneng.2009.11.004.

Myers, L., and A. Bahaj (2012), An experimental investigation simulating flow effects in first generation marine current energy converter arrays, *Renewable Energy*, *37*(1), 28–36, doi:10.1016/j.renene.2011.03.043.

Neill, S. P., J. R. Jordan, and S. J. Couch (2012), Impact of tidal energy converter (tec) arrays on the dynamics of headland sand banks, *Renewable Energy*, *37*(1), 387 – 397.

Nieuwstadt, F. T. M., B. J. Boersma, and J. Westerweel (2016), *Turbulence - Introduction to Theory and Applications of Turbulent Flows*, chap. Correlation Function and Spectrum, pp. 183–213, Springer International Publishing, doi:10.1007/978-3-319-31599-7.

Nishino, T., and R. H. Willden (2012a), Effects of 3-d channel blockage and turbulent wake mixing on the limit of power extraction by tidal turbines, *International Journal of Heat and Fluid Flow*, *37*, 123 – 135, doi:https://doi.org/10.1016/j.ijheatfluidflow.2012.05.002.

Nishino, T., and R. H. J. Willden (2012b), The efficiency of an array of tidal turbines partially blocking a wide channel, *Journal of Fluid Mechanics*, *708*, 596–606, doi:10.1017/jfm.2012.349.

Nishino, T., and R. H. J. Willden (2013), Two-scale dynamics of flow past a partial cross-stream array of tidal turbines, *Journal of Fluid Mechanics*, *730*, 220–244, doi:10.1017/jfm.2013.340.

Nortek AS (), *Operations Manual – Signature 250, 500 and 1000*, Nortek Group, Red, Norway.

Nortek AS (2019), *Operations Manual – Vectrino*, Nortek Group, Red, Norway.

NWO, N. (2016), The new delta, https://www.nwo.nl/onderzoeksprogrammas/new-delta, *Tech. rep.*

O'Mahoney, T. S. D., A. de Fockert, A. Bijlsma, and P. de Haas (2019), Hydrodynamic impact and power production of tidal turbines in a storm surge barrier, in *13th EWTEC*.

Ouro, P., and T. Stoesser (2019), Impact of environmental turbulence on the performance and loadings of a tidal stream turbine, *Flow, Turbulence and Combustion*, *102*, doi:10.1007/s10494-018-9975-6.

Schmitt, P., B. Elsaesser, S. Bischof, and R. Starzmann (2015), Field testing a full-scale tidal turbine part 2: In-line wake effects, in *11th European Wave and Tidal Energy Conference*, edited by A. H. Clément, Ecole Centrale Nantes, France.

Smeaton, M., R. Vennell, and A. Harang (2016), The effect of channel constriction on the potential for tidal stream power, *Renewable Energy*, *99*, 45 – 56, doi:10.1016/j.renene.2016.06.013.

Stallard, T., R. Collings, T. Feng, and J. Whelan (2013), Interactions between tidal turbine wakes: Experimental study of a group of three-bladed rotors, *Philosophical Transactions of the Royal Society A: Mathematical, Physical and Engineering Sciences*, *371*(1985), doi:10.1098/rsta.2012.0159.

Stallard, T., T. Feng, and P. Stansby (2015), Experimental study of the mean wake of a tidal stream rotor in a shallow turbulent flow, *Journal of Fluids and Structures*, *54*, 235–246, doi:10.1016/j.jfluidstructs.2014.10.017.

Steenman, Y. (2020), Numerical modelling of shallow jet flows - case study of waterdunen, Master's thesis, Delft University of Technology, Faculty of Civil Engineering and Geosciences.

Talstra, H. (2011), Large-scale turbulence structures in shallow separating flows, Ph.D. thesis, Delft University of Technology.

Talstra, H., B. Van Leeuwen, and L. De Wit (2019), Improving accuracy of weir/groyne discharge formulations for highly sub-critical (submerged) conditions, *Land of Rivers, NCR Days 2019 Utrecht*, (2019-43), 83–84.

Valle-Levinson, A., and X. Guo (2009), Asymmetries in tidal flow over a seto inland sea scour pit, *Journal of Marine Research*, *67*, 619–635, doi:10.1357/002224009791218850.

van Leeuwen, B. (2016), Validatie van het oosterscheldemodel, sophiastrand, *Svasek Hydraulics*, pp. 1–3.

Vennell, R. (2010), Tuning turbines in a tidal channel, *Journal of Fluid Mechanics*, *663*, 253–267, doi:10.1017/S0022112010003502.

Vennell, R., S. Funke, S. Draper, C. Stevens, and T. Divett (2015), Designing large arrays of tidal turbines: A synthesis and review, *Renewable and Sustainable Energy Reviews*, *41*, 454–472, doi:10.1016/j.rser.2014.08.022.

Verbeek, M., R. Labeur, and W. Uijttewaal (2020a), The performance of a weir-mounted tidal turbine: Field observations and theoretical modelling, *Renewable Energy*, *153*, 601 – 614, doi:https://doi.org/10.1016/j.renene.2020.02.005.

Verbeek, M., H. Talstra, R. Labeur, and W. Uijttewaal (2022), Supporting material, https://link.to.supplementary.material.

Verbeek, M. C., R. J. Labeur, A. C. Bijlsma, and T. S. D. O'Mahoney (2019), How bathymetric features affect turbine performance: Insights from a cfd model, in *7th Oxford Tidal Energy Workshop 8-9 April 2019, Oxford, UK*, pp. 13–14.

Verbeek, M. C., R. J. Labeur, and W. S. J. Uijttewaal (2020b), The performance of a weir-mounted turbine - experimental investigation, *Renewable Energy*, *168*, 64–75, doi:10.1016/j.renene.2020.12.013.

Verbeek, M. C., R. J. Labeur, and W. S. J. Uijttewaal (2020c), Estimating the stability of a bed protection of a weir-mounted tidal turbine, *International Marine Energy Journal*, *3*(1), 21–24, doi:10.36688/imej.3.21-24.

Vogel, C., and R. Willden (2017), Multi-rotor tidal stream turbine fence performance and operation, *International Journal of Marine Energy*, *19*, 198 – 206, doi:10.1016/j.ijome.2017.08.005.

Vogel, C., G. Houlsby, and R. Willden (2016), Effect of free surface deformation on the extractable power of a finite width turbine array, *Renewable Energy*, *88*, 317–324, doi:10.1016/j.renene.2015.11.050.

Vreugdenhil, C. (1994), *Numerical methods for shallow-water flow*, Kluwer Academic Publishers.

Whelan, J., J. Graham, and J. Peiro (2009a), A free-surface and blockage correction for tidal turbines, *Journal of Fluid Mechanics*, *624*, 281–291, doi:10.1017/S0022112009005916.

Whelan, J. I., J. M. R. Graham, and J. Peiro (2009b), A free-surface and blockage correction for tidal turbines, *Journal of Fluid Mechanics*, *624*, 281–291, doi:10.1017/S0022112009005916.

Wimshurst, A., and R. Willden (2016), Tidal power extraction on a streamwise bed slope, *Ocean Engineering*, *125*, 70–81.

Xia, J., R. A. Falconer, and B. Lin (2010), Hydrodynamic impact of a tidal barrage in the severn estuary, uk, *Renewable Energy*, *35*(7), 1455–1468, doi:https://doi.org/10.1016/j.renene.2009.12.009, special Section: IST National Conference 2009.

Acknowledgements

This work was supported by the Netherlands Organisation for Scientific Research (NWO) within the research programme The New Delta with project number 869.15.008 and the European Regional Development Fund (ERDF) within the project OP-Zuid 2014-2020. We are grateful to Tocardo for the use of their velocity and turbine performance measurements and to Deltares for the assistance in the data processing. Svasek Hydraulics is thanked for the help in the computer modelling and the use of their computer cluster. A special thanks goes to the personnel of DEMO and Environmental Fluid Mechanics laboratory of TU Delft for their assistance in the laboratory tests. The partners of the research project of NWO are also thanked for the collaboration: Tocardo, Svasek Hydraulics, Deltares, Rijkswaterstaat and Dutch Marine Energy Centre. Another thanks goes to the collaboration partners in the OP Zuid project of the EU: Utrecht University and Wageningen Marine Research.

Word of thanks

Many people contributed to this dissertation. Here, I like to thank a few of them with a personal note.

Robert Jan, if there is one person I like to thank it is you. You trained me in analysing flow problems and writing with coherency. Furthermore, you contributed to the articles with a lot of wise suggestions. Thank you for being there to discuss questions and set backs.

Wim, thank you for your wise suggestions to the articles we wrote and the laboratory and numerical tests we did. Thank you also for giving me trust and freedom in the project.

Harmen, thank your for you valuable contribution to Chapter 4. The chapter would not have been written without your modelling effort and patience to check my formula's. Besides, I like to thank for making me feel always welcome at Svašek Hydraulics.

Yorick, Zeinab, Erik, Maria, Lodewijk, Jianwei and Gonzalo, thank you for sharing happiness and set backs in our office. It was always a save and happy place for me.

All people working in the hydraulics laboratory of TU Delft, thank you for the nice working environment, the parties, and the many many coffees we drank together.

Thank you organisation of the Oxford Tidal Energy Workshops. The sessions with tidal energy researchers from all over Europe were instructive and inspiring to me.

Rico and Jeannette, thank you for the flexibility and trust to take time off to finish the thesis while working at RWS.

Arnout, Anton, Magnus, Pieter, Hans, Peter, Britta, Harmen, Paul, Leon, Martin, Michaela, Lonneke, Marco, and Mascha, thank you for the nice and fruitfull collaboration in the Oosterschelde Tidal Power project and the New Delta project.

Clàudia and María, thank you for being my paranimfs at the thesis defence and for being good friends.

A

APPENDIX

A.1. APPENDICES TO CHAPTER 2

A.1.1. SOLUTION OF FLOOD MODEL

The proposed model equations can be solved by following the approach described below, defining the head at station 1 (see Fig. 2.10), $h_1 = p_1/(\rho g)$ [m], to be zero. The pressures at stations 2 and 5, p_2 and p_5 are expressed, using Eq. 2.5 and 2.6:

$$p_2 = 1/2\rho u_1^2(1-\alpha_2^2), \tag{A.1}$$
$$p_5 = 1/2\rho u_1^2(1-\beta_5^2\alpha_2^2). \tag{A.2}$$

The expression for the pressures p_2 and p_5 can be substituted in the momentum equation (Eq. 2.9). A non-dimensional equation can be derived, using the energy balances given in Eq. 2.6, 2.7, and 2.8.

$$\begin{aligned} &R\alpha_2^2 + R(1+a)/2(1-\alpha_2^2) - 1/2\alpha_2^2(\beta_5^2-\alpha_5^2) - \alpha_2^2\beta_5(R-\alpha_3) \\ &-\alpha_2^2\alpha_3\alpha_5 - R(1+a)/2(1-\alpha_2^2\beta_5^2) = 0. \end{aligned} \tag{A.3}$$

Furthermore, Eq. 2.3 gives the relative bypass velocity at station 3 and 5: *Nishino and Willden* (2013)

$$\beta_3 = (R-\alpha_3)/(R-1), \tag{A.4}$$
$$\beta_5 = (R-\alpha_3)/(R-\alpha_3/\alpha_5). \tag{A.5}$$

Lastly, Eq. 2.2 gives the relative velocity at station 1:

$$\alpha_2 = 1+a. \tag{A.6}$$

Eq. A.3 to A.6 form a closed set of equations solving for the unknowns α_5, β_3, β_5, and α_2, respectively, when of a, R, and α_3 are supposed to be known values.

The momentum balance between stations 5 and 7 is considered,

$$Q_B u_1 \alpha_2 \beta_5 + Q_D u_1 \alpha_2 \alpha_5 + A_5 p_5/\rho = A_7(u_1^2 + p_7/\rho), \tag{A.7}$$

A

to determine the dimensional velocity u_1 [ms^{-1}]. This equation enables the solution of the dimensional part of the problem for a given head difference between stations 1 and 7.

A.1.2. SOLUTION OF EBB MODEL

The relative velocity at station 3 and 4 in the bypass streamtube is defined using Eq. 2.3, giving:

$$\beta_3 = (R + Ra - \alpha_3)/(R + Ra - 1), \tag{A.8}$$

$$\beta_5 = (R + Ra - \alpha_3)/(R - \alpha_3/\alpha_5) \tag{A.9}$$

Using Eq. 2.18, a non-dimensional momentum balance can be set up between stations 2 and 5, giving:

$$\alpha_3(1-\alpha_5) - (\beta_5^2 - \alpha_5^2)/2 - (\alpha_3 + \alpha_3/\alpha_5)(1-\beta_5^2)/4 = 0, \tag{A.10}$$

in which the head at station 2 is defined to be zero. Equations A.8, A.9, and A.38 form a closed set to solve for the unknowns β_3, β_5, and α_5, as the values of a, R, and α_3 are assumed to be known values.

The dimensional part of the flow problem can be solved, using a balance of horizontal momentum between station 5 and station 7 given by:

$$Q_B u_1 \beta_5 + Q_D u_1 \alpha_5 + A_5 p_5/\rho + p_6 a R A_D/\rho = A_7(u_1^2 + p_7/\rho), \tag{A.11}$$

where aRA_D is the area of the weir in the model. To solve this equation the pressure in station 6 should be known. The pressure distribution between station 6^-, which is located before the weir, and 6^+, which is located after the weir, is assumed to be continuous. The pressure is defined in the horizontal momentum balance between station 5 and 6.

$$Q_B u_1 \beta_5 + Q_D u_1 \alpha_5 + A_5 p_5/\rho = A_{6^-}(u_1^2 \alpha_2^2 \alpha_6^2 + p_6/\rho), \tag{A.12}$$

where α_6 is given, using a mass balance between station 1 and 6 as:

$$\alpha_6 = 1 + a. \tag{A.13}$$

The pressure at station 7, p_7, is an input of the model. As a result, the flow velocity u_1 [ms^{-1}] can be calculated.

A.1.3. INPUT VARIABLES FOR MODEL VALIDATION

The modelled thrust ratio's of Fig. 2.9 required four input values: the relative velocity at the rotor plane, α_3, the blockage, $1/R$, the relative weir height, a and the available head at the structure, Δh. A constant value of $\alpha_3 = 2/3$ is used in the validation, in line with the observations. For the comparison with the model of Garrett and Cummins a relative weir height of 0 is used and for the comparison with model of Betz also a blockage of 0 is modelled. The blockage, $1/R$, and relative weir area, a, are a function of the channel

Table A.1: The water level in the gate h_L as a function of the water level head Δh for different tidal stages during the field monitoring.

	Ebb				Flood			
Δh [m]	−0.50	−0.40	−0.30	−0.20	0.20	0.30	0.40	0.50
h_L [m NAP]	−2.00	−2.00	−2.00	−2.00	1.60	1.40	1.10	0.70

depth, H, and the local water level, h_L, at the weir, as the water level at the weir crest varied over the different tidal stages (Tab. A.1). The blockage is defined as the rotor swept area divided by the channel area:

$$1/R \quad = \quad A_D/(A_D R) = N(D/2)^2\pi/(HW + h_L W),$$

where A_D is the rotor area with diameter D (5.3 m), N is the number of turbines (5), H is the reference channel depth (9 m), and W is the gate width (39.5 m). The relative weir area is defined as the frontal area of the weir divided by the channel area:

$$a \quad = \quad A_a/(RA_D) = H_a W/(HW + h_L W),$$

where H_a is the height of the weir (4 m).

It is assumed that 2/3 of the head available at the weir, Δh, is lost in friction before reaching the barrier, in order to compare the model results with the field data.

A

A.2. APPENDICES TO CHAPTER 3

Fig. A.1 presents measured flow velocity, the turbulence intensity and the lateral velocity for all tests of Chapter 3.

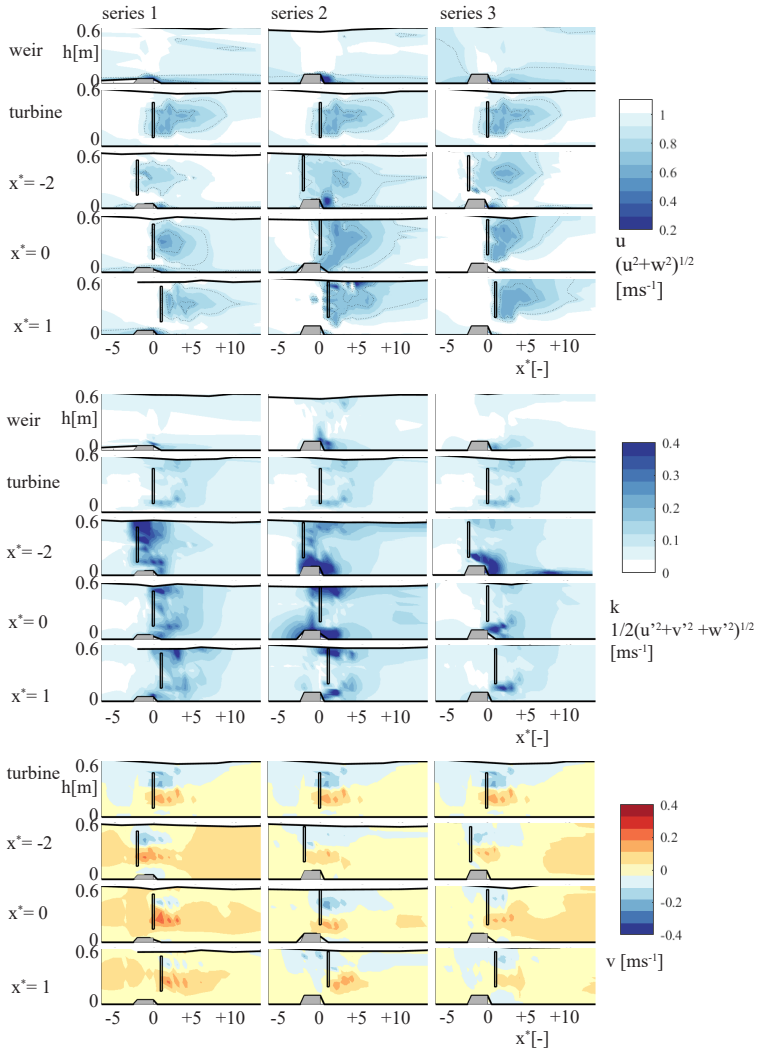

Figure A.1: Measured flow velocity in a streamwise plane at the flume center line, the turbulence intensity in the same plane and the lateral velocity in this plane for all tests.

A.3. APPENDICES TO CHAPTER 4

A.3.1. SUB-GRID TURBINE MODEL

TURBINE PARAMETRIZATION

The turbine parametrization relates the local water level difference over the turbine-weir configuration to the following output,

- the discharge q (per unit width) through a barrier gate with or without turbines (discharge relation),
- the net thrust force T on the turbines,
- the power yield P of the turbines[1].

The parametrization is based on an analytical model proposed in *Verbeek et al.* (2020a) which was validated experimentally in *Verbeek et al.* (2020b). The corresponding discharge relations have been adapted to include the cases of a weir without turbines and turbines on a flat bed as well. The resulting discharge relation takes the following general form,

$$q = d_c u_c = d_c \sqrt{\frac{2g\Delta h}{f}} \tag{A.14}$$

in which d_c and u_c are, respectively, the depth and the depth-averaged flow velocity at the weir crest, g is the gravitational acceleration, Δh is the local head difference over the turbine/weir, and f is a dimensionless head loss coefficient.

The expression for f is specific to the chosen turbine-weir configuration. Four different cases are distinguished,

1. turbine on a flat bed (no weir)
2. turbine upstream of a weir
3. turbine downstream of a weir
4. weir only (no or idle turbine)

These cases are characterized by two dimensionless parameters. The relative weir height a is defined as the height of the weir relative to the water depth near the weir, as follows,

$$a = \frac{d_1 - d_c}{d_c} = \frac{d_7 - d_c}{d_c} \tag{A.15}$$

in which d_1 is the water depth upstream of the weir, assumed equal to the downstream water depth d_7, see Fig. A.2. The so-called inverse blockage ratio R is defined as the (reciprocal) fraction of the flow cross-section at the weir blocked by the turbines, as follows,

$$R = \frac{1}{B_L} = \frac{d_c}{A_D} \tag{A.16}$$

in which D is the turbine diameter, s_L is the intra-turbine spacing, and A_D is the rotor swept area of the turbine per unit width, see also Eq. (4.2). Note that for a turbine on a flat bed a equals zero, while for a weir without turbine R tends to infinity.

[1] The gross amount of energy extracted from the flow will always be reduced by some efficiency factor $\eta < 1$, to obtain the effective net electrical power yield. However, this efficiency factor has no feedback on the local hydrodynamics and is therefore omitted from the analyses.

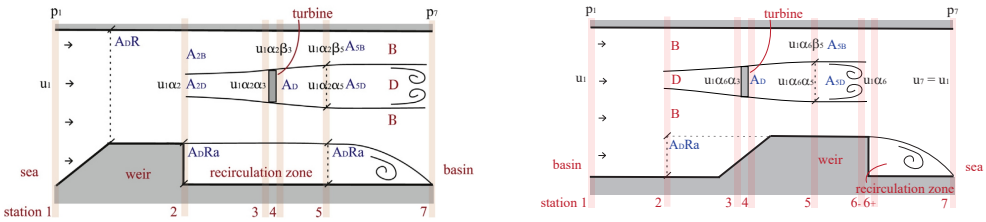

Figure A.2: Schematization of the flow passing the weir and turbine: turbine downstream of weir as during flood (a), turbine upstream of weir as during ebb (b)

The flow distribution over the weir and turbines is schematized by means of two streamtubes (see Fig. A.2), a stream tube passing the turbine rotor, indicated D, and a stream tube covering the flow bypass, indicated B. In addition, we discern a flow recirculation zone downstream of the weir. Furthermore, the schematization assumes a uniform water level over the weir-turbine, for which a weighted average of the upstream and downstream water levels is used (*Verbeek et al.*, 2022). Thus, the water level difference Δh only acts in a dynamic way, driving the flow, while its effect on the flow kinematics (i.e., flow cross-section) is ignored. This is allowed if the water level difference Δh is negligeable relative to the local water depth.

For both streamtubes one-dimensional balances of mass, momentum and energy apply. These balances are expressed in terms of dimensionless velocity coefficients α_n (streamtube D) and β_n (streamtube B), where n is an index referring to the corresponding station (see Fig. A.2). In particular, the coefficient α_5 (velocity in the turbine wake relative to u_c) is treated as an independent input parameter, representing the actual operational settings of the turbine system. Assuming a constant discharge (quasi-steady flow) and a hydrostatic pressure in every station but 3 and 4, the balances are coupled which results in a set of equations that, given a, R and α_5, can be solved to yield the flow and presure distributions along both streamtubes. The algebra is lengthy, and the complete derivation and solution are provided in the supplementary material (*Verbeek et al.*, 2022). The resulting expressions for the head-loss coefficient are given by,

$$
\begin{aligned}
&\text{turbine on a flat bed (no weir)*} && f = \frac{\beta_5^2 - \alpha_5^2}{R} \\
&\text{turbine upstream of a weir} && f = \frac{\beta_5^2 - \alpha_5^2}{R} + 2\left(\frac{a}{1+a}\right)^2 + \frac{a}{2+a}\left[\left(\frac{1}{1+a}\right)^2 - \beta_5^2\right] \\
&\text{turbine downstream of a weir} && f = \frac{\beta_5^2 - \alpha_5^2}{R(1+a)} + \left(\frac{a}{1+a}\right)^2 \\
&\text{weir only, no turbine**} && f = \left(\frac{a}{1+a}\right)^2
\end{aligned}
\tag{A.17}
$$

*(*Garrett and Cummins*, 2007), ** (*Talstra et al.*, 2019)

in which the coefficient β_5 (velocity in the wake bypass relative to u_c) is implicitly given

by,

$$Ry\beta_5^2 - 1 - \beta_5^2 - \alpha_5^2 + 2R1 - \beta_5 1 - \alpha_5 = 0 \tag{A.18}$$

where y is a flow expansion factor defined by $2+2a/2+a$ for an upstream turbine, and by $1+a$ otherwise. After solving for β_5, the coefficient α_3 (velocity at the rotor plane relative to u_c, or *induction*), follows from,

$$\alpha_3 = \frac{R1 - \beta_5}{1 - \beta_5/\alpha_5} \tag{A.19}$$

To complete Eq. (A.14), the water level difference Δh is obtained from the shallow water flow model. The resulting specific dicharge q is fed back into the flow model by imposing it as an interior boundary condition.

The following general formula holds for the net axial force T on the turbines (thrust force) per unit width,

$$T = \frac{1}{2}\rho u_c^2 A_D \left(\beta_5^2 - \alpha_5^2\right) = \frac{1}{2}\rho u_c^2 A_D C_T \tag{A.20}$$

in which $C_T = \beta_5^2 - \alpha_5^2$ is the dimensionless thrust coefficient. Multiplying the thrust force by the local flow velocity $\alpha_3 u_c$ at the turbine disk returns the corresponding power yield P per unit width,

$$P = \frac{1}{2}\rho u_c^3 A_D \alpha_3 \left(\beta_5^2 - \alpha_5^2\right) = \frac{1}{2}\rho u_c^3 A_D C_P \tag{A.21}$$

in which $C_P = \alpha_3 C_T = \alpha_3 \left(\beta_5^2 - \alpha_5^2\right)$ is the dimensionless power coefficient. We recall that P must be scaled by the electrical efficiency η to obtain the effective power yield ηP.

A.4. SUPPLEMENTARY MATERIAL TO CHAPTER 4

This note provides the background information of the turbine-weir sub-grid model as implemented in the large-scale shallow water flow model of the Eastern Scheldt. In Sec. A.4.1 the head-discharge relations of the relevant weir-turbine configurations are derived, followed in Sec. A.4.2 by a description of the forthcoming sub-grid parametrization in the shallow water flow model. Finally, Sec. A.4.3 discusses the verification, validation and calibation of the resulting coupled model.

A.4.1. TURBINE SUB-GRID MODEL

The turbine-weir sub-grid model is based on the model equations given in *Verbeek et al.* (2020a), which have been slightly adapted and tailored to the current application. This is done for robustness; the sub-grid model must yield physically meaningful results over the entire possible input parameter space to ensure consistent results in generic large-scale computations. Furthermore, the sub-grid model has been made much faster and easier to implement by replacing iterations by an exact solution. To this end, the original model in *Verbeek et al.* (2020a) has been rewritten in the form of a discharge-head relation.

SET-UP AND NOTATION

Two primary cases are considered, a sub-grid model for a turbine downstream of a weir (which corresponds to the flood situation in the Eastern Scheldt pilot), and upstream of a

A

weir (ebb). Two other cases, namely a turbine on a flat bed (no weir) and a weir only (no or idle turbine), can be trivially derived from both of the former two cases. The setups of the flood and ebb cases have been sketched in Fig. A.3 and Fig. A.4, respectively. The flow passing the weir and turbines is schematized by means of two streamtubes, a streamtube passing the rotor disk (D) and a streamtube following the bypass flow (B). We use the following notation,

- A_D is the average turbine-swept area per unit width
- d_c is water depth at the weir crest
- $R = d_c / A_D$ is the 'inverse blockage ratio' of the turbine
- d_1 and $d_7 = d_1$ are the depths at either side of the weir
- $a = (d_1 - d_c)/d_c = (d_7 - d_c)/d_c$ is the weir step height relative to the depth d_c
- u_c is the depth-averaged flow velocity at the weir crest
- $\alpha_n u_c$ is the flow velocity in turbine streamtube D at station n
- $\beta_n u_c$ is the flow velocity in bypass streamtube B at station n
- h_n is the piezometric head at station n (defined at stations where it is vertically uniform)

(This notation slightly differs from that used in *Verbeek et al.* (2020a).)

To account for the influence of the free surface height on the blockage, we use a time-variable, uniform water level by averaging the water levels upstream and downstream of the gate. The depth at the weir crest is defined by,

$$d_c = (1-\gamma)h_1 + \gamma h_7 - b_c \tag{A.22}$$

where $\gamma \in [0,1]$ is a weight factor and b_c is the weir crest height. This approximation is allowed if the head difference $(h_1 - h_7)$ is small relative to the water depth, and only acts as a pressure force driving the flow.

TURBINE DOWNSTREAM OF A WEIR (FLOOD CASE)

Fig. A.3 shows the schematization of the flow over the weir passing a turbine sitated downstream of it. In the Eastern Scheldt case this situation corresponds to the flood tidal stage. The associated cross-sectional areas and flow velocities are summarized in Table A.2. The flow through and around the turbine mainly interferes with the flow expansion (recirculation) zone downstream of the weir, whereas upstream of the turbine, which is a zone of flow contraction, the flow dynamics are basically undisturbed by the turbine. We summarize the physical balance principles that have been applied to derive the associated $q-h$ relation.

Between stations 1 and 2 energy conservation (Bernoulli's law) can be applied, which yields,

$$h_1 - h_2 = \frac{u_c^2}{2g}\left(1 - \frac{1}{(1+a)^2}\right) \tag{A.23}$$

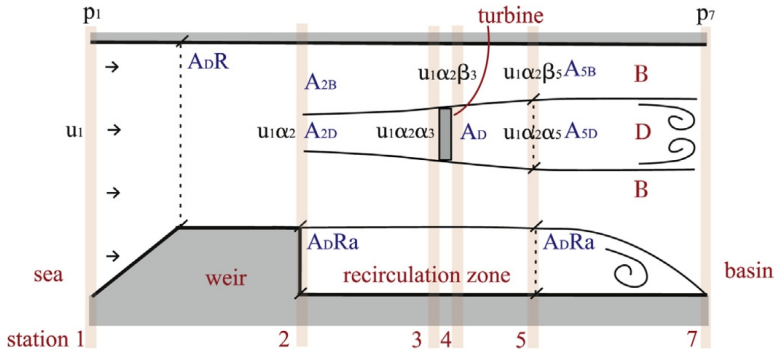

Figure A.3: Schematization of the case with a turbine downstream of a weir, containing a turbine streamtube (D), bypass streamtube (B), and recirculation zone behind the weir; station numbers indicate cross sections; velocities along streamtubes are expressed as the mean velocity above the weir crest u_c times a velocity coefficient α_n (turbine tube) or β_n (bypass), where n is the station number; by definition $d_c = A_D R$.

Table A.2: Definitions of streamtube cross sections and velocities at stations n for the case with a turbine downstream of a weir; A_{nB} is the bypass cross-sectional area, A_{nD} is the cross section of the stream tube passing the turbine, and A_n is the entire cross-sectional area (i.e. total water depth), all per unit width; u_{nB}, u_{nD} and u_n are the corresponding flow velocities; see Fig. A.3 for the corresponding schematization.

n	1, 7	2	3, 4	5
A_{nB}	-	$A_D(R-\alpha_3)$	$A_D(R-1)$	$A_D(R-\alpha_3/\alpha_5)$
A_{nD}	-	$A_D\alpha_3$	A_D	$A_D\alpha_3/\alpha_5$
A_n	$d_c(1+a)$	$A_D R$	$A_D R(1+a)$	$A_D R(1+a)$
u_{nB}	-	u_c	$u_c\beta_3$	$u_c\beta_5$
u_{nD}	-	u_c	$u_c\alpha_3$	$u_c\alpha_5$
u_n	$u_c/(1+a)$	u_c	-	-

A

As explained in *Verbeek et al.* (2020a), conservation of energy can also be applied between stations 2-3-4-5 along both the turbine tube (D) and bypass tube (B), with a discontinuity across the turbine disk. This yields the following expression for the thrust force T upon the turbines, per unit width,

$$T = \frac{1}{2}\rho u_c^2 A_D \left(\beta_5^2 - \alpha_5^2\right) = \frac{1}{2}\rho u_c^2 A_D C_T, \tag{A.24}$$

in which $C_T = \beta_5^2 - \alpha_5^2$ is the thrust coefficient. Also, the following relation holds between h_2 and h_5,

$$h_2 - h_5 = \frac{u_c^2}{2g}\left(\beta_5^2 - 1\right) \tag{A.25}$$

Applying conservation of mass over the bypass tube (B) between stations 2 and 5 yields a continuity constraint which relates the velocity coefficients α_3, α_5 and β_5,

$$\beta_5 = \frac{R - \alpha_3}{R - \alpha_3/\alpha_5} \quad \text{or equivalently} \quad \alpha_3 = \frac{R(1-\beta_5)}{1 - \beta_5/\alpha_5} \tag{A.26}$$

in which α_5 is treated as an independent input parameter, representing the actual operational settings of the turbine system, while α_3 and β_5 are derived quantities (in fact β_3 is never needed). The system of equations for α_3 and β_5 is closed by applying a full momentum balance between stations 2 and 5,

$$\rho d_c u_c^2 - \rho A_D (R - \alpha_3) u_c^2 \beta_5 - \rho A_D \alpha_3 u_c^2 \alpha_5 + \rho g d_c y (h_2 - h_5) - T = 0, \tag{A.27}$$

in which the first three terms are momentum advection terms, the fourth term is the net pressure force over the full water depth, and the last term is the turbine thrust (all per unit width). The factor $y = 1 + a$ represents the relative flow expansion downstream of the weir. Substituting (A.24) and (A.25) into (A.27) and dividing by $\rho u_c^2 A_D$ gives,

$$\alpha_3 = \frac{R - R\beta_5 + \frac{1}{2}Ry\left(\beta_5^2 - 1\right) - \frac{1}{2}\left(\beta_5^2 - \alpha_5^2\right)}{\alpha_5 - \beta_5} \tag{A.28}$$

Combining this with (A.26), and dropping the common denominator $(\alpha_5 - \beta_5)$, yields the following quadratic equation,

$$\left[1 - \beta_5 + \frac{1}{2}y\left(\beta_5^2 - 1\right) - \frac{1}{2R}\left(\beta_5^2 - \alpha_5^2\right)\right] = \alpha_5(1 - \beta_5) \tag{A.29}$$

This equation can be solved exactly for β_5, after which substitution of the result in Eq. (A.26) yields α_3. Compared to the iterative approach used in *Verbeek et al.* (2020a), this exact solution is fast and prevents possible convergence issues. Furthermore, it follows that for the limit $\alpha_5 \to 1$ (the so-called idle-turbine limit) the expansion factor y must go to 1 as well in order to ensure a momentum balance that is consistent with the 'weir-only' case (no turbine). This can be achieved by using the expression $y = y_0 - (y_0 - 1)\alpha_5$, where $y_0 = 1 + a$. This scaling will ensure that $\alpha_3 \to 1$ if $\alpha_5 \to 1$, while $\alpha_3 \geq \alpha_5$ will always hold, whereas it has virtually no impact on β_5 (which tends to 1 if $\alpha_5 \to 1$).

The final balance principle to be applied is the overall momentum balance between stations 2 and 7,

$$\rho d_c u_c^2 - \frac{\rho d_c u_c^2}{1+a} + \rho g d_c (1+a)(h_2 - h_7) - T = 0 \tag{A.30}$$

which, after substitution of Eq. (A.24), can be rewritten as,

$$h_2 - h_7 = \frac{u_c^2}{2g}\left[\frac{2}{(1+a)^2} - \frac{2}{1+a} + \frac{\beta_5^2 - \alpha_5^2}{R(1+a)}\right] \tag{A.31}$$

Adding this equation to Eq. (A.23) yields,

$$h_1 - h_7 = \frac{u_c^2}{2g}\left[\left(\frac{a}{1+a}\right)^2 + \frac{\beta_5^2 - \alpha_5^2}{R(1+a)}\right] \tag{A.32}$$

Defining the specific discharge $q = d_c u_c$ (i.e., the discharge per unit width), and defining,

$$f = \left(\frac{a}{1+a}\right)^2 + \frac{\beta_5^2 - \alpha_5^2}{R(1+a)} \tag{A.33}$$

this equation can be rewritten equivalently as,

$$q = d_c \sqrt{\frac{2g(h_1 - h_7)}{f}} \tag{A.34}$$

which is in fact our sought after discharge relation for the weir and turbine, with the head-loss coefficient f defined by Eq. (A.33).

Multiplying the turbine thrust force T by the local velocity $\alpha_3 u_c$ across the turbine disk, returns the power yield P per unit width,

$$P = \frac{1}{2}\rho u_c^3 A_D \alpha_3 \left(\beta_5^2 - \alpha_5^2\right) = \frac{1}{2}\rho u_c^3 A_D C_P \tag{A.35}$$

in which $C_P = \alpha_3 C_T = \alpha_3\left(\beta_5^2 - \alpha_5^2\right)$ is the dimensionless power coefficient. We note that P must be scaled by the electrical efficiency η to obtain the effective power yield ηP. Furthermore, applying an additional energy balance between stations 5 and 7, we find the following energy losses due to the turbine wake and the recirculation zone (gyre), respectively,

$$P_{\text{wake}} = \frac{1}{2}\rho u_c^3 d_c \left(\frac{1}{1+a} - \alpha_3\right)\left(\frac{\beta_5^2 - \alpha_5^2}{R}\right) \tag{A.36}$$

and

$$P_{\text{gyre}} = \frac{1}{2}\rho u_c^3 d_c \left(\frac{a}{1+a}\right)^2 \tag{A.37}$$

Summation of Eqs. (A.35), (A.36) and (A.37) yields, $P + P_{\text{wake}} + P_{\text{gyre}} = \frac{1}{2}\rho u_c^3 d_c f$, which using Eq. (A.34) is equivalent to $\Delta P = \rho g q (h_1 - h_7)$, the total energy dissipation per unit width over the entire structure.

A

Table A.3: Definitions of streamtube cross sections and velocities at stations n for the case turbine upstream of weir; A_{nB} is the bypass cross-sectional area, A_{nD} is the cross section of the streamtube passing the turbine, and A_n is the entire cross-sectional area (i.e. total water depth), all per unit width; u_{nB}, u_{nD} and u_n are the corresponding flow velocities; see Fig. A.4 for the corresponding schematization.

n	1, 7	2	3, 4	5	6^-	6^+
A_{nB}	-	$A_D(1+a)(R-\alpha_3)$	$A_D(R(1+\frac{1}{2}a)-1)$	$A_D(R-\alpha_3/\alpha_5)$	-	-
A_{nD}	-	$A_D(1+a)\alpha_3$	A_D	$A_D\alpha_3/\alpha_5$	-	-
A_n	$d_c(1+a)$	$A_DR(1+a)$	$A_DR(1+\frac{1}{2}a)$	A_DR	d_c	$d_c(1+a)$
u_{nB}	-	$u_c/(1+a)$	$u_c\beta_3$	$u_c\beta_5$	-	-
u_{nD}	-	$u_c/(1+a)$	$u_c\alpha_3$	$u_c\alpha_5$	-	-
u_n	$u_c/(1+a)$	$u_c/(1+a)$	-	-	u_c	u_c

TURBINE UPSTREAM OF A WEIR (EBB CASE)

Using similar notation and balance principles as for a turbine downstream of a weir (see Sec. A.4.1), but using different definitions of the cross-section numbers, we derive a $q-h$ relation for the case with a turbine upstream of a weir. In this case turbine dynamics mainly interfere with the flow contraction (acceleration) zone upstream of the weir, whereas the downstream expansion and recirculation are basically undisturbed (see Fig. A.4 and Table A.3).

Between stations 1 and 2 the flow does not change, and consequently $h_1 = h_2$. As explained in *Verbeek et al.* (2020a), conservation of energy can be applied between stations 2-3-4-5 along both the turbine streamtube (D) and the bypass (B), with a streamwise discontinuity at the turbine disk. This yields Eq. (A.24) for the thrust force T, using however a different relation between h_2 and h_5 due to contraction of streamlines between stations 2 and 5,

$$h_2 - h_5 = \frac{u_c^2}{2g}\left[\beta_5^2 - \left(\frac{1}{1+a}\right)^2\right] \tag{A.38}$$

Applying conservation of mass to bypass tube (B) between stations 2 and 5 yields the same continuity constraint Eq. (A.26) as for the flood case. Again, α_5 is treated as an independent (operational) input parameter. The system of equations for α_3 and β_5 is closed by the momentum balance between stations 2 and 5,

$$\frac{\rho d_c u_c^2}{1+a} - \rho A_D(R-\alpha_3)u_c^2\beta_5 - \rho A_D\alpha_3 u_c^2\alpha_5 + \rho g d_c[(1+a)h_2 - h_5] - \rho g d_c a\left[\frac{(1+a)h_2 + h_5}{2+a}\right] - T = 0 \tag{A.39}$$

in which the first three terms are momentum advection terms, the fourth term is the pressure force difference between stations 2 and 5, the fifth term is the pressure force upon the upstream side of the weir, and the last term is the turbine thrust. Unlike in *Verbeek et al.* (2020a), this balance is taken over the entire water depth instead of the turbine tube only. Also, the expression for the upstream force on the weir is chosen algebraically consistent with the 'weir-only' case (see (*Battjes and Labeur*, 2017)), which improves robustness of the solution for large values of α_5 (idle-turbine limit).

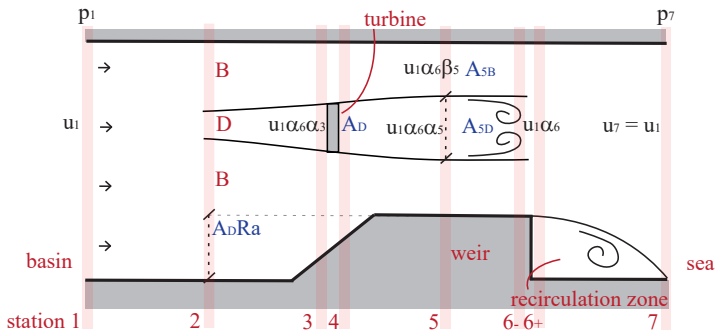

Figure A.4: Schematization of the case turbine upstream of a weir, discerning a turbine streamtube (D), bypass streamtube (B), and recirculation zone behind the weir; station numbers indicate cross sections; velocities along streamtubes are expressed as the mean velocity above the weir crest u_c times a velocity coefficient α_n (turbine tube) or β_n (bypass), where n is the station number; by definition $d_c = A_D R$.

Substituting Eqs. (A.24) and (A.38) into Eq. (A.39), dividing by $\rho u_c^2 A_D$ and using the identity

$$\frac{1}{1+a} - \left(\frac{1+a}{2+a}\right)\left(\frac{1}{1+a}\right)^2 = 1 - \frac{1}{2}\left(\frac{2+2a}{2+a}\right) \tag{A.40}$$

gives

$$\alpha_3 = \frac{R - R\beta_5 + \frac{1}{2}Ry\left(\beta_5^2 - 1\right) - \frac{1}{2}\left(\beta_5^2 - \alpha_5^2\right)}{\alpha_5 - \beta_5} \tag{A.41}$$

in which the factor $y = (2+2a)/(2+a)$ is a measure for the relative flow contraction upstream of the weir. Combining this with Eq. (A.26) and dropping the common denominator $(\alpha_5 - \beta_5)$ yields a quadratic equation in β_5,

$$\left[1 - \beta_5 + \frac{1}{2}y\left(\beta_5^2 - 1\right) - \frac{1}{2R}\left(\beta_5^2 - \alpha_5^2\right)\right] = \alpha_5(1 - \beta_5) \tag{A.42}$$

This equation is algebraically identical to Eq. (A.29), except for the alternative definition of y (!). We can solve exactly for β_5, and substitution of the result in Eq. (A.26) yields α_3. Again, it follows that for $\alpha_5 \to 1$ (idle-turbine limit) the factor $y \to 1$ in order to ensure a momentum balance that is consistent with the 'weir-only' case (no turbine). This is achieved by using $y = y_0 - (y_0 - 1)\alpha_5$, where $y_0 = (2+2a)/(2+a)$. This definition will ensure that $\alpha_3 \to 1$ precisely if $\alpha_5 \to 1$, while $\alpha_3 \geq \alpha_5$ will always hold, whereas it has virtually no impact on β_5 (which tends to 1 if $\alpha_5 \to 1$).

Between stations 5 and 6^-, conservation of momentum governs the final part of the turbine wake,

$$\rho A_D(R - \alpha_3)u_c^2\beta_5 + \rho A_D \alpha_3 u_c^2 \alpha_5 + \rho g d_c (h_5 - h_6) - \rho d_c u_c^2 = 0 \tag{A.43}$$

which is combined with Eq. (A.39) to give,

$$h_2 - h_6 = \frac{u_c^2}{2g}\left[2 - \frac{2}{1+a} + \frac{a}{2+a}\left[\left(\frac{1}{1+a}\right)^2 - \beta_5^2\right] + \frac{\beta_5^2 - \alpha_5^2}{R}\right] \tag{A.44}$$

Between stations 6^+ and 7, conservation of momentum governs the expansion (recirculation) area,

$$\rho d_c u_c^2 - \frac{\rho d_c u_c^2}{1+a} + \rho g d_c (1+a)(h_6 - h_7) = 0 \tag{A.45}$$

Substituting Eqs. (A.39) and (A.43), and using $h_1 = h_2$, this is rewritten as,

$$h_1 - h_7 = \frac{u_c^2}{2g}\left[2\left(\frac{a}{1+a}\right)^2 + \frac{a}{2+a}\left[\left(\frac{1}{1+a}\right)^2 - \beta_5^2\right] + \frac{\beta_5^2 - \alpha_5^2}{R}\right] \tag{A.46}$$

Using $q = d_c u_c$ we find the following $q-h$ relation,

$$q = d_c\sqrt{\frac{2g\,(h_7 - h_1)}{f}} \tag{A.47}$$

with the head-loss coefficient f defined by,

$$f = 2\left(\frac{a}{1+a}\right)^2 + \frac{a}{2+a}\left[\left(\frac{1}{1+a}\right)^2 - \beta_5^2\right] + \frac{\beta_5^2 - \alpha_5^2}{R} \tag{A.48}$$

Finally, if additional energy balances are applied between stations 2-6^- and stations 6^+-7, respectively, we find that the expressions for the power yield P and the energy dissipation rate in the recirculation zone P_{gyre} will be identical to, respectively, Eqs. (A.35) and (A.37). The energy dissipation rate in the turbine wake will however differ from Eq. (A.36), and reads,

$$P_{\text{wake}} = \frac{1}{2}\rho u_c^3 d_c\left[\left(\frac{a}{1+a}\right)^2 + \frac{a}{2+a}\left[\left(\frac{1}{1+a}\right)^2 - \beta_5^2\right] + (1-\alpha_3)\,\frac{\beta_5^2 - \alpha_5^2}{R}\right] \tag{A.49}$$

Summation of Eqs. (A.35), (A.37) and (A.49) yields $\sum P \equiv P + P_{\text{wake}} + P_{\text{gyre}} = \frac{1}{2}\rho u_c^3 d_c f$, which (using Eq. (A.47)) is equivalent to $\sum P = \rho g q (h_1 - h_7)$, the total energy dissipation rate per unit width over the entire structure.

TURBINE ON A FLAT BED (NO WEIR)

The sub-grid model for a turbine on a flat bed follows after setting $a = 0$ (zero weir step height) throughout in Sec. A.4.1 as well as in Sec. A.4.1. The resulting $q-h$ relation is then given by Eq. (A.47), with the head-loss factor f defined by,

$$f = \frac{\beta_5^2 - \alpha_5^2}{R} \tag{A.50}$$

This formulation is consistent with the result given in (*Garrett and Cummins*, 2007). Eqs. (A.24) and (A.35) for, respectively, the thrust T and power yield P are unchanged. The energy dissipation rate in the turbine wake is given by,

$$P_{\text{wake}} = \frac{1}{2}\rho u_c^3 A_D\,(1-\alpha_3)\left(\beta_5^2 - \alpha_5^2\right) \tag{A.51}$$

whereas the energy dissipation rate in the gyre (P_{gyre}) equals zero, by definition.

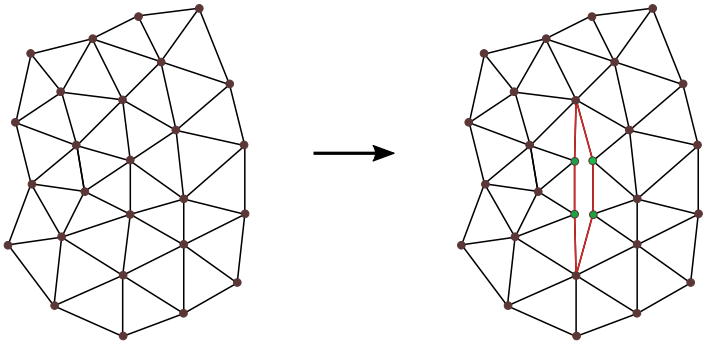

Figure A.5: Creation of an interior boundary (indicated red) by duplication of associated nodes (indicated green).

WEIR-ONLY CASE (NO TURBINE); IDLE-TURBINE LIMIT

A situation with effectively no turbine is described by either setting $A_D = 0$ (weir only), which also implies $R \to \infty$, or setting $\alpha_5 = 1$, which implies an 'idle-turbine limit' - though a turbine is present, it exerts no force upon the flow and will neither extract power from it (see Fig. A.6). Consistent with the derivations in Secs. A.4.1 and A.4.1, it then follows that $\alpha_3 = \beta_5 = 1$, and hence $T = 0$ and $P = P_{\text{wake}} = 0$. The $q - h$ relation is given by Eq. (A.47), with a head-loss factor f defined by,

$$f = \left(\frac{a}{1+a}\right)^2 \tag{A.52}$$

Eq. (A.37) for P_{gyre} remains unchanged; this represents the usual energy dissipation rate for subcritical weir flow.

A.4.2. NUMERICAL IMPLEMENTATION

The turbine-weir parametrization derived in Sec. A.4.1 is coupled to a shallow water flow model. We apply a finite element discretization of the depth-averaged shallow water equations, using the FINEL modelling package (provided by Svašek Hydraulics), which is based on a numerical approach introduced in *Labeur* (2009) and developed further in *Labeur and Wells* (2009, 2012).

The method involves a partitioning of the spatial domain into triangular elements, defining the global state variables (horizontal velocity vector $\vec{u}$ and water level h) at the vertices (nodes) of each triangle, see Fig. A.5. Such a partitioning (or mesh) conveniently deals with irregular geometries and allows for a flexible local refinement in regions of specific interest. In particular, this is needed near the barrier gates where the sub-grid turbine parametrization is coupled to the flow model. The latter has been achieved by locally disconnecting the mesh, creating an interior boundary, along which the $q - h$ relation representing a specific turbine-weir configuration is imposed as a boundary condition.

This section describes the implementation of this approach. It is noted that the use of a finite element based method is not crucial as, in principle, the sub-grid turbine parametrization can be coupled to any type of spatial discretization that allows $q - h$ relations to be imposed on interior boundaries or cell interfaces.

A

INTERIOR BOUNDARY CONDITIONS

At element interfaces that are aligned with a gate opening an interior boundary is created. This is done by splitting the respective interfaces, which defines two separate boundaries that are delineated by the resulting pairs of adjacent nodal points, see Fig. A.5. The state variables ($\vec{u}$ and h) are now represented by functions that are piecewise continuous on elements, but that are discontinuous across interior boundaries. The mass flux (discharge) remains continuous however, which is enforced by expressing it as a single-valued function of the water level difference between the opposing segments of an interior boundary. This function is provided by a $q-h$ relation.

For embedding this relation as a boundary condition, it is sufficient to consider the structure of the depth-averaged continuity equation (conservation of mass). Omitting details (for a complete treatment see e.g. (*Vreugdenhil*, 1994),*Battjes and Labeur* (2017)), the continuity equation takes the following form (assuming a uniform density ρ),

$$\frac{\partial h}{\partial t} + \nabla \cdot (d\vec{u}) = 0 \tag{A.53}$$

in which h is the water level, d is water depth, $\vec{u}$ is the velocity vector, t denotes time and ∇ is the horizontal gradient operator. Typical of the finite element method is to multiply this balance equation by weight functions v, and applying integration by parts over the entire flow domain Ω (using Gauss' divergence theorem), which yields the so-called weak formulation of the continuity equation, as follows,

$$\int_\Omega \frac{\partial h}{\partial t} v \,\mathrm{d}\Omega - \int_\Omega d\vec{u} \cdot \nabla v \,\mathrm{d}\Omega + \int_{\Gamma_{\text{ext}} \cup \Gamma_{\text{int}}} d\vec{u} \cdot \vec{n}\, v \,\mathrm{d}\Gamma = 0, \quad \forall \quad v \in V \tag{A.54}$$

in which Ω denotes the interior flow domain, Γ_{ext} and Γ_{int} denote, respectively, the exterior and interior boundaries, $\vec{n}$ is the outward normal unity vector on each boundary element, and V is the space of weight functions. The class of interpolation functions for the variables h and $\vec{u}$, and weight functions v, basically determines the type of finite element method, see for instance (*Labeur*, 2009; *Labeur and Wells*, 2009). The key point here is that the third term of Eq. (A.54) involves a boundary volume flux, $d\vec{u} \cdot \vec{n}$, which is the boundary-normal discharge q per unit width. Substituting the expression for q given in Eq. (A.34) at interior boundaries, we obtain a dynamic coupling between the water levels h at neighbouring nodes on both sides of the barrier-turbine system.

From the above it follows that the discharge-head relation is applied to the normal flow component only. This is in accordance with the physics of turbines, as horizontal-axis turbines mainly extract streamwise momentum from the flow. However, it also requires that the mesh contours align well with the turbine-swept planes. The tangential momentum component is not affected by the interior boundary, which is actually required to model the horizontal flow contraction across barriers properly. This process can be viewed as physically independent from the $q-h$ relation, which only involves the normal momentum component.

SOLUTION PROCEDURE

To advance the solution for h in time (from time t^n to time t^{n+1}, say) we use an implicit time integration method. This leads to a system of equations for the nodal values representing h

at the new time level $n+1$. This requires that the discharge terms appearing in the second[2] and third intergrals of Eq. (A.54) are expressed in terms of h^{n+1}. As the discharge relation Eq. (A.34) is non-linear, imposing it at interior boundaries would render the resulting system of equations nonlinear, which is undesirable regarding computational effort. Therefore, at each time step we apply the following linearization,

$$q^{n+1} \approx q(h_1^n, h_7^n) + (h_1^{n+1} - h_1^n) \left.\frac{\partial q}{\partial h_1}\right|_{t=t^n} + (h_7^{n+1} - h_7^n) \left.\frac{\partial q}{\partial h_7}\right|_{t=t^n} \tag{A.55}$$

The first term of this sum is an explicit predictor for q, using Eq. (A.34), as a function of the known water levels h_1^n and h_7^n at time t^n. The two other terms are implicit correctors for q, based on first-order derivatives of q in Eq. (A.34) with respect to both h_1 and h_7. (Here it is allowable that the highly non-linear head-loss factor f can be computed based upon the previous time level.) Using Eq. (A.34) with d_c defined by Eq. (A.22), the derivatives of q with respect to the water levels up- and downstream of the weir are given by,

$$\frac{\partial q}{\partial h_1} = (1-\gamma)\frac{q}{d_c} + \frac{g}{f}\frac{d_c^2}{q} \tag{A.56}$$

$$\frac{\partial q}{\partial h_7} = \gamma\frac{q}{d_c} - \frac{g}{f}\frac{d_c^2}{q} \tag{A.57}$$

Again, it should be noted that local definitions of h_1 and h_7 (and hence the respective derivatives of q) will depend on the local flow orientation (i.e., h_1 is the upstream water level).

A.4.3. MODEL PERFORMANCE

Before applying the sub-grid turbine model to realistic scenarios, the performance of the model is examined in detail. This involves the correct implementation of the governing equations (verification), the accurate reproduction of the governing physical processes (validation), and the ability of the model to represent the actual conditions by means of adjusting its free input parameters (calibration). The following sections describe these respective steps.

MODEL VERIFICATION

For consistency, the output of the sub-grid turbine model must depend continuously on the input data. To this end, Fig. A.6 illustrates the behaviour of the model output (i.e., coefficients for wake - and bypass flow velocities, turbine thrust and - power, and head loss), for variations of the wake velocity coefficient α_5, using a fixed inverse blockage ratio R and relative weir height a. The figure shows that the output parameters vary smoothly with α_5, and also converge to the correct values in the various limiting cases: full blockage ($\alpha_5 = 0$), idle turbine ($\alpha_5 = 1$), and no weir. It has been verified that the model behaviour is similarly consistent when varying R and a (results not shown).

[2] The second term in Eq. (A.54) is replaced by substituting a reduced form of the momentum equations having h^{n+1} as the only unknown (pressure correction method).

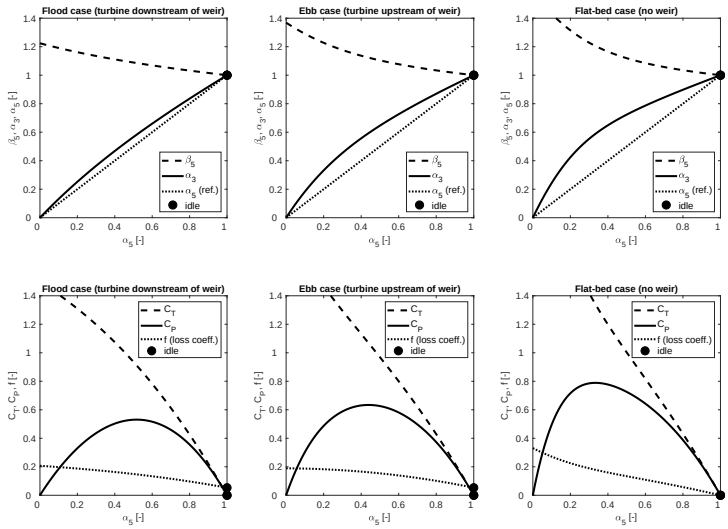

Figure A.6: Behaviour of dimensionless model coefficients as function of the relative wake velocity (α_5), for an inverse blockage ratio R of 7.5 and a relative weir height a of 0.3; upper panels: velocity coefficients α_3 and β_5; lower panels: thrust coefficient C_T, power coefficient C_P and head-loss coefficient f; left panels: turbine downstream of weir; middle panels: turbine upstream of weir; right panels: flat-bed case; black dots indicate the idle-turbine limit (or no weir).

MODEL VALIDATION

The model validation involves the comparison of the model results with measured data. We consider the coupled model, that is, the shallow water flow model including the sub-grid parametrization of the weir and turbine. The data used for validation concern the laboratory experiments conducted in (*Verbeek et al.*, 2020b). In the model, the discharge and the relative wake velocity α_5 are prescribed and the computed head loss, power and thrust are compared with the measurements.

Fig. A.7 shows that the model predicts the magnitudes of the head loss and performance parameters for a weir with turbines quite well, with a relative error of less than 20%, which is close to the accuracy of the measurements. Furthermore, the model very accurately predicts the turbine thrust and power. The head loss, though, is always approximately 1 cm larger in the experiment than in the model. Likely this is caused by the neglect of friction over the turbine-weir section in the model, which is actually present in the experiments. The corresponding relative error in the predicted head loss differs among the different turbine-weir configurations, but is always less than 15%.

CALIBRATION

The wake velocity factor α_5 is used as a calibration parameter for which the operational characteristics of the turbine must be known beforehand in order to predetermine a realistic range of values. To this end we use measurements from previous work. In the experimental tests described in *Verbeek et al.* (2020b) the relative wake velocity α_5 varies between 0.56 and 0.95. This provides a reliable range in which the relative wake velocity α_5 can be

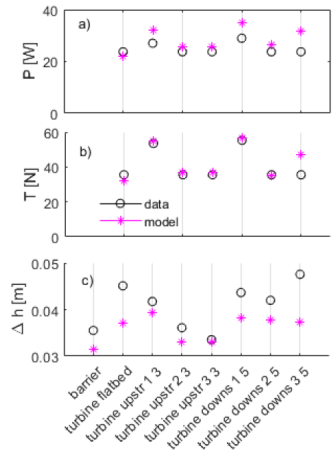

d)

Case (x-axis of figure)	Water depth [m]	Weir height [m]	Distance [m]
barrier/weir only	0.65	0.05	
Turbine only	0.65		
Turb. upstr. of weir 1 3	0.65	0.05	-1D
Turb. upstr. of weir 2 3	0.65	0.10	-1D
Turb. upstr. of weir 3 3	0.70	0.10	-1D
Turb. downstr. of weir 1 5	0.65	0.05	+2D
Turb. downstr. of weir 2 5	0.65	0.10	+2D
Turb. downstr. of weir 3 5	0.70	0.10	+2D

Figure A.7: Model validation: observed and computed power output (a), thrust (b) and water level head over the turbine and/or weir (c) for the different experimental test cases as summarized in the table (d); the table gives the water depth, weir height, and streamwise distance from the weir end to the turbine swept plane (relative to the rotor diameter D) for the different experimental cases from *Verbeek et al.* (2020b).

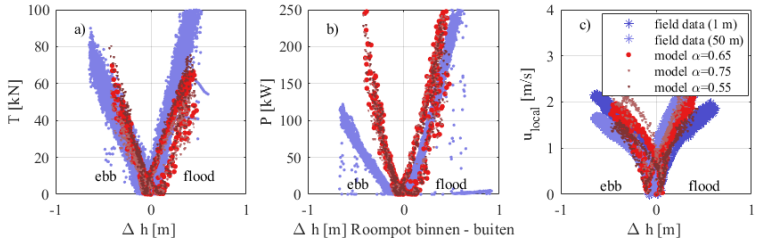

Figure A.8: Model calibration: measured and computed turbine thrust (a), power (b) and gate-normal velocity (c) versus water level head over the Eastern Scheldt storm surge barrier, for different values of α_5 (field data from *Verbeek et al.* (2020a))

chosen. In the field (*Verbeek et al.*, 2020a), the observed wake velocity factor amounted to 0.65, which falls neatly in the range of measured values in the experimental tests. However, this value bears some uncertainty as it was converted from in-situ velocity measurements in the wake center, assuming a parabolic velocity variation over the wake cross section, to obtain an average value representing the overall wake.

In order to select the appropriate value for α_5 we therefore perform a sensitivity analysis, varying the velocity coefficient α_5, and comparing the resulting thrust, power and local velocity in the gate, see Fig. A.8. For the considered range of α_5, the computed turbine power and thrust are almost similar, but the computed local velocity at the turbine shows a better agreement for a velocity factor of 0.65, confirming the value proposed in (*Verbeek et al.*, 2020a), and which is adopted here. At the same time, the computed thrust and power agree well with the measured values during the flood phase, while during ebb these are overestimated by approximately 60%. This overestimation is caused both by the decelerating effect of the turbine strut, which in front of the swept plane during ebb - a

factor which is not incorporated in the model, and an overestimation of the wake expansion during the ebb phase (see *Verbeek et al.* (2020a)). In line with the observations, the computed added resistance of the turbines is larger during ebb (turbine upstream of the weir) than during flood (turbines downstream of the weir), where the latter is also slightly underestimated in the computations.

Finally, it should be noticed that the adopted value for α_5 is not necessarily the optimal value regarding power extraction, rather it is a value that corresponds to the observed turbine performance parameters and that we wish to reproduce.

Curriculum Vitæ

Merel Clasien Verbeek

Education

2010–2016	Master Earth and Environment (Environmental Fluid Mechanics)
Thesis:	Tidal motion and salt dispersion at a tidal junction
Supervisor:	Prof. dr. ir. A.J.F. Hoitink
2016-2022	PhD Hydraulic Engineering
Thesis:	Optimizing the configuration of tidal turbines in storm surge barriers
Promotor:	Prof. dr. ir. W.S.J. Uijttewaal and dr. ir. R.J. Labeur

Work

2016	Teaching assistant Fluid Mechanics (Wageningen University)
2016	Intern hydraulic modelling (Port of Rotterdam)
2020-now	Hydraulic river expert (Rijkswaterstaat Oost-Nederland)

List of Publications

Journal publications

- **M. C. Verbeek**, R. J. Labeur, and W. S. J. Uijttewaal, 2020, "The performance of a weir-mounted tidal turbine: Field observations and theoretical modelling", Renewable Energy, 153, 601 – 614, https://doi.org/10.1016/j.renene.2020.02.005
- **M. C. Verbeek**, R. J. Labeur, and W. S. J. Uijttewaal, 2021 "The performance of a weir-mounted tidal turbine: Experimental investigation. Renewable Energy, 168, 64-75, https://doi.org/10.1016/j.renene.2020.12.013
- **M. C. Verbeek**, T. Talstra, R. J. Labeur, and W. S. J. Uijttewaal, 2022, Modelling and optimizing the configuration of tidal fences in barrages, in subm.
- **M. C. Verbeek**, R. J. Labeur, and W. S. J. Uijttewaal, 2020, Estimating the stability of a bed protection downstream of a weir-mounted tidal turbine. International Marine Energy Journal, 3(1), 21–2, https://doi.org/10.36688/imej.3.21-24
- M. K. Chowdhury, A. Blom, C. Ylla Arbos, **M. C. Verbeek**, M. H. I. Schropp and R. M. J. Schielen, 2023, "Semicentennial Response of a Bifurcation Region in an Engineered River to Peak Flows and Human Interventions", Water Resources Research 59(4), 21, https://doi.org/10.1029/2022WR032741

Conference papers (peer-reviewed)

- M. C. Verbeek, R. J. Labeur, W. S. J. Uijttewaal, and P. de Haas, "The near-wake of horizontal axis tidal turbines in a storm surge barrier", in Proceedings of the Twelfth European Wave and Tidal Energy Conference, A. Lewis, Ed., ISSN: 2309-1983, EWTEC, vol. 1179, University College Cork, Ireland, 2018, pp. 1–6.

Conference abstracts

- M. C. Verbeek, R. J. Labeur, W. S. J. Uijttewaal, and P. de Haas, "Large scale piv applied to flow interaction downstream a semi-open barrier", in 4th International Symposium on Shallow Flows, IAHR, Technical University of Eindhoven, 2017.
- M. C. Verbeek, R. J. Labeur, and W. S. J. Uijttewaal, "Field observations of rotor thrust and bypassacceleration at a tidal fence", in 6th Oxford Tidal Energy Workshop 26-27 March 2018, Oxford, UK, in prep., 2018, pp. 8–9.
- M. C. Verbeek, R. J. Labeur, and W. S. J. Uijttewaal, "Measuring two-scale flow response to resistance at tidal turbines in the eastern scheldt", in Book of abstracts, NCK days 2018, Geo-logic in coastal and shelf research: a matter of multi-disciplinarity, 2018, p. 62.

- M. C. Verbeek, R. J. Labeur, A. C. Bijlsma, and T. S. D. O'Mahoney, "How bathymetric features affect turbine performance: Insights from a cfd model", in 7th Oxford Tidal Energy Workshop 8-9 April 2019, Oxford, UK, 2019, pp. 13–14.
- M. C. Verbeek, R. J. Labeur, and W. S. J. Uijttewaal, "Modelling weir-mounted tidal turbines", in NAC Netherlands Earth Sciences conference Abstracts, B. Westerop, S. de Vet, R. Prop, and D. Liauw, Eds., 2019, p. 55.
- M. C. Verbeek, B. Vermeulen, and A. J. F. Hoitink. 2016, Including tidal models in adcp processing. In *18th Physics of Estuaries and Coastal Seas Conference*.

TECHNICAL REPORTS

- M. Leopold and M. Scholl, "Monitoring getijdenturbines oosterscheldekering jaarrapportage 2018", Wageningen Marine Research Den Helder, Wageningen UR (University and Research centre), Tech. Rep. C010/19, Mar. 2019, pp. 1-58. doi: 10.18174/470409.

MEDIA ATTENTION

- Omroep Zeeland, Onderzoek getijdencentrale voor Tocardo, 26/05/2017, 'youtu.be/-FdjVhfKdM8'